An-Najah National University

Faculty of Graduate Studies

DESIGN A SHUNT ACTIVE POWER FILTER FED BY 27-LEVEL INVERTER AND WIND TURBINE

By

Manar Wael Shtaya

Supervisor

Dr. Kamel Saleh

This Thesis is Submitted in Partial Fulfillment of the Requirements for the Degree of Master of Electrical Power Engineering, Faculty of Graduate Studies, An-Najah National University, Nablus – Palestine

2023

DESIGN A SHUNT ACTIVE POWER FILTER FED BY 27-LEVEL INVERTER AND WIND TURBINE

By

Manar Wael Shtaya

This Thesis was Defended Successfully on 3/10/2023 and approved by

Dr. Kamel Sobhi	
Supervisor	Signature
Dr. Baseem AL-Saied	
External Examiner	Signature
Dr. Moien Omar	Dr. Moien Omar
Internal Examiner	Signature

II

Dedication

أهدي هذا العمل إلى:

أبي وإمي اللذان من دونهما لم أكن أستطيع إتمام مسيرتي التعليمية والمهنية..

رفيق دربي وشريك حياتي الغالي أحمد..

صغيري المدلل الغالي ابني سلطان..

إلى الأهل والأقارب الأعزاء..

إلى أستاذي الفاضل الدكتور كامل صبحي..

إلى أرواح شهداء شعبنا العظيم..

الى كل يد وقلب سار معي درب الانجاز لأكون..

الى كل هؤلاء اهدي هذه الرسالة... راجيا من الله تعالى ان تكون نافذة علم، وبطاقة معرفة... وان ينفعنا وينفع بنا

Acknowledgment

First of all, I would like to thank my supervisor, Dr. Kamel Saleh, for his unwavering support for my master's degree and research. My sincere thanks also goes to each of my university “An-Najah National University”, graduate study faculty, specifically Electrical Power Engineering.

And all thanks to my family: my parents, my husband and my son for supporting me in all phases of my life.

Special thanks to Dr. Baseem Al-Saied and Dr. Moien Omar my external examiner and the internal examiner.

Declaration

I, the undersigned, declare that I submitted the thesis entitled:

DESIGN A SHUNT ACTIVE POWER FILTER FED BY 27-LEVEL INVERTER AND WIND TURBINE

I declare that the work provided in this thesis, unless otherwise referenced, is the researcher's own work, and has not been submitted elsewhere for any other degree or qualification.

Student's Name: **Manar Wael Shtaya**

Signature: Manar Shtaya

Date: **3/10/2023**

V

List of Contents

List of Tables

List of Figures

List of Appendices

DESIGN A SHUNT ACTIVE POWER FILTER FED BY 27-LEVEL INVERTER AND WIND TURBINE

By
Manar Wael Shtaya
Supervisor
Dr. Kamel Saleh

Abstract

The need for energy is increasing rapidly along with the world's population. The generation of power assumes a critical role in facilitating national development by addressing the demands of the populace. Renewable energy sources, including solar energy, wind power, and others, have been utilised for centuries, predating the present era. Solar and wind energy are commonly acknowledged as the most promising modalities of renewable energy, and their utilisation is becoming increasingly prevalent.

The widespread use of non-linear loads in modern electrical systems leads to harmonic pollution of the main network. Apart from the issues instigated by harmonic currents, reactive power represents an additional challenge in power systems.

Enhancing the power of delivery quality to the system and achieve a power factor of unity, it is imperative to employ electrical filters to eliminate harmonics and reactive power. To improve the quality of the electricity, a parallel active filter is utilized.

In this research, a 27-level multi-level inverter besides an active power filter have been integrated with a wind turbine as a renewable energy source by using MATLAB/SIMULINK. The system has been designed to work under different operation scenarios, the system effects, if it is connected with separated load or with network, have been evaluated for each scenario.

In this project, the active power filter was simulated in MATLAB, and the results obtained were as follows: in the first operating condition, when the system connected with separated non linear load, the total harmonic distortion of the source output current was reduced from 21.02% to 8.90% after the inverter has started working. Furthermore, the THD of the inverter output current was increased from 6.74% to756.93%.

In the second operating condition, the system connected with fifteen buses radial network, when the active filter connected near to the power source, the THD of the source output current was reduced from 26.67% to 13.19 %, on the contrary, when the active filter is connected near to the load, the THD of the source output current was reduced from 26.67% to 8.28%. The results confirm that the active filter at this location is effective in reducing THD values.

Keywords: renewable energy sources, active power filter, multi-level inverter, wind turbine, non-linear loads, radial network, total harmonic distortion.

Chapter 1
Introduction

1.1 Motivation

1.1.1 Power system quality

The maintenance of a high level of power quality in the distribution networks is vitally essential, Therefore, addressing the various issues that contribute to diminished power quality, such as the presence of harmonics, reactive power injection, and real power injection, it is imperative to employ active filters within distribution networks [1].

1.1.2 Reliability of renewable energy system

The reliability of the energy source isn’t a function of independent generation method, but a function of the whole of electricity system. Therefore, the wind energy resource is a reliable resource although its classified as variable resource because it depend on wind speed.

1.2 Objectives

1. The primary aim of this research endeavour is to design and construct an active power filter that possesses the capacity to efficiently mitigate the adverse effects of harmonics, adding reactive power injection to the distribution network's regular actual power injection, which includes:

a- Selection and design of wind power system size required to meet load reactive and active power requirements.
b- Design the symmetric three-legs cascaded H-Bridge multi-level inverter.
c- Design the controller needed to integrate the Wind System with multi-level inverter.

The MATLAB/SIMULINK program will be used to implement the designed models which are described above, to ensure that these models can be operated correctly under different scenarios.

Figure 1.1 below shows the general schematic for single phase of the designed system in this research.

Figure 1.1
General schematic of the designed system

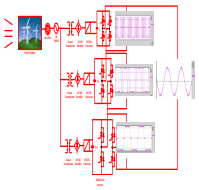

1.3 Thesis structure

1.3.1 Chapter One: Introduction

The first chapter has been introduced in this thesis to examine the effects of the proliferation of nonlinear loads and this study examines the integration of renewable energy sources into the power grid, with a specific emphasis on the emergence of harmonics in distribution networks and its associated phenomena. Furthermore, the chapter presents techniques which will be used for counteracting these effects in spite of these expansion on nonlinear loads and renewable energy sources. Finally, state the motivation and goals for this work.

1.3.2 Chapter Two: Wind Energy Resources Systems

The second chapter compares and contrasts many distinct types of wind generators. It also explains factors that influence wind resource potential. Additionally, the text discusses various aspects pertaining to wind energy conversion systems, including

an examination of distinct classifications of wind turbine generators, as well as a comprehensive analysis of their respective merits and drawbacks.

The chapter also discussing the Buck Converters and its Output Waveforms.

Finally, it shows the Design of wind system with step down linear transformers and with 36V ,108V and 324V DC Buck Converters by using MATLAB/SIMULINK to simulate the aerodynamic and mechanical parts of the energy resources and discuss the buck output voltage and the absolute value of the wind turbine torque behaviors from wind system under different operation conditions.

1.3.3 Chapter Three: Multilevel Inverter

This chapter reviews different topologies of the multilevel inverters besides their principle of operation and limitations. It also explains the design of multilevel inverter and the reasons for the project's choice of an H-bridge with a 27-level inverter. Finally, it shows the designed multilevel inverter model with controller and DC sources for one leg by using MATLAB/SIMULINK.

1.3.4 Chapter Four: Shunt Active Filter

Chapter 4 discusses the different topologies of the of shunt active power filters and their operation and limitations. Furthermore, the chapter reviews the harmonic extraction techniques especially the PQ and DQ techniques and their equations. A Finally, at the end of this chapter, the shunt active filter with its controllers is introduced and simulated MATLAB SIMULINK.

1.3.5 Chapter Five: Compensation Scenarios and System Result

This chapter shows the system schematic overview with Separate nonlinear load and with IEEE network by using MATALAB/SIMLUINK. This chapter also illustrates the system behavior and effects on the source and networks under different compensation scenarios for each operation conditions.

1.3.6 Chapter Six: Conclusions

This chapter illustrates the thesis conclusions based on system results.

Chapter 2
Wind Energy Resources Systems

2.1 Introduction

Wind energy is a form of solar energy that is generated through various mechanisms, such as the uneven heating of the Earth's atmosphere by solar radiation, alterations in topography, and the Earth's rotation. As a result, the Wind Energy Conversion System (WECS) has gained significant appeal as a renewable energy option. To power an electrical generator, in order to convert the kinetic energy of the air into useful mechanical energy, a Wind Turbine (WT) is used. In contrast to scattered wind energy, which consists of wind turbines with a combined capacity of less than 100 kilowatts, utility-scale wind energy refers to wind turbines with a capacity of more than 100 kilowatts that are connected to the grid. The term "distributed wind" refers to the installation of smaller wind turbines, often for usage in residences and off-grid systems [2].

Several factors affect how much wind energy can be generated at a given location. The quantity of energy captured is based on three basic factors: the wind speed, the air density, and the radius of the blades. Wind farms need areas with consistent wind speeds, not only those with periodic gusts [3].

2.2 Types of wind turbines

Two primary types of wind turbines exist, those that revolve around a horizontal axis and those that rotate around a vertical axis, respectively. HAWT's widespread use may be attributed to its several benefits, such as its low cost, great efficiency, and simple design, particularly at higher speeds.

2.2.1 Horizontal axis wind turbines (HAWTs)

The majority of wind turbines currently in use can be categorised as horizontal-axis wind turbines. The turbines employ airfoils, which are aerodynamic rotor blades, that are connected to the rotor through positioning either in an upwind or downwind configuration. The HAWT is offered in configurations featuring either two or three blades, and it functions by operating at elevated blade tip velocities. Figure 2.1 in appendix A shows the horizontal axis wind turbines line diagram [4].

2.2.2 Vertical axis wind turbines (VAWTs)

Vertical axis wind turbines are commonly characterised by their compact size and a rotational axis that is perpendicular to the Earth's surface. The ability of the VAWT to function autonomously regardless of wind direction is a significant benefit, particularly in urban settings where wind direction may exhibit rapid fluctuations. The two primary designs of VAWTs are based on either the Savonius rotors, which are driven by drag forces, or the Darrieus rotors, which are driven by lift forces. Figure 2.2 in appendix A is an illustration of a vertical-axis wind turbine's setup [5].

2.3 Factors that influence the potential of the wind resource

2.3.1 Wind Speed

The pace at which the wind blows has a major impact on how much electricity a wind turbine can produce. In most cases, the rotor blades' rotational speed increases in response to a rise in wind speed, leading to a proportional increase in electrical power output. The faster rotating speed of the generator increases its mechanical and electrical output [3].

The power curve of a wind turbine shows how the amount of electricity generated by the turbine varies with the wind speed. It's a helpful tool for simulating how well wind turbines work.

The Figure 2.3 in appendix A shows a curve of typical wind turbine power output with steady wind speed.

In the first region, the wind turbine's output power is rendered as zero due to the wind speed falling below a designated minimum threshold, commonly referred to as the cut-in speed. In the second region, the power output of the wind turbine experiences a rapid increase when the wind speed surpasses the cut-in speed but remains below the rated speed. In the third region, when the wind speed exceeds the rated speed but remains below the maximum operational speed (cut-out) of the turbine, a constant power output (rated power) is generated by the wind turbine. In Region 4, it is necessary to deactivate the wind turbine when the wind speed surpasses the cut-out threshold in order to safeguard the turbine from potential harm, resulting in a complete cessation of power generation [6].

Prior to construction, the type and size of the turbine are used to establish the cut-in and cut-out speeds [7].

2.3.2 Air density

Wind turbine performance is significantly affected by changes in air density. A wind's potential energy is related to the density of the air around it. If you raise the density of the air, you can generate more energy. The determination of air density is contingent upon the combined influence exerted by air pressure and temperature. The variable in question exhibits an upward trend in response to a decrease in temperature or an increase in air pressure. As a result, variations in elevation have a big impact on the power produced due to variations in air density [8].

2.3.3 Turbine design

In order to enhance operational efficiency and augment power generation, wind turbines are engineered with a substantial radius for their rotor blades. By increasing the airflow through a rotor equipped with larger blades, the turbine is able to enhance its capacity to harness a greater amount of kinetic energy derived from the wind. Conversely, larger blades necessitate a larger surface area and higher wind velocities. In general, it is common practice to arrange turbines at a distance equal to four times the diameter of the rotor. In order to mitigate turbine interference and subsequently minimise the reduction in power output, it is necessary to maintain a specific distance [9].

2.4 Wind energy conversion system elements

The wind energy conversion system is composed of three distinct stages, specifically the aerodynamic, mechanical, and electrical phases. The aerodynamic phase encompasses the conversion of energy from a moving air mass with a defined velocity, leading to the rotational motion of the turbine and the subsequent production of mechanical energy in the generator shaft. The mechanical stage serves as a visual representation of the available mechanical power, which is determined by the rotational speed of the rotor and the torque exerted on the system's shaft. The electrical phase refers to the conversion of mechanical energy into electrical energy at the output of the generator. The procedure is visually illustrated in Figure 2.4, as shown in appendix A [10].

2.5 Types of wind turbine generators (WTGs)

A WTG is an electromechanical device employed for the purpose of electricity generation. Electrical generators operating at low revolutions per minute (rpm) are designed to efficiently convert the mechanical rotational power harnessed from wind energy into electrical energy that can be readily utilised.

2.5.1 Doubly fed induction generator (DFIG)

The DFIG is the prevailing choice for power generation in WECS due to its ability to directly connect the stator to the grid and the rotor via a converter with a partial rating. The utilisation of a gearbox is imperative in order to establish a connection between generators and rotors, as the rotor and stator exhibit disparate rotational velocities. The prevalent configurations include variable frequency, back-to-back AC/DC/AC, and AC/AC voltage source types. Rotor and grid-side converters utilise power electronics components, including bipolar junction transistor BJT, metal-oxide-semiconductor field-effect transistors MOSFETs, insulated-gate bipolar transistors IGBTs and other similar devices. The power converter assumes the responsibility of providing the necessary voltage to the rotor. The responsibility of regulating the power factor and ensuring its maintenance at an optimal level lies with the grid side converter GSC. In contrast, the responsibility of the rotor side converter RSC encompasses the regulation of both active and reactive power, alongside the administration of harmonics. The schematic of a DFIG is depicted in Figure 2.5 in appendix A [11-12].

DFIG advantages

- The speed range is limited (-30% to 30%) around the synchronous speed.
- Low cost, small capacity PWM inverter.
- Complete control over reactive and active power.
- High energy yield and efficiency.

DFIG disadvantages

- Need slip rings.
- Need for gearbox.
- It has a short lifespan and medium dependability due to bearing and gear failures [13].

2.5.2 Permanent magnet synchronous generator (PMSG)

PMSGs enable direct-drive systems. In the PMSGs drive, there is no gear system required because they don't have a rotor current with minimum rotational speed, since the drive is gearless small wind turbines are easily possible at consumer side with high efficiency at low maintenance cost.

PMSGs eliminate the need for gearboxes, resulting in low-maintenance systems. In the AC/DC/AC full power converter, the PMSG provides voltage. This allows generator disengagement from the grid. In this project, the PMSG was chosen because this type is differentiated by a low maintenance grade, this facilitates the integration of turbine generators utilizing unconventional approaches.

Figure 2.6 in appendix A shows a PMSG schematic [14].

PMSG advantages

- Full speed range.
- No gear system required.
- Complete control over reactive and active power.
- Brushless (low maintenance).
- The power converter for field is not required.

PMSG disadvantages

- A full scale the power converter.
- In case of direct drive topologies, multi-pole generators are required (big and heavy).
- A permanent magnet is needed [13].

2.6 Buck converters

A buck or step-down converter is a type of DC/DC converter that reduces the input DC voltage in order to generate the desired voltage at the output. In the context of a DC-DC converter, it is important to note that both the input and output voltages are direct current (DC). Power semiconductors are employed as switches in order to control the activation and deactivation of the direct current power supply to the load. The process of switching can be achieved through the utilisation of various semiconductor devices

such as the (BJT), (MOSFET), or (IGBT). There exist three distinct categories of converters, namely buck converters, boost converters, and buck-boost converters. Regardless of the input DC voltage, these converters have the capability to deliver the appropriate DC output voltage, as indicated below:

1. Buck converter: The output voltage of the converter is less than or equal to the input voltage.
2. Boost Converter: A converter whose output voltage is greater than or equal to the input voltage.
3. Buck-Boost Converter: A converter has the capability to produce an output voltage that is either lower than, higher than, or equal to the input voltage.

Buck converters are employed within wind systems to mitigate the voltage of the wind output. The buck converter consists of the components illustrated in Figure 2.7 in appendix A.

- Inductor L.
- Controlled switch S.
- Diode D.
- Capacitor C.

where:

Vi: Converter DC Input Voltage.
S: controlled switching element. IGBTs are used in this thesis design.
D: A shunt diode was connected in parallel with the source.
L: An inductor was connected in series with the load.
C: A capacitor connected across the load.
Vo: Converter output voltage.

The voltage at the output exhibits variation in accordance with the duty cycle and can be calculated by multiplying the input voltage by the switching duty cycle (D).

2.6.1 The operation of buck converter

Buck converters operate in two modes. Switch S activates the initial mode when closed and the following mode when open. The supply voltage Vi flows via the closed switch S during the Ton time. This current enters the load and charges the inductor. This

charging procedure increases the magnetic field and Vo. Reverse bias opens the shunt diode, blocking current. Figure 2.8 in appendix A shows it.

The inductor stores more energy as its current increases. Switch S and diode D are actuated when Vo reaches the desired value.

The inductor acts as a source and maintains load resistor current throughout the Toff phase when switch S is purposefully activated. Figure 2.9 in appendix A shows that the inductor's energy decreases, lowering its electrical current. After the inductor discharges, D activates and S deactivates, starting a repeated cycle.

2.6.2 Output waveforms of buck converters

The buck converter operates in Continuous Conduction Mode (CCM) and Discontinuous Conduction Mode (DCM). CCM's inductor current never reaches zero. The buck converter is in continuous mode if the inductor current never reaches zero throughout the commutation cycle. Within the domain of power electronics, it is evident that the discontinuous conduction mode encompasses a distinct time interval during which the current passing through the inductor undergoes a decrement until it reaches a state of complete cessation. The converter possesses the capacity to operate in two discrete modes, thereby offering enhanced convenience to the user. Figure 2.10 in appendix A visually represents the CCM and DCM modes, whereas Figure 2.11 in appendix A provides a graphical representation of the waveforms associated with the buck converter mode [15-16].

2.7 Design of wind system with converters

In this research, A shunt filter employing a 27-level inverter, which is supplied by wind energy sources, is designed and simulated with the objective of improving the power system's quality.

The following sections present a comprehensive overview of the design of the Wind system, which includes the integration of a PMSG, step-down linear transformers, and buck converters. Where a 36V, 108 V and 324 V as an output voltages from the wind system, which are required to integrate them with the multi-level inverter.

2.7.1 Design the wind turbine with PMSG.

The Wind Turbine and PMSG models have been used in the MATLAB/SIMULINK to simulate the aerodynamic and mechanical parts of this energy resources. The models' detailed specs are shown in Table 2-1 below.

Table 2.1
Technical specifications for wind turbine and PMSG model.

Value	Specifications Data for Wind Turbine
1500 KW	Nominal mechanical output power
1666.6 KVA	Base apparent power
12 m/s	Base wind speed
0.73 Pu of nominal mechanical power	Maximum Power @ base wind speed
1.2 Pu of base generator speed	Base rotational speed
0	Pitch angle beta
55%	Wind energy utilization ratio
2500Kw	Maximum output power
1.8 m/s	Start-up speed
2-25 m/s	Working speed
30 m	Blade dimeter
Value	Specifications Data for PMSG model
Three (3)	Number of Phases
Sinusoidal	EME waveform
Round	Rotor Type
3000 RPM	Synchronous speed
0.05 Ω	Stator resistance (Rs)
0.635 mH	Armature inductance

The instantaneous mechanical output power of wind turbines is primarily influenced by wind speed. The equation that represents the theoretical mechanical power harnessed by a wind turbine (Pm) is as follows:

$$P\text{m} = 1/2\ \rho\ Aw\ C\text{p}\ \upsilon\ 3 \tag{2.1}$$

where:

Pm: Mechanical power output of the wind turbine in watts.

Cp: Wind energy utilization coefficient (power coefficient).

ρ: Air density in Kg/m3, it's usually 1.225Kg/m3.

Aw: Turbine swept area in m2,

Aw = Π* (D/2)^² , where D is turbine blade's diameter in m.

= 706.50 m2.

υ: Wind speed in m/s.

The MATLAB/SIMULINK wind turbine model converts mechanical power into mechanical output torque per unit (p.u) of the nominal generator torque. MATLAB/SIMULINK has been enhanced to translate the output torque per unit (p.u) value into its true mechanical output value using the following equation.

$$Base\ tourqe(N.M) = \frac{Base\ Power\ (VA)}{Base\ Speed\ (\frac{rad}{s})} \tag{2.2}$$

$$Base\ tourqe = \frac{1666.6\ \text{KVA}}{2 * 3.14 * 3000/60} = 5307\ \text{N.M}$$

The Figure 2.12 below shows the designed Wind system with PMSG by using MATLAB/SIMULINK.

Figure 2.12
Wind system design by using MATLAB/SIMULINK

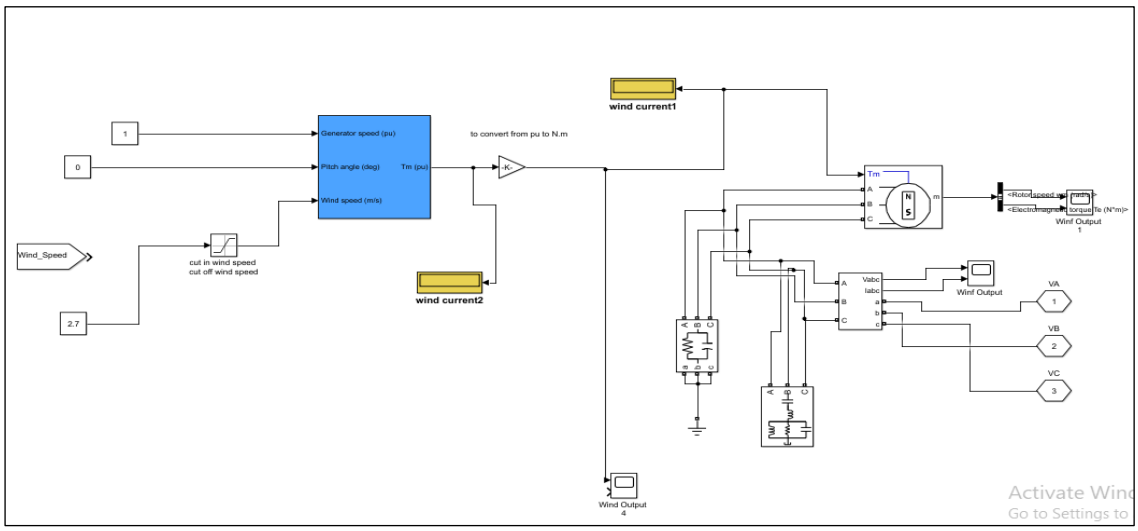

The output of PMSG shall be connected with three step down Linear Transformers, These linear transformers have been combined with multi-level inverter via Buck DC converters to achieve the desired fixed value at the inverter input.

A Universal Diode Bridge model has been used in the MATLAB/SIMULINK to converter the sinusoidal output from PMSG to DC waveform.

After that, Buck converters have been designed to convert this DC waveform to a 36V, 108 V and 324V as a fixed DC voltages at first, second and third DC input buses of multi-level inverter despite the change of operation conditions during the day.

These values of voltages were chosen to make the voltage of the active filter to be near and matches the voltage of the buses at the PCC, which equal 400 V.

2.7.2 Design the 36 V DC buck converter.

The voltage required for the first DC input bus of the multilevel inverter in the designed system is 36 V, but the received DC voltage from the designed wind system is almost equal to 66 volts, for that, the buck converter has been used to achieve this voltage at multi-level inverter input.

This converter has been designed to achieve a 36 V as fixed output voltage at first DC input bus of multilevel inverter.

The first step down linear transformer has a Turn Ratio A1 = voltage at primary side/ voltage at secondary side = 900 Vrms /100 Vrms = 9, and apparent power S1 = voltage at secondary side $*$ maximum current of the inverter = 141.4 Volt $*$ 11 A =1555.6 VA.

Figure 2.7 shows the buck converter circuit. The wind system output voltage equals the buck input voltage. The Insulated Gate Bipolar Transistor (IGBT) controls the switching device, and the equations calculated the inductance and capacitance values. The wind turbine should supply a voltage almost equal to 66 volts to the buck converter whose output voltage is fixed at 36 volts on the first DC input bus of the multilevel inverter. Table 2.2 illustrates the 36V buck controller's design specifications.

Table 2.2
Design specifications of 36 V buck converter

Parameter Value	
66 V	Maximum Input Voltage
36	Output Voltage
10kHz	Switching frequency

(Vout < Vin) is the buck converter's output voltage.

Table 2.2 shows how to calculate the buck converter duty cycle from input and output voltages. This equation calculates it:

$$\mathrm{Vout} = \mathrm{Vin} * \mathrm{D} \tag{2.3}$$

Then

$$D = \frac{Vout}{Vin}$$

Where:

V_{out}: is the buck output voltage as per above table

V_{in}: is the input voltage as per the above table.

Buck converters aim to maintain the output voltage. Buck converter duty cycle directly affects wind power system output voltage. The following equation shows that the buck converter's workload is lowest when the wind turbine system's output voltage is maximum:

$$Dmin = \frac{Vout}{Vin\ max} \tag{2.4}$$

$$Dmin = \frac{36}{66} = \sim 54\%$$

The minimum value of the buck converter series inductance is chosed according to equation (2.5):

$$Lmin = \frac{(1-D)R}{2f}$$

(2.5)

If the resistence value is chosen to be 10 **Ω** , then

$$Lmin = \frac{(1-0.54)*10}{2*10*10^3} = 0.23*10^{-3}\ \ F$$

The determination of the minimum capacitor size for the buck converter's output can be achieved by employing the subsequent formula, assuming a voltage ripple of 0.05.

$$C_{min} = \frac{\boldsymbol{V0(1-D)}}{\boldsymbol{8Lf^2\Delta V}}$$

(2.6)

$$C_{min}=\frac{\boldsymbol{36(1-0.54)}}{\boldsymbol{8*0.23}*10^{-3}*(10*10^3)^{\boldsymbol{2}}*0.05} = 1.8\ mF$$

2.7.3 Design the 108 V DC buck converter.

The regulation of the second DC input bus voltage in the multilevel inverter within the wind system design is necessary to maintain a constant value of 108 V, as specified in Table 2.1 in the preceding section.

But the received DC voltage from the designed wind system is almost equal to 200 volts. The second step down linear transformer has a Turn Ratio A2 = voltage at primary side/ voltage at secondary side = 900 Vrms /300 Vrms = 3, and apparent power S2 = voltage at secondary side $*$ maximum current of the inverter = 424.2 Volt $*$ 11 A =4666.2 VA.

The wind turbine should supply a DC voltage is almost equal to 200 volts to the buck converter whose output voltage is fixed at 108 volts on the second DC input bus of the multilevel inverter. Table 2.3 illustrates the 108 V buck controller's design specifications.

Table 2.3
Design specifications of 108 V buck converter

Parameter Value	
200 V	Maximum Input Voltage
108	Output Voltage
10kHz	Switching frequency

Using equation (2.4) above, the minimum duty cycle for this buck converter is about 54%. The minimum duty cycle of the 108 buck converter is equivalent to that of a 36V buck converter which is calculated in section 2.7.2. Based on that, the passive elements values of this converter are close to values which are used on 36 V Buck converter as calculated in previous section above. So, the same values have been used to simulate this converter.

2.7.4 Design the 324 V DC buck converter

The voltage required for the third DC input bus of the multilevel inverter in the designed system, which its specifications are mentioned in Table 2.1 in the previous section, is 324 V, but the received DC voltage from the designed wind system is almost equal to 600 volts, for that, the buck converter has been used to achieve this voltage at multilevel inverter input.

The third step down linear transformer has a Turn Ratio A3 = voltage at primary side/ voltage at secondary side = 900 Vrms /900 Vrms = 1, and apparent power S3 = voltage at secondary side $*$ maximum current of the inverter = 1272.8 Volt $*$ 11 A =14$*$ 10^3 VA.

The wind turbine is expected to provide a DC voltage to the buck converter, with a voltage is almost equal to 600 volts. The primary objective of the buck controller is to regulate and sustain a consistent output voltage of 324 volts at the third DC input bus of the multi-level inverter. Table 2.4 illustrates the 324V buck controller's design specifications.

Table 2.4
Design specifications of 324 V buck converter

Parameter Value	
600 V	Maximum Input Voltage
324	Output Voltage
10kHz	Switching frequency

Using equation (2.4) above, the minimum duty cycle for this buck converter is about 54%. Based on the formula presented in subsection 2.7.2, the 108 buck converter's minimum duty cycle is identical to that of the 36V buck and the 108V converters.

Based on that, the passive elements values of this converter are close to values which are used on 36 V Buck converter as calculated in previous section above. So, the same values have been used to simulate this converter.

The Figure 2.13 below shows the designed linear transformers with buck converters for one phase by using MATLAB/SIMULINK.
The Figure 2.14 below shows a 36V buck converter design by using MATLAB/SIMULINK.

Figure 2.13
Design of linear transformers with buck converters for one phase by using MATLAB/SIMULINK

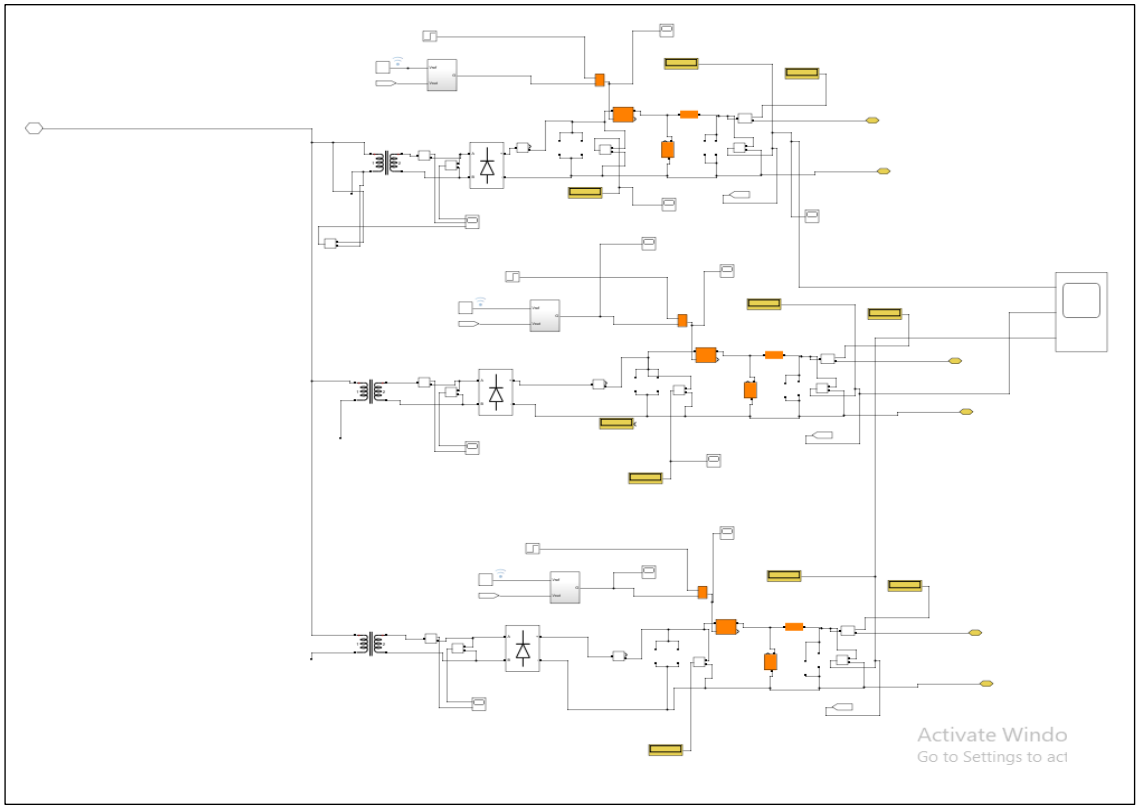

Figure 2.14
Design of 36V buck converter by using MATLAB/SIMULINK

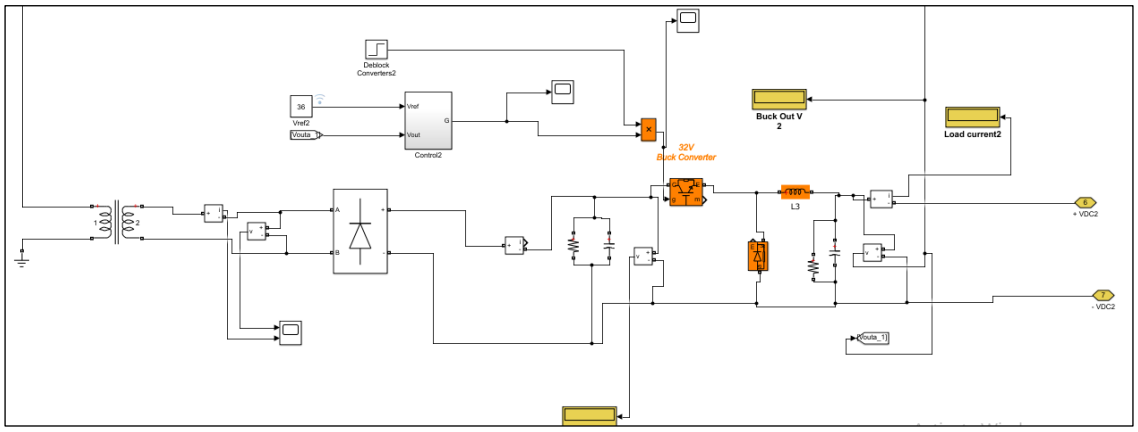

The wind energy system configuration and the reference value of voltages (V ref) have been changed according to the required voltage, and set in the MATLAB/SIMULINK design as described above.

Chapter 3
Multilevel Inverter

3.1 Introduction

An inverter is a piece of power electronics that changes the input voltage and the conversion of direct current (DC) to alternating current (AC) occurs at the designated settings, altering the frequency as well. In the world of industrial applications, multilevel converters are an interesting field today. Conventional power electronic converters can only generate output voltages that switch between two voltage levels. The conventional two-level inverter is associated with elevated switching losses, functions at a high switching frequency, and is restricted in its capacity to handle high power and voltage applications. It also suffers from high levels of total harmonic distortion. These problems make it more difficult to use the two-level inverter in high and medium voltage settings. Several types of multilayer inverter topologies are needed [17].

For medium power and high voltage situations, multilevel inverters can be used instead of conventional converters. To generate the required output voltage, it uses several DC voltage levels as input. This boosts the inverter's power production and creates a sinusoidal output signal with low harmonics. Multi-level inverters are employed as a viable substitute for step-up transformers in order to establish a connection between low-voltage renewable energy sources, such as wind and solar, and the higher voltages of the grid [18].

The inception of multilevel converters can be traced back to 1975. The term "multi-level" refers to a converter that possesses three or more levels. There are many topologies that are introduced for the multilevel converters. These topologies employ a sequence of power semiconductor switches in conjunction with multiple direct current sources to achieve a high level of power. The multi-level inverter's significantly high output voltage does not necessitate an increase in the switches' rated voltage, as it solely relies on the rating of the linked DC voltage sources [16].

One notable drawback pertains to the significant quantity of power semiconductor switches that are necessary. The system experiences an escalation in both complexity

and cost due to the necessity of a dedicated drive circuit for each switch. The field of electrical engineering has witnessed a decline in circuit complexity due to advancements in power electronics switches and gate drive circuits.

The purpose is to reduce circuit complexity by reducing power electronics switches and gate drive circuits [17].

3.2 Multilevel converter structure

Multilevel converters are comprised of three or more levels. Multilevel converters are referred to as converters rather than inverters due to their utilisation of bidirectional switches capable of functioning as both rectifiers and inverters. As the quantity of levels increases, the total harmonic distortion (THD) diminishes and the overall performance of the system enhances.

A multilayer voltage source inverter (VSI) uses a DC source to get the DC link voltage (Vdc). In Figure 3.1, a configuration of interconnected capacitors functions as an energy reservoir, enabling the generation of diverse DC voltage levels for the inverter. The equation presented herein demonstrates that every capacitor possesses a voltage denoted as Vc [18].

$$Vc=Vdc/ (n-1) \tag{3.1}$$

Where n is the number of levels.

The principal operation of a single-phase multi-level inverter, in terms of generating various voltage levels, is depicted in Figure 3.1 in appendix A. The generation of various voltage levels can be achieved by solid-state switches through the connection of the output with a series of input DC sources. In general a n-level inverter could generates n output voltage level.

The most common three topologies of the multilevel converter that is exists in literature and in industry are depicted in Figure 3.2 in appendix A. These topologies are:

- Cascaded H-bridge
- Diode clamped
- Flying capacitor [19].

3.2.1 Diode-clamped multilevel inverter

In the present topology, diodes are employed as a clamping device to produce distinct levels of output voltage. The utilisation of these diodes serves the purpose of mitigating the voltage strain on solid-state switches.

Figure 3.3 in appendix A shows a single-phase three-level diode-clamped inverter. C1 and C2 form the DC bus in this setup [18-19].

Table 3.1 illustrates the various output levels that can be produced from this topology based on the switching states [19].

Table 3.1
Switching states of the three-level diode-clamped inverter

van	Switch State
Vo=Vdc/2	T1=ON, T2=ON T3=OFF, T4=OFF
Vo=0	T1=OFF, T2=ON T3=ON, T4=OFF
Vo=-Vdc/2	T1=OFF, T2=OFF T3=ON, T4=ON

In General, in order to generate n-level voltage using the diode-clamped multi-level inverter topology, it requires (n-1) capacitors, 2(n-1) solid-state switches, and (n-1)(n-2) diodes per leg. Due to the increased number of switching devices, increasing the output level to reduce harmonic content complicates the inverter's design and management [20].

3.2.2 Capacitor clamped multilevel inverter

The capacitor-clamped topology uses flying capacitors instead of diodes. Figure 3.4 in appendix A shows these capacitors clamping voltages.

In general, to generate n-level output of leg of the capacitor clamped multi-level inverter topology, it requires (2n – 2) solid-state switches, (n-1) capacitors and no clamped diodes. The output level of the capacitor clamped topology according to the switching states of the solid-state switches are the same as that given in table 3.1 for the diode clamped topology.

3.2.3 Cascaded multilevel inverter

Cascaded Multilevel Inverters (CMI), also known as series H-bridge inverters, are an additional alternative to multilevel inverters [21].

The converter under consideration exhibits a topology that relies on a concatenation of H-bridge converters featuring distinct direct current sources, as depicted in Figure 3.5 in appendix A.

The H-Bridge configuration offers three distinct levels of direct current voltage: positive (V), neutral (0), and negative (V), with V representing the voltage of the H-Bridge's DC link. The DC-link can consist of various components such as PV systems, diode rectifiers, batteries, or other DC sources. The scalability of the output voltage levels in the CMI can be readily achieved through the augmentation of H-Bridges within each leg. The correlation between the quantity of output voltage levels (n) produced by the CMI and the number of H-Bridges (s) utilised as DC sources is expressed as n = 2s+1. CMI has been widely utilised in various applications, specifically those with high power requirements, owing to its adaptability and modular nature [22-23].

3.3 Multilevel inverter design.

For this project, an H-bridge with a 27level inverter was chosen because of the reasons listed below:

- The output waveform's distortion will be reduced as the level number is increased to (27) levels.
- Compared to conventional inverters, it is better appropriate for high-power, high-voltage applications.
- The controller of the solid-state switches is easier compared to other topologies.
- The voltage stress on the switches will become less intense when the level’s number is increased.
- Since the inverter structure consists of many single-phase full-bridge converters that are each fed by a separate DC sources, there is no need to use voltage balance circuits (sharing circuits) or voltage matching of switching devices.
- For each H-bridge, a separate DC energy source can be applied.

The diagram presented in Figure 3.6 in appendix A illustrates a hierarchical arrangement comprising three H-bridges that are interconnected in a series configuration. The DC-link input voltage is unique to each H-bridge. Three input DC link voltages have a 1:3:9 voltage ratio. The DC links of the H-bridges are sourced from wind energy generators and transformers, as indicated by the respective ratings provided in Table 3.2.

Table 3.2
The dc sources of the inverter

Required input voltage	Inverter Bus name	DC Energy Source Type
36 V	Vdc1	Wind System
108 V	Vdc2	Wind System
324 V	Vdc3	Wind system

To generate a near sinusoidal output, the solid-state switches of each H-bridge are fed from pulsating signals. These pulsating signals are generated using Amplitude modulation technique. This modulation technique is simple and can be easily implemented compared to other modulation techniques. The operational principle of this methodology is depicted in Figure 3.7 in appendix A. This technique involves the utilisation of various solid-state components that exhibit distinct switching states based on the amplitude of the input reference signal.

Where: the reference signal's absolute value divided on maximum value is represented by the symbol a, and y is the reference signal's value divided by the maximum value.

Figure 3.8 shows the designed multilevel inverter model with controller and DC sources for one leg by using MATLAB/SIMULINK.

Figure 3.8
Simulink Modelling of a symmetric 27 level inverter

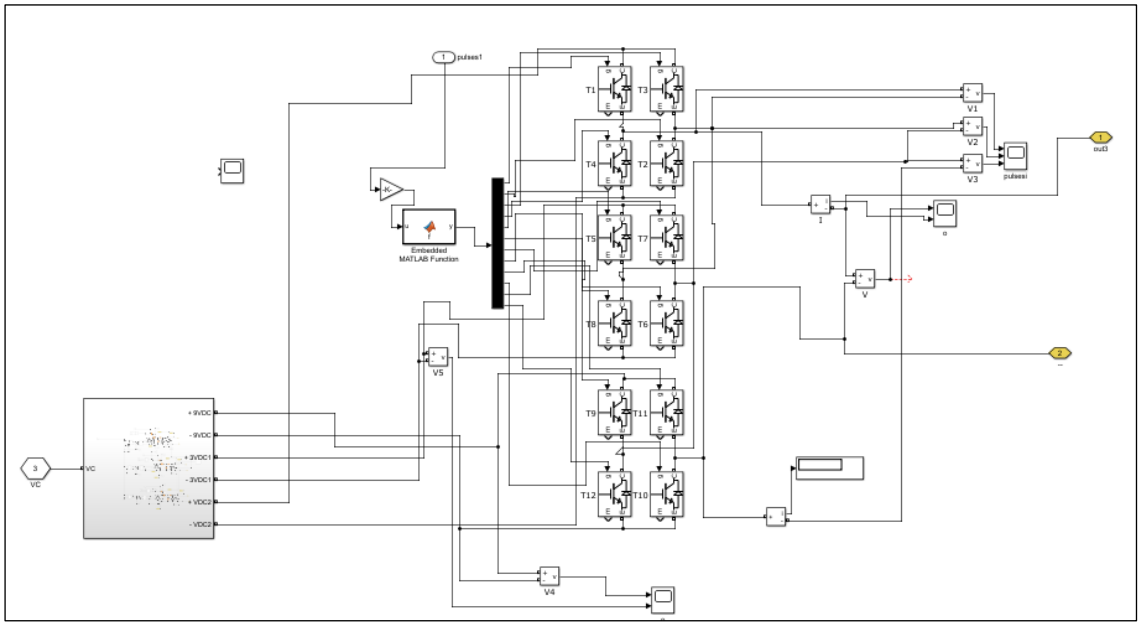

The inverter output behavior with its controller under different operating conditions is described in Chapter 5 of this research.

Chapter 4
Shunt Active Filter

4.1 Introduction

Power electronic devices are frequently utilised in various settings, including commercial, industrial, and consumer applications. The aforementioned appliances produce harmonics and reactive power within the utility system. A major issue today is reducing harmonics to improve power quality [24].

The occurrence of harmonics in electrical systems results in the distortion and deviation of current and voltage from sinusoidal waveforms. Power distribution system-connected non-linear loads generate harmonic currents. Nonlinear loads have been categorised as current sources due to the deviation of their waveform from pure sine waves at the fundamental frequency. Harmonic voltages arise as a result of the passage of harmonic currents through impedances within a system, leading to the distortion of the supplied voltage [25].

There exist several techniques to enhance the effectiveness and excellence of an AC source. These include the advancement of electronic converters that augment the power factor in accordance with the source, That the development of electronic devices aimed at improving the power factor of electrical equipment, as well as the enhancement of supply voltage quality, have been subjects of significant interest and research in recent years [26].

4.2 Harmonic mitigation techniques

There are two techniques to compensate the harmonics in power system. The first technique is using suited circuit topology to reduce or prevent the generation of harmonics. The typical example of this technique is the use of the transformer-less UPS system with PWM rectifier. In this case, there is no need for filtering equipment because just a small amount of distortion may remain.

The second method entails the utilisation of power filtering apparatus, which employs techniques to mitigate the overall harmonic distortion of the electric current, commonly referred to as total harmonic distortion (THD). Passive and active filtering are the main

methods of reducing harmonic distortion in power distribution systems. Passive filtering technique is the traditional filter that uses R, L, and C components as depicted in Figure 4.1 in appendix A. The parallel passive filter possesses the ability to attenuate the desired harmonic by introducing a low impedance that is placed in parallel with the load, or by impeding it through a high impedance that is connected in series with the load (referred to as a series passive filter) [27]. The utilisation of a blend of shunt and series connections could be employed based on the nonlinear load utilised. The utilisation of these filters is occasionally advantageous due to their straightforwardness, low cost, and effectiveness [28]. However, passive filters have several disadvantages, including fixed compensation, high size, and resonance issues.

Active power filters offer several benefits compared to their passive counterparts. Primarily, apart from providing contemporary harmonics, they possess the capability to diminish reactive currents. In addition, it is worth noting that active filters do not induce adverse resonances with power distribution systems, which is not the case with passive filters.

4.3 Types of active power filters

Figure 4.2 in appendix A shows active filter topologies. Active Power Filters (APFs) may be shunt, series, or hybrid [29].

4.3.1 Shunt active power filters

In active filtering applications, this class is the most significant and most widely used. Shunt Active Power Filters (SAPFs) are employed for the purpose of mitigating harmonics in a network that arise from non-linear loads. This is achieved by injecting harmonics of opposite polarity into the load. Additionally, SAPFs are capable of balancing the currents in a three-phase system and compensating for reactive power. This task could be accomplished by using a proper controller to drive the switching element (IGBT) to provide a reference signal.

Figure 4.3 in appendix A illustrates the schematic representation of the SAPF. The presence of a nonlinear load introduces distortion in the real power (P) and reactive power (Q) due to their nonlinearity. Shunt filters are a potential solution for compensating for power distortion.

It is advisable for the SAPF to generate the filter current (I_F) by consistently monitoring the load current IL. This approach ensures the attainment of a sinusoidal current IL that is synchronised with the voltage of the source.

In order to accomplish this goal, sensors are utilised to monitor the load current (IL) in conjunction with either the filter current (I_F) or the source current I_S [30].

One advantage of shunt filters is their ability to generate harmonic currents that are a small fraction of the active fundamental current, resulting in a significantly reduced rated current. Moreover, it is possible to connect multiple filters in parallel when the level of harmonics current is elevated. Hence, this particular circuit configuration is suitable for a diverse spectrum of power ratings [30]. The SHAPF can be categorised into two main types: the current source active filter (CSAF) and the voltage source active filter (VSAF). The selection of the filter type is contingent upon the choice of storage element employed in these filters. Specifically, capacitors are utilised in Voltage Source Active Power Filters, while inductors are employed in Current Source Active Power Filters.

In this project, VSAF was chosen over CSAF because it is lighter, less expensive, higher efficiency and easier to control [31].

4.3.2 Series active power filters

The utilisation of a series active power filter (SEAPF) can also serve the purpose of mitigating the adverse effects caused by higher harmonics present in the current IL. In this particular case, the monitoring of the load current (IL) is carried out, while the power circuit generates the voltage UF, thereby effectively mitigating the presence of higher harmonics in the current. The block diagram of the series active power filter is depicted in Figure 4.4 in appendix A.

It is more common to use a series filter as a solution for eliminating source voltage quality distortion. The device known as the dynamic voltage restorer (DVR) is commonly utilised to monitor and regulate the waveform of either the load voltage (UL) or the source voltage (US). The filter generates a voltage (UF) that aligns with the source voltage, leading to a sinusoidal voltage that delivers power to the load [30].

In an industrial context, parallel active filters are more prevalent compared to series active filters. The primary drawback of series circuits is their requirement to accommodate high load currents, resulting in a substantial increase in their current rating relative to parallel filters, Specifically, the focus of this study is on the secondary side of the coupling transformer. On the other hand, series filters offer several advantages when compared to parallel filters. Notably, they excel in the elimination of harmonics from voltage waveforms and the achievement of three-phase voltage balance. This implies that the utilisation of such a filter contributes to the enhancement of the voltage stability within the system, thereby resulting in advantageous effects for the connected load. The provision of a pure sinusoidal waveform to the load holds significance for voltage-sensitive equipment [29].

4.3.3 Hybrid active power filters

The implementation of a hybrid active power filter configuration allows for the resolution of technical limitations associated with conventional active power filters. Commonly, these systems are comprised of a blend of fundamental active power filters and passive power filters. Hybrid active power filters amalgamate the advantageous features of passive filters and APFs, thereby yielding improved operational effectiveness and a financially viable resolution. The main goal of this approach is to reduce the occurrence of both switching noise and electromagnetic interference. The present design integrates an economical passive high-pass filter (HPF) in conjunction with the conventional active power filter. Both filters have the common objective of filtering harmonics. The high-pass filter is responsible for attenuating higher order harmonics, whereas the active power filter is designed to nullify lower order harmonics. Hence, the primary objective of hybrid Active Power Filters is to enhance the filtering efficacy of high-order harmonics, while simultaneously providing cost-effective mitigation of low-order harmonics [34]. Figure 4.5 in appendix A illustrates the block diagram of the hybrid Active Power Filter (APF), comprising a shunt APF and a passive filter interconnected in a series configuration [31].
In the electronic industry nowadays, a variety of hybrid APFs are used, although Figure 4.6 in appendix A depicts the two most common ones.

The system configuration of the hybrid shunt Active Power Filter is illustrated in Figure 4.6(a) in appendix A. In the given scenario, a shunt active power filter and a passive

filter are interconnected in parallel with a nonlinear load. As a result, the function of the hybrid active power filter can be divided into two distinct elements: the shunt APF addresses low-order harmonics, and the passive high pass filter reduces high-frequency harmonics. The configuration of the hybrid series active power filter is illustrated in Figure 4.6(b) in appendix A. In the given context, the conversion transformer facilitates the interconnection between the series active power filter and the distribution line.

4.4 Harmonic currents extraction methods

The reference extraction technique chosen affects the APF's efficiency. Many techniques are employed for extracting the reference signal. There exist two fundamental methodologies, namely frequency domain and time domain, which are employed in various academic disciplines [32]. The utilisation of reference signal estimation is applicable to both single-phase and three-phase systems using the frequency domain technique. The origins of these concepts can be traced back to the fundamental principles of Fourier analysis. One of the main limitations associated with this approach is the inherent time delay that occurs during the sampling of system variables and the subsequent computation of Fourier coefficients. Therefore, it is not appropriate for real-time applications that experience dynamically fluctuating loads. Consequently, this approach is exclusively applicable to load conditions that undergo gradual changes. On the other hand, time-domain techniques are dependent on the instantaneous estimation of the reference signal by utilising voltage and current signals that are subject to distortion and contamination from homophonic noise. The outcome will exhibit increased speed due to the utilisation of the time domain method, which is characterised by its simplicity and reduced computational requirements compared to the frequency domain method [32].

4.4.1 Instantaneous PQ method

4.4.1.1 Introduction

The theory known as the instantaneous real and reactive power theory (PQ theory), commonly referred to as the instantaneous power theory, provides an explanation for the physical significance of the instantaneous real and imaginary power in a three-phase circuit. Additionally, it elucidates the manner in which energy is transmitted within a three-phase circuit, either between phases or from a source to a load. This approach

enables the design and comprehension of flexible AC transmission system (FACTS) compensators. Since p-q theory operates within the time domain, it is equipped with the ability to efficiently control the Active Power Filters in real-time. This includes the regulation of steady-state and transient conditions, as well as different voltage and current waveforms. The determination of the instantaneous power method (p-q theory) in a three-phase power system relies on the utilisation of the voltage and current waveforms' instantaneous values [33].

The p-q theory relies on instantaneous power, which is defined within the time domain, as previously elucidated. According to this theory, both three-phase systems with and without a neutral wire can be utilised. The first step in the theory entails transforming three-phase current and voltage measurements from a-b-c coordinates to Clarke or α-β-0 coordinates. Following that, the calculation of instantaneous power can be performed using the α-β-0 coordinates. The utilisation of the Clarke transformation is implemented, which encompasses the utilisation of a matrix that establishes a correlation between the components of a three-phase system and the α-β-0 stationary reference frames. The generation of the reference current is ultimately determined by the active and reactive power of the non-intuitive load [33].

4.4.1.2 Instantaneous active and reactive power (p-q) calculation

"Generalized Theory of the Instantaneous Reactive Power in Three-Phase Circuits," The Akagi-Nabae theory, which has been put forth, presents a novel approach to active filter control in three-phase power systems. The harmonic and fundamental components of nonlinear load power are separated using the (p-q) theory [34]. The following is an expression for three-phase systems without zero sequence:

$$\mathbf{va} + \mathbf{vb} + \boldsymbol{v}\mathbf{c} = \mathbf{0} \tag{4.1}$$

Based on the aforementioned equation, it can be demonstrated that the third voltage can be inferred from the remaining two voltages. This phenomenon is also applicable to the flow of electric currents.

The determination of the real and reactive power in a three-phase system can be achieved by utilising the voltages and currents of the three phases, employing the subsequent procedures: Firstly, the signals are transformed from the a-b-c coordinates to

a stationary reference coordinate system known as α-β-0. This transformation is achieved using the equations provided below and illustrated in Figure 4.7 in appendix A.

$$\begin{bmatrix} vo \\ v\alpha \\ v\beta \end{bmatrix} = \sqrt{2}/\sqrt{3} \begin{bmatrix} 1/\sqrt{2} & 1/\sqrt{2} & 1/\sqrt{2} \\ 1 & -1/2 & -1/2 \\ 0 & \sqrt{3}/2 & -\sqrt{3}/2 \end{bmatrix} \begin{bmatrix} va \\ vb \\ vc \end{bmatrix} \quad (4.2)$$

$$\begin{bmatrix} io \\ i\alpha \\ i\beta \end{bmatrix} = \sqrt{2}/\sqrt{3} \begin{bmatrix} 1/\sqrt{2} & 1/\sqrt{2} & 1/\sqrt{2} \\ 1 & -1/2 & -1/2 \\ 0 & \sqrt{3}/2 & -\sqrt{3}/2 \end{bmatrix} \begin{bmatrix} ia \\ ib \\ ic \end{bmatrix} \quad (4.3)$$

$$\begin{bmatrix} ia \\ ib \\ ic \end{bmatrix} = \sqrt{2}/\sqrt{3} \begin{bmatrix} 1/\sqrt{2} & 1 & 0 \\ 1/\sqrt{2} & -1/2 & \sqrt{3}/2 \\ 1/\sqrt{2} & -1/2 & -\sqrt{3}/2 \end{bmatrix} \begin{bmatrix} io \\ i\alpha \\ i\beta \end{bmatrix} \quad (4.4)$$

Secondly, the power can be then calculated according to the equations below:

$$\begin{bmatrix} po \\ p\alpha\beta \\ q\alpha\beta \end{bmatrix} = \begin{bmatrix} vo & 0 & 0 \\ 0 & v\alpha & v\beta \\ 0 & -v\beta & v\alpha \end{bmatrix} \begin{bmatrix} io \\ i\alpha \\ i\beta \end{bmatrix} \quad (4.5)$$

Where:

va, vb, vc are the phase voltages and ia, ib, ic are the phase currents.

po: the zero sequence power component.

$p\alpha\beta$: is the instantaneous P in stationary frame .

$q\alpha\beta$: is the instantaneous Q in stationary frame $\alpha\beta$.

Furthermore, equation (4.5) can be rewritten as follows to obtain the currents from the voltages and the powers:

$$\begin{bmatrix} io \\ i\alpha \\ i\beta \end{bmatrix} = 1/vov\alpha\beta^2 \begin{bmatrix} v\alpha\beta & 0 & 0 \\ 0 & vov\alpha & -vov\beta \\ 0 & vov\beta & vov\alpha \end{bmatrix} \begin{bmatrix} po \\ p\alpha\beta \\ q\alpha\beta \end{bmatrix} \quad (4.6)$$

Where:

$$v\alpha\beta^2 = v\alpha^2 + v\beta^2 \quad (4.7)$$

In the p-q theory, there are six main types of power as following [35]:

- $\overline{p0}$ = average value of instantaneous zero-sequence power
- $\widetilde{p0}$ = harmonic components of the instantaneous zero-sequence power.
- $\bar{p}$ = average value of the instantaneous real power
- $\tilde{p}$ = harmonic components of the instantaneous real power
- $\bar{q}$ = average value of instantaneous reactive power
- $\tilde{q}$= harmonic components of the instantaneous reactive power

Figure 4.8 in appendix A illustrates the flow of these component in the power system.

In the absence of a connected neutral wire, it can be observed that both the zero-component voltage and the zero-current components will assume null values. Considering the harmonics, the components $\tilde{p}$, and $\tilde{q}$ should be filtered out In order to mitigate the effects of harmonics, it is necessary to employ either a low pass or high pass filter. The depicted process can be observed in Figure 4.9 in appendix A.

If there is a desire to control the active filter in order to compensate for reactive power, in addition to harmonic compensations, it is necessary to modify the harmonic extraction scheme as illustrated in Figure 4.10 in appendix A.

4.4.2 Instantaneous synchronous frame method (d-q) method

This method involves the extraction of harmonics within the d-q synchronous frame. Initially, the currents undergo a transformation in the synchronous reference frame. The synchronous frame (dq) is aligned with the voltage. The utilisation of a phase-locked loop on the voltage components enables the acquisition of an angle, which is subsequently employed in the orientation, as demonstrated in equation 4.9.

$$\begin{bmatrix} id \\ iq \\ io \end{bmatrix} = \sqrt{\frac{3}{2}} \begin{bmatrix} cos\theta & \cos(\theta - \frac{2\pi}{3}) & \cos(\theta + \frac{2\pi}{3}) \\ -sin\theta & -sin\theta(\theta - \frac{2\pi}{3}) & -sin\theta(\theta + \frac{2\pi}{3}) \\ 1/\sqrt{2} & 1/\sqrt{2} & 1/\sqrt{2} \end{bmatrix} \begin{bmatrix} ia \\ ib \\ ic \end{bmatrix} \quad (4.8)$$

The variable θ denotes the angular position of the synchronous reference obtained by employing a phase-locked loop. The expressions for the d and q components of the current can be further represented as demonstrated below:

$$id=\widetilde{id}+\overline{id} \tag{4.9}$$

$$iq=\widetilde{iq}+\overline{iq} \tag{4.10}$$

Where:

$\widetilde{id}$ and $\widetilde{iq}$ are harmonics components and $\overline{id}$ *and* $\overline{iq}$ are average terms.

The above equations show a number of things, including the following:

- The average current, under sinusoidal and balanced condition, represents the first harmonic (fundamental) current.
- The oscillating terms corresponding to each higher harmonic.

According to that, if the active filter is wanted to compensate the harmonics only, the schematic depicted in Figure 4.11 in appendix A can be used.

4.5 Control of the shunt active power filter (SAPF)

In order to ensure the efficient execution of multiple tasks, including harmonic compensation, real and reactive power compensation, and load changes, it is crucial to implement proper control mechanisms for the SAPF. The regulation of the SAPF can be accomplished using one of two approaches, which are contingent upon the magnitude of the current being measured.

- Direct Control Method.
- Indirect Control Method.

4.5.1 Direct control method

The proposed method involves the utilisation of the SAPF to produce currents that rely solely on the load current, rather than the source currents. Consequently, any measurement or control inaccuracies may manifest as unfiltered harmonics in the grid current. Conversely, many sensors are employed, and the system will be steady [35]. The schematic of direct control method is depicted in Figure 4.12 in appendix A.

4.6 Design of shunt active power filter controller

The simulation employed the indirect control method based on synchronous reference (Id-Iq) theory. The load currents are initially measured and subsequently transformed into the dq synchronous frame. Subsequently, the load currents' dq components underwent filtering procedures, which were implemented in accordance with the active filter's purpose. These procedures aimed to extract the reference current, encompassing both harmonic compensation and power compensation. At the same time the inverter generated currents is transformed also to the same synchronous dq frame. Subsequently, PI controllers are employed to ensure that the currents of the inverter align with the previously determined reference currents [36]. The derivation of the active filter model can be obtained by utilising the equations provided below, as depicted in Figure 4.13 in appendix A.

According to the figure the voltage va,b,c are the voltages at the PCC and the voltages v a1,b1,c1 are the inverter output voltages. Using KVL the following equations hold true:

$$V_a = i_1 R + L\frac{di1}{dt} + V_{a1} \quad (4.11)$$

$$V_b = i_2 R + L\frac{di2}{dt} + V_{b1} \quad (4.12)$$

$$V_c = i_3 R + L\frac{di3}{dt} + V_{c1} \quad (4.13)$$

The above equation then can be transformed into the synchronous dq frame and the results shown below;

$$(Va_d - Va_{1d}) = R*i_d R + L*d_{id}/dt - \omega L\, i_q \quad (4.14)$$

$$(Va_d - Va_{1d}) = R*i_d + L*d_{id}/dt - \omega L\, i_q \quad (4.15)$$

$$(Va_q - Va_{1q}) = R*iq + L*d_{iq}/dt + \omega L\, i_q \quad (4.16)$$

The above equations can be rewritten by using the

$$L\, d_{id}/dt + i_d R = V_d$$

$$L\, d_{id}/dt + i_d R = V_q$$

Where:

$\mathbf{V_d = (Va_d - Va_{1d}) - \omega L\, i_q}$

$\mathbf{V_q = (Va_q - Va_{1q}) + \omega L\, i_d}$

Based on the above equations the controlled closed loop for the d and the q components will be as depicted in Figure 4.14 in appendix A [36].

The following is the transfer function of the PI controller:

$$\mathbf{G_{PI}(S) = K_1 + K_2/S} \qquad (4.17)$$

When comparing the transfer function of the controller with the canonical form of a second-order transfer function, the following values are assumed:

- The Damping factor ξ value is 0.707
- Resistor R equal 3.9 **Ω**
- Inductor L equal 3.89 $*10^{-3}$ H
- Band width 200 Hz.

According to that, the values for K1 and K2 will be as follows: K1 = 100 and K2 = 10,000, correspondingly.

The control methodology for SHAPF is depicted in Figure 4.15 and experimentally evaluated using MATLAB software.

Figure 4.15
Shunt active power filter controller by using MATLAB/SIMULINK

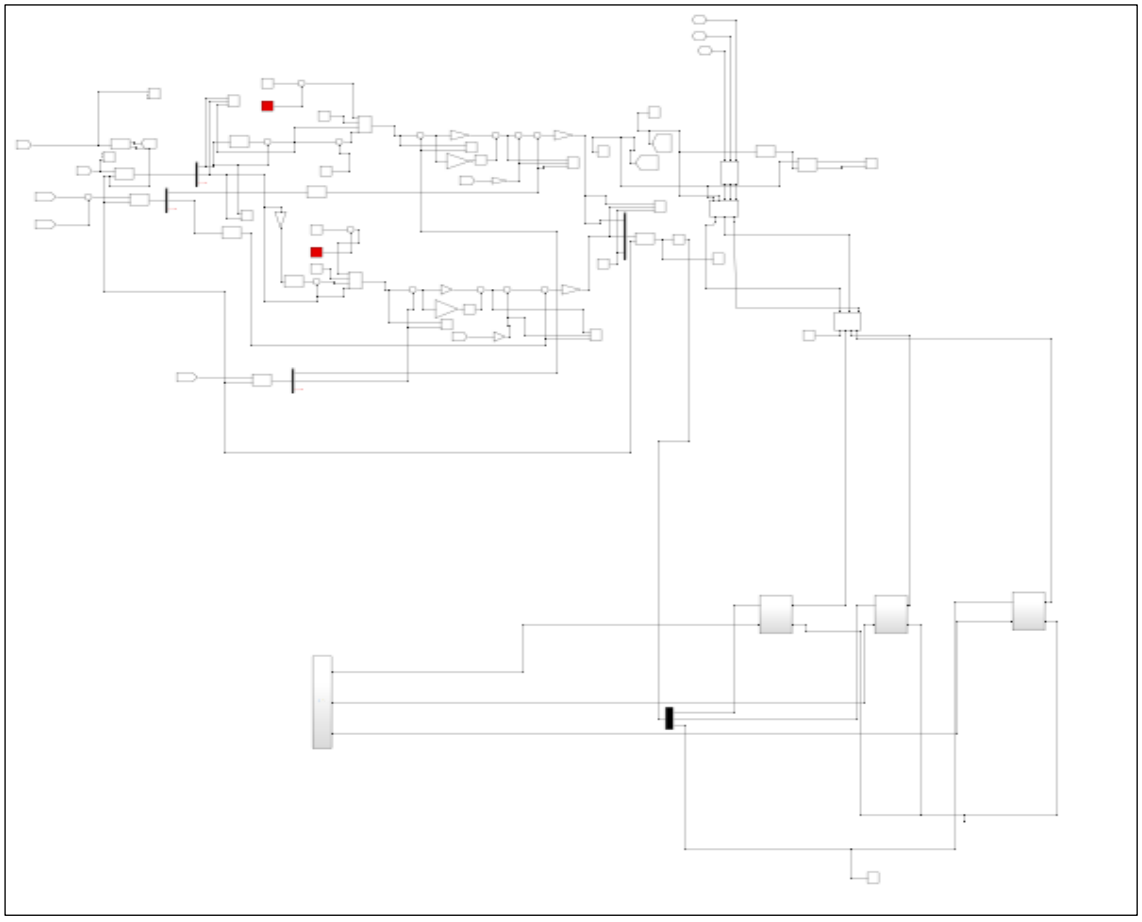

The inverter output behavior with its controller under different operation conditions is discussed in chapter 5 of this research.

Chapter 5

Compensation Scenarios and System Results

To complete the goals of this research, a wind renewable energy source has been employed by using an active filter, a multi-level inverter and their controllers as previously indicated, and to check the complete system's performance and the correct working, MATLAB SIMULINK is used to model the system and run simulations.

The system was analyzed under two separate working conditions: the first simply included a non-linear load, while the second studied the system's effect on the IEEE Network. The controllers have been designed to operate as per the following scenarios in each of these operational conditions:

1. 0-0.2s: The inverter was disabled and does not work, and the system remains the same (previous situation), so the output signal of the source current is irregular and has distortion.
2. 0.2-0.3s: The inverter has been turned on in a standby state, but the inverter current is zero.
3. 0.3-0.5s: The primary purpose of starting the inverter is to address the issue of harmonics. Specifically, the inverter is utilised to inject the necessary load harmonics of active and reactive power, thereby improving the power quality of the AC source.
4. 0.5-0.7s: The inverter commenced the injection of reactive power alongside its harmonic mitigation function. Consequently, the inverter persisted in injecting both harmonics and reactive power, thereby enhancing the power factor of the source.
5. 0.7 -1.0s: The practice of injecting harmonics and reactive power, alongside a targeted injection of active power, serves to enhance the power factor and network quality while reducing reliance on the power source.

5.1 System compensation scenarios effects on separate non-linear load (Parallel RLC load)

The first operating condition is study the effect of connecting the system with a separated non-linear load (Parallel RLC load). The objective of this study is to evaluate the capacity of the inverter to introduce reactive power, and real power, and mitigate

harmonics. The active power consumption of the non-linear load is measured at 8.0 kWp, while the reactive power consumption is recorded at 4 kVar. The reference signal of the controller is responsible for providing the voltage sources that are being controlled.

Figure 5.1 illustrates the complete system subsequent to its integration with a non-linear load and the subsequent application of a MATLAB/SIMULINK simulation.

Figure 5.1
A schematic for combined system simulation with non-linear load by using MATLAB/SIMULINK

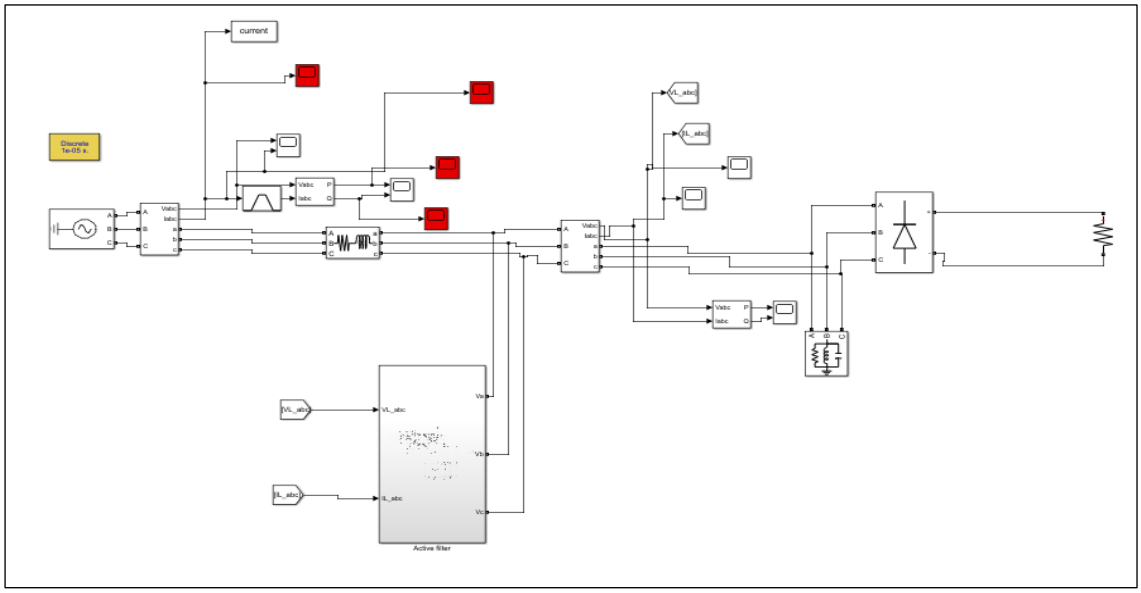

After implementing the previously mentioned five scenarios above, Figure 5.2, Figure 5.3 and Figure 5.4 presented in appendix A depict the active and reactive power characteristics of the source, inverter, and load under different operational scenarios.

From the above three figures, it was noticed that when the inverter starts working after (t>=0.3s), the source active power harmonic has been eliminated while it is compensated for the load through the inverter, meanwhile the source active power is reduced by around (2kWp-3kWp) during the last operation scenario (t>=0.7s), In addition to the enhancement of harmonics observed in the previous scenario, an additional quantity is introduced into the load via the inverter. The active power load remains constant during all operational activities.

Furthermore, the reactive power harmonic originating from the source has been effectively eliminated. This is achieved by compensating for the load through the

inverter, which initiates operation at a time greater than or equal to 0.3 seconds (t>=0.3s). As a result, during the operation scenarios involving reactive power injection (t>=0.5s), the reactive power from the source is almost negligible. This indicates that the inverter is solely responsible for producing the required reactive power for the load, leading to a power factor of 1 at the source. Meanwhile, the inverter's output reactive power is adjusted to meet the reactive power demand of the load. The load's reactive power remains constant during all operational activities.

The curves of the current behavior for the source and the inverter between all five scenarios described above are illustrated in the Figures from 5.5 to 5.12 in appendix A.

From the above Figures, it was noticed the following explanation in each of operation scenarios:

- During first and second scenarios: I_{Source} is not affected, and $I_{inverter}$ is zero as shown in Figures 5.5, 5.9 in appendix A.
- During third scenario: The harmonics of the I_{Source} are eliminated, and $I_{inverter}$ has harmonics instead of the source, accordingly, as shown in Figures 5.6 and 5.10 in appendix A, It is evident that as the total harmonic distortion diminishes, the source current approaches a state of near-pure sinusoidal waveform. Consequently, the presence of harmonics in the source current will decrease due to the inverter's ability to effectively cancel them out.
- During fourth scenario: The magnitude of the $I_{inverter}$ is increased, and I_{Source} is decreased slightly due to the injection of reactive power, in addition to the harmonic elimination process in the previous point as shown in Figures 5.7,5.11 in appendix A.
- During fifth scenario: The magnitude of the $I_{inverter}$ is increased, and I_{Source} is reduced, due to the injection of the high active power in addition to the previous point as shown in Figure 5.8, 5.12 in appendix A. The decrease in source current that has been observed indicates that the inverter is presently generating a fraction of the real power consumed by the load.

The results of the Fast Fourier Transform FFT analysis for the source current and inverter current for each of the above-mentioned operation scenarios are presented in

the Table 5.1 below as a fundamental value (50Hz) and total harmonic distortion (THD).

According to IEEE standard, THD is defined as the ratio of the square root of the sum of all harmonic components except fundamental to the fundamental component. The proportion of distortion from its fundamental wave form is expressed as THD.

Both voltage and current harmonics are assessed using THD, which can be calculated according to these two formulas:

$$\textbf{THD v (\%)} = \frac{\sqrt{(V2)^2+(V3)^2+(V4)^2+(V5)^2+(V6)^2+(V7)^2}*100}{V1} \quad (5.1)$$

where V2, V3, V4 are harmonic voltage and V1 is Fundamental Voltage.

$$\textbf{THD i (\%)} = \frac{\sqrt{(I2)^2+(I3)^2+(I4)^2+(I5)^2+(I6)^2+(I7)^2}*100}{I1} \quad (5.2)$$

where I2, I3, I4 are harmonic current and I1 is Fundamental Current.

Table 5.1
Total harmonics distortion of Source and inverter output currents

Scenario	Source output current		Inverter output current	
	Fundamental (50Hz)	THD (%)	Fundamental (50Hz)	THD (%)
First and Second scenarios (0-0.3s)	18.01	21.02%	0.0002937	6.74%
Third scenario (0.3-0.5s)	18.63	8.90%	0.578	756.93%
Fourth scenario (0.5-0.7s)	17.93	6.69%	2.75	152.44%
Fifth scenario (0.7-1s)	13.12	24.35%	5.792	90.97%

Figures from 5.13 to 5.20 in appendix A presented below depict the results of the FFT analysis conducted on the source current and inverter current, respectively, throughout the operational scenarios.

The results in the Figures from 5.21 to 5.25 in appendix A shows the source voltage and inverter voltage respectively during the operation scenarios.

Figures 5.22, 5.23, 5.24 and 5.25 in appendix A displays initial measurements showing a total harmonic distortion of the inverter voltage signal of 3.53% before inverter operation began. After the inverter started injecting reactive power and actual power to

reduce harmonics, the THD steadily increased until it reached 37.55%. The inverter voltage also rises progressively from a low of roughly 312 v to a maximum of 615 v.

To check the PI controllers performance, Id measured and Id reference are compared. Moreover, Iq measured and Iq reference as in the Figures 5.26, 5.27 in appendix A.

From the above two Figures 5.26 and 5.27 in appendix A, it was observed that the measured current signals are more accurate and similar to the reference current signals.

5.2 System compensation scenarios effects on IEEE network

The second operating condition is study the effect of connecting the system with IEEE fifteen buses radial network operating at 400 V.

According to the voltage distortion limits in IEEE standard, the THD should not exceed 8% when the bus voltage V at the PCC is less or equal 1 kV ($V \leq 1.0$ kV). The standard acknowledges that the utility has a duty to supply consumers with a voltage that is almost sine wave.

There are two tests of this operation condition:

- **First Test**: This test utilized an IEEE 15 bus network with a 400 V nominal voltage, as illustrated in Figure 5.28, with a non-linear load on Bus no 5. In this particular scenario, the SAPF is strategically connected in close proximity to the power source, specifically on Bus no 1, while being positioned at a considerable distance from the nonlinear load. The network as a whole is regarded as a unified load, with any harmonics present within the network being excluded from consideration. There are harmonic components injected as a current source to some buses.

Figure 5.28
The model of IEEE 15 Bus network, SAPF connected near the source at bus no 1. by using MATLAB/SIMULINK

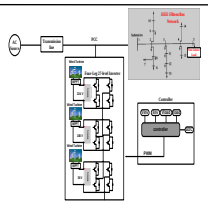

The source current and voltage waveforms on Bus No. 1 were measured after running the aforementioned five scenarios, and the THD was then calculated. Figures 5.29, 5.30, 5.31, 5.32 and 5.33 in appendix A demonstrate the source current and voltage respectively during different operational situations. Figures 5.34, 5.35, 5.36 and 5.37 in appendix A displays initial measurements showing a THD of the source output current during different operational situations.

Analysis of the waveform of the source current and the use of the FFT in this experiment show that the reduction in the source current's harmonic components is insignificant. THD values determined for the source current also supported these conclusions.

The examination of the impact of the system on the entire network during this experiment, measurements were taken of the waveforms of currents and voltages, and the THD was subsequently calculated at various randomly selected buses. The bus routes numbered 7, 9, 11, and 15 were selected.

Current and voltage waveforms for the selected buses and their respective operational circumstances are shown in Figure 5.38 and Figure 5.39 in appendix A, respectively.

The results of FFT analysis for buses current and buses voltage for each of the above-mentioned operation scenarios are presented in the two tables below as a total harmonic distortion percent (THD).

Table 5.2
Total harmonics distortion of the Buses output currents in the first test

Scenario	Bus 7 output current THD (%)	Bus 9 output current THD (%)	Bus 11 output current THD (%)	Bus 15 output current THD (%)
First and Second scenarios (0-0.3s)	6.29%	8.92%	8.58%	11.46%

Third scenario (0.3-0.5s)	2.74%	5.77%	5.55%	7.83%
Fourth scenario (0.5-0.7s)	4.78%	7.79%	6.24%	9.11%
Fifth scenario (0.7-1s)	4.92%	7.68%	6.66%	8.71%

Table 5.3
Total harmonics distortion of the Buses output voltage in the first test

Scenario	Bus 7 output voltage THD (%)	Bus 9 output voltage THD (%)	Bus 11 output voltage THD (%)	Bus 15 output voltage THD (%)
First and Second scenarios (0-0.3s)	7.01%	7.05%	9.04%	11.46%
Third scenario (0.3-0.5s)	3.05%	3.67%	5.86%	7.83%
Fourth scenario (0.5-0.7s)	5.27%	5.17%	6.56%	9.11%
Fifth scenario (0.7-1s)	5.43%	5.71%	7.01%	8.71%

Figures 5.38 and 5.39 in appendix A exhibit the current and voltage waveforms of buses 7, 9, 11, and 15. This study shows a little enhancement of these waveforms. This suggests that the current within the network continues to exhibit distortion. The total harmonic distortion within the network remains elevated, thereby giving rise to numerous complications in power quality within the network.

The preceding Tables 5.2 and 5.3 present the THD calculations pertaining to the buses in question. These calculations serve to validate the assertion that the SAPF situated at this particular location exhibits ineffectiveness and inefficiency in its capacity to mitigate THD within the network. This inadequacy can be attributed to the SAPF's placement at a considerable distance from the non-linear power load present on bus 5.

- **Second Test**: The identical IEEE 15 bus network featuring a nominal voltage of 400V was employed In the other test. The source was connected to Bus no 1, while a nonlinear load was introduced to Bus no 5. In this particular scenario, the SAPF is integrated within the network and positioned in proximity to the nonlinear load, specifically on Bus no 5. The goal of this configuration, as shown in Figure 5.40, is to examine how SAPF affects losses and harmonics of the remaining buses.

Figure 5.40

The model of IEEE 15 Bus network, SAPF connected near the nonlinear at bus no 5. by using MATLAB/SIMULINK

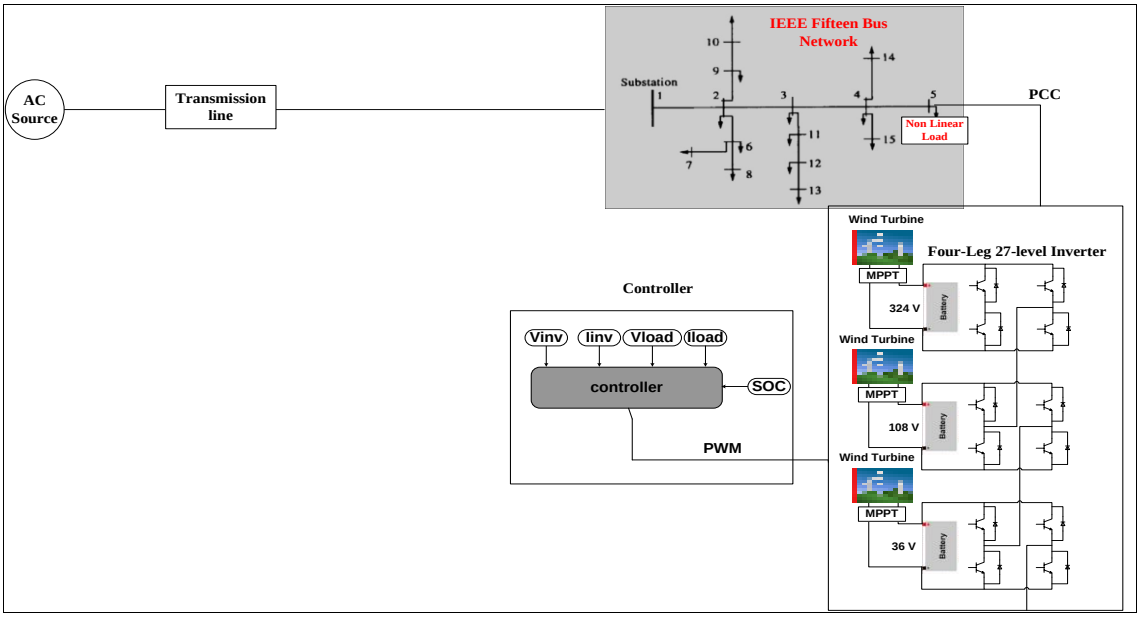

After conducting the aforementioned five scenarios, the waveforms of the source current and voltage at Bus No. 1 were recorded, and the Total Harmonic Distortion was calculated for each operational scenario. The findings are illustrated in Figure 5.41 to Figure 5.49 in appendix A, correspondingly.

The test yielded a substantial reduction in the harmonic content of the source current, as evidenced by the outcomes of the Fast Fourier Transform analysis and the observed waveforms of the source current. The computed THD values for the source current provided additional support for the results indicated above. The results pertaining to the source currently demonstrate superior performance when the SAPF is connected to bus 1.

In the examination of the impact of the system on the entire network during this experiment, measurements were taken of the waveforms of currents and voltages, and the THD was subsequently calculated at various randomly selected buses. The buses no 7,9,11, and 15 were chosen.

Figure 5.50 and Figure 5.51 in appendix A shows the results of the current and voltage waveforms for the chosen different buses during the operation scenarios.

The results of FFT analysis for buses current and buses voltage for each of the above-mentioned operation scenarios are presented in the table below as a total harmonic distortion percent (THD).

Table 5.4
Total harmonics distortion of the Buses output currents and voltages in the second test

Scenario	Bus 7 output current THD (%)	Bus 9 output current THD (%)	Bus 11 output current THD (%)	Bus 15 output current THD (%)
First and Second scenarios (0-0.3s)	6.29%	8.92%	8.58%	11.46%
Third scenario (0.3-0.5s)	1.54%	4.21%	2.47%	2.83%
Fourth scenario (0.5-0.7s)	1.6%	3.96%	2.44%	2.97%
Fifth scenario (0.7-1s)	1.51%	3.53%	2.43%	2.80%
Scenario	Bus 7 output voltage THD (%)	Bus 9 output voltage THD (%)	Bus 11 output voltage THD (%)	Bus 15 output voltage THD (%)
First and Second scenarios (0-0.3s)	7.01%	7.05%	9.04%	11.46%
Third scenario (0.3-0.5s)	1.70%	2.09%	2.60%	2.83%
Fourth scenario (0.5-0.7s)	1.77%	2.06%	2.58%	2.97%
Fifth scenario (0.7-1s)	1.67%	2.00%	2.56%	2.80%

Based on the analysis of the current and voltage waveforms observed at buses 7, 9, 11, and 15, as depicted in Figures 5.50 and 5.51 in appendix A, it is evident that a notable enhancement has been achieved in the aforementioned waveforms. This observation implies that the network exhibits a remarkably low level of harmonic distortion.

Tables 5.4 and 5.5 presented above depict the THD calculations pertaining to the respective buses. The findings validate the efficacy and efficiency of the SAPF deployed at this specific location. The SAPF successfully mitigates THD within the network, primarily owing to its close proximity to the nonlinear load situated on bus 5.

The following two charts 5.52 and 5.53 in appendix A present a comparative analysis of the impact of the first and second tests on the THD values of the current and voltage waveforms across various selected buses during the fourth scenario, specifically within the time interval of 0.5 to 0.7 seconds.

Chapter 6
Conclusion

The demand for renewable energy sources has experienced a substantial rise in order to address the growing energy requirements and mitigate the environmental impact associated with conventional energy sources. Consequently, there has been a growing demand for the utilisation of an H-Bridge multi-level inverter due to its capacity to efficiently harness power from multiple diverse energy sources, as elucidated in the preceding discussion in Chapter 3. As previously stated in Chapter 4, the utilisation of the shunt active power filter and its corresponding controller techniques enables the accomplishment of the following objectives:

- Mitigating the harmonics in the source current to improve the system power quality.
- Reducing the system loss power by injecting active power near to the load, which will reduce the source current.
- Improving the source power factor by compensating reactive power, which will improve the bus voltage value.

The integration of a wind turbine within a system, alongside a controller and a 27-level H-Bridge multi-level inverter with a shunt active power filter, serves as a means to harness renewable energy, employ modulation techniques, and manage the load. The system was evaluated by employing the MATLAB Simulink software to analyse the behaviour of a single non-linear load, followed by its application to an IEEE grid as a load. The controller has been specifically developed to address the harmonic mitigation and reactive power compensation functionalities of the power filter. To evaluate its performance, the MATLAB software was utilised for testing purposes.

The suggested Shunt Active Power Filter can be employed in situations where the load consists exclusively of a non-linear load, as well as in instances where the load constitutes an entire power system network. The installation of a power filter results in a decrease in the total harmonic distortion of the current source from 21.02% to 8.90% when a single nonlinear load is connected. Furthermore, the total harmonic distortion in both the current source and voltage source exhibits a reduction in order to conform to the prescribed standard level. Moreover, it is evident that the power factor experienced a

rise to approximately 1, indicating a substantial decrease in the reactive power produced by the source, approaching zero.

If the network being analysed is a power system network, it is recommended to locate the SAPF in close proximity to the load in order to improve the overall performance of the network.

List of Abbreviations

Abbreviations	Meaning
AC	Alternative Current
DC	Direct Current
IEEE	Institute of Electrical and Electronics Engineers
PF	Power factor
WECS	Wind Energy Conversion System
WTG	Wind Turbine Generator
HAWT	Horizontal Axis Wind Turbine
VAWT	Vertical Axis Wind Turbine
DFIG	Doubly Fed Induction Generator
PMSG	Cell output current.
IGBT	Insulated Gate Bipolar Transistor
MOSFET	Metal Oxide Semiconductor Field Effect Transistor
BJT	Bipolar Junction Transistor
GSC	Grid Side Converter
RSC	Rotor Side Converter
PWM	Pulse Width Modulation
THD	Total Harmonic Distortion.
CCM	Continuous Conduction Mode
DCM	Discontinuous Conduction Mode
rpm	revolutions per minute
VSI	Voltage Source Inverter
PCC	Point of Common Coupling
FFT	Fast Fourier Transform
PV	Photovoltaic
kWp	kilowatt peak
SAPF	Shunt Active Power Filter
Us	Source voltage
UL	Load voltage
UF	Filter voltage
Is	Source current
IL	Load current
IF	Filter current
HPF	High Pass Filter
CSAF	Current Source Active Filter
VSAF	Voltage Source Active Filter

References

[1] Thakur, Y., & Sakravdia, D. (2018). *Active Filters: A Reliability and Performance Analysis.* IEEE.

[2] U.S. Department of Energy. (n.d.). *Wind Energy Market Sectors.* Office of Energy Efficiency & Renewable Energy.

[3] El-Ahmar, M. H., El-Sayed, A. H., & Hemeida, A. H. (2017). Evaluation of factors affecting wind turbine output power. *Nineteenth International Middle East Power Systems Conference (MEPCON).* Cairo, Egypt.

[4] Johari, M., Khudri, M., & Shariff, M. (2018). Comparison of horizontal axis wind turbine (HAWT) and vertical axis wind turbine (VAWT). *International Journal of Engineering and Technology 7.4.13*.

[5] Whittlesey, R. (2017). *Vertical Axis Wind Turbines," in Wind Energy Engineering.* Elsevier.

[6] Sohoni, V., Gupta, S. C., & Nema, R. K. (2016). A Critical Review on Wind Turbine Power Curve Modelling Techniques and Their Applications in Wind Based Energy Systems. *Journal of Energy*.

[7] Veers, P., & et al. (2003). Trends in the design, manufacture and evaluation of wind turbine blades. *Wind Energy: An International Journal for Progress and Applications in Wind Power Conversion Technology 6.3*.

[8] Badran, O., Abdulhadi, E., & Mamlook, R. (2009). *Evaluation of parameters affecting wind turbine power generation.* 7th APCWE .

[9] Tong, W. (2010). *Wind power generation and wind turbine design.* WIT press.

[10] Buaossa, N., & et al. (2018). Practical design and performance evaluation of micro-wind turbine in Libya. *2018 9th international renewable energy congress (IREC).* IEEE.

[11] Cadirci, I., & Ermis, M. (2015). *Double-output induction generator operating at sub-synchronous and super-synchronous speeds: steady-state optimization and wind-energy recovery.* IEE Proc B Electric Power Applications.

[12] Molina, M., & Alvarez, J. (2011). *Technical and regulatory exigencies for grid connection of wind generation.* Wind Farm-Technical Regulations, Potential Estimation and Siting Assessment.

[13] Benelghali, S., Benbouzid, M., & Charpentier, J. (2012). Generator Systems for Marine Current Turbine Applications: A Comparative Study. *in IEEE Journal of Oceanic Engineering*.

[14] Yin, M., Gengyin, L., Zhou, M., & Zhao, C. (2007). *Modeling of the Wind Turbine with a Permanent Magnet Synchronous Generator for Integration.* IEEE PES.

[15] Majumder, D., Mehta, M., Mukherjee, S., & Mondal, S. (n.d.). *ELECTRICAL ENGINEERING.*

[16] KWIZERA, J. (2020). *DC converter design for a DC direct use. Case study solar powered irrigation system at Kabuga.* Rwanda. Diss: College of science and Technology.

[17] Krishna, A. R., & Suresh, L. P. (2016). A brief review on multilevel inverter topologies. *2016 International Conference on Circuit, Power and Computing Technologies (ICCPCT).* Nagercoil, India.

[18] Mittal, N., Singh, B., Singh, S. P., Dixit, R., & Kumar, D. (2012). Multilevel inverters: A literature survey on topologies and control strategies. *2012 2nd International Conference on Power, Control and Embedded Systems.* Allahabad, India.

[19] Divya, K., & Srinivasan, S. (2015). International Research Journal of Engineering and Technology (IRJET).

[20] Zheng, X., Song, L. A., & Hongying, P. (2012). Study of Five-level diodes-clamped Inverter Modulation Technology Based on Three-harmonic Injection Method. *2nd International Conference on Electronic & Mechanical Engineering and Information Technology.*

[21] Balachandran, S., & Hansdah, S. (2007). *Study and analysis of three phase multilevel inverter.* Diss.

[22] Singh, A., & Singh, R. (2018). *A Comparative Study of Multilevel Inverter Topologies. no. 03.*

[23] Krishna, R., & Suresh, L. (2013). A brief review on multilevel inverter topologies. *International Conference on Power, Energy and Control (ICPEC).*

[24] Moran, L., Dixon, J., Espinoza, J., & Wallace, R. (2019). *Using active power filters to improve power Quality.* IEEE Transactions.

[25] Miller, T., & Wiley, J. (1982). *Reactive Power Control in Electric Systems.* A Wiley Intercedence Publication.

[26] Gyugyi, L., & Strycula, E. (1976). *Active AC power filters.* IEEE Industrial Applications Society Annual Meeting.

[27] Patil, A., Katkar, R., & Vijay, C. (2017). Harmonic metigation using Passive Filter. *International Journal of Engineering Trends and Technology (IJETT).*

[28] Dekka, A., Beig, A., & Poshtan, M. (2011). *Comparison of Passive and Active Power Filters in Oil Drilling Rigs.* Abu Dhabi, UAE: The Petroleum Institute.

[29] Anju, J., & et al. (2014). A review of active power filters in power system applications. *International Journal of Advanced Research in Electrical, Electronics and Instrumentation Engineering 3.6.*

[30] Antchev, M. (2018). Classical and recent aspects of active power filters for power quality improvement. *Classical and Recent Aspects of Power System Optimization. Academic Press.*

[31] Routimo, M., Salo, M., & Tuusa, H. (2007). *Comparison of Voltage and Current Sources Active Power Filters.* IEEE.

[32] Candrsekaran, S., & Ragavan, K. (2013). *Reference current extraction through sliding DFT assisted single phase p-q theory for shunt active power filter.* IJEEPS.

[33] Afonso, L., Feritas, M., & Martins, S. (2003). *p-q Theory Power Components Calculations.* IEEE.

[34] Akagi, H. (1996). *New Trends in Active Filters for Power Conditioning.* IEEE.

[35] Noguchi, T., Tomiki, H., Kondo, S., & Takahashi, I. (2001). *Direct Power Control of PWM converter without power-source voltage sensors.* IEEE .

[36] Chelladurai, J., Saravana Ilango, G., Nagamani, C., & Senthil Kumar, S. (2008). Investigation of Various PWM Techniques for Shunt Active Filter. *International Journal of Electrical, Computer, Energetic, Electronic and Communication Engineering*.

Appendices

Appendix A

Figures

Figure 2.1
Horizontal Axis Wind Turbines (HAWT)

Note: Johari, M., Khudri, M., & Shariff, M. (2018). Comparison of horizontal axis wind turbine (HAWT) and vertical axis wind turbine (VAWT). International Journal of Engineering and Technology 7.4.13

Figure 2.2
Vertical axis wind turbines (VAWT)

[Stock Photos|Vertical Axis Wind Turbine]

Figure 2.3
Wind power curve

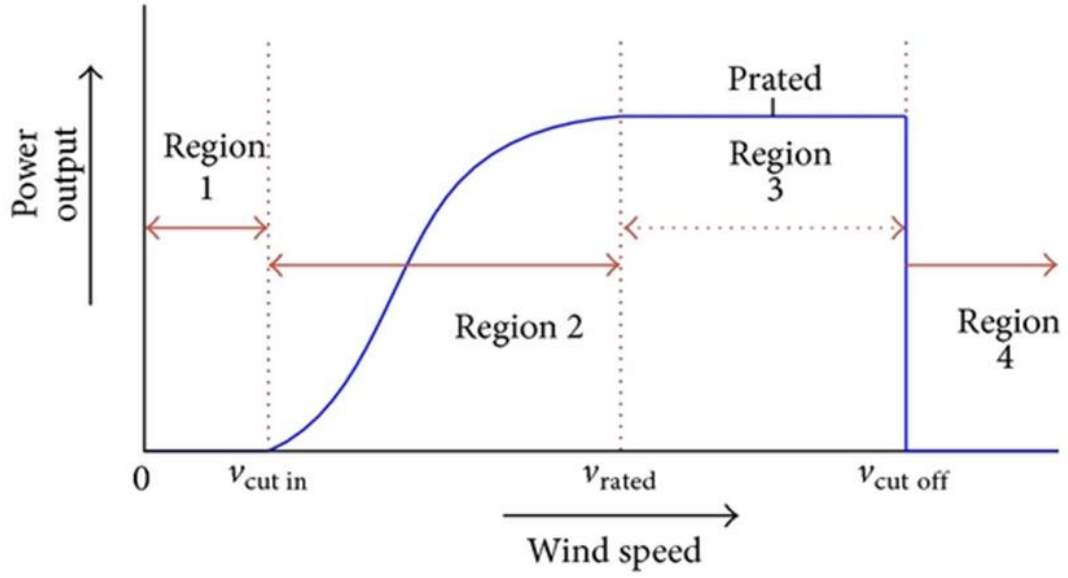

Note: Sohoni, V., Gupta, S. C., & Nema, R. K. (2016). A Critical Review on Wind Turbine Power Curve Modelling Techniques and Their Applications in Wind Based Energy Systems. Journal of Energy

Figure 2.4
Three stages of WECS

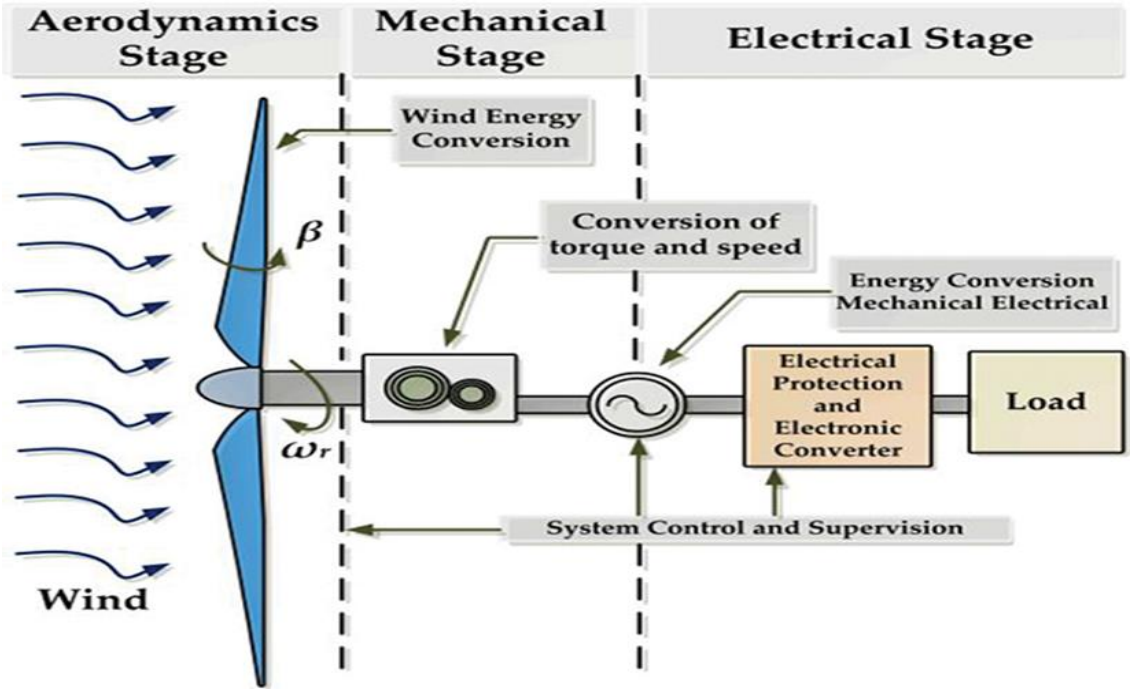

Note: Buaossa, N., & et al. (2018). Practical design and performance evaluation of micro-wind turbine in Libya. 2018 9th international renewable energy congress (IREC). IEEE

Figure 2.5
Schematic of a doubly-fed induction generator (DFIG)

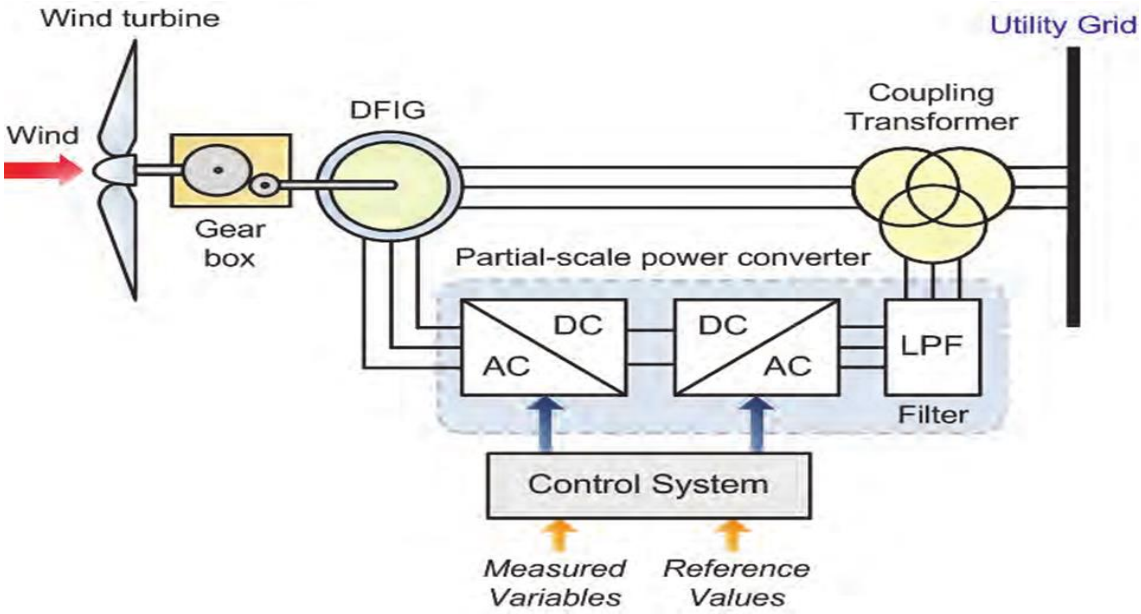

Note: Molina, M., & Alvarez, J. (2011). *Technical and regulatory exigencies for grid connection of wind generation.* Wind Farm-Technical Regulations, Potential Estimation and Siting Assessment

Figure 2.6
Schematic of permanent magnet synchronous generator (PMSG)

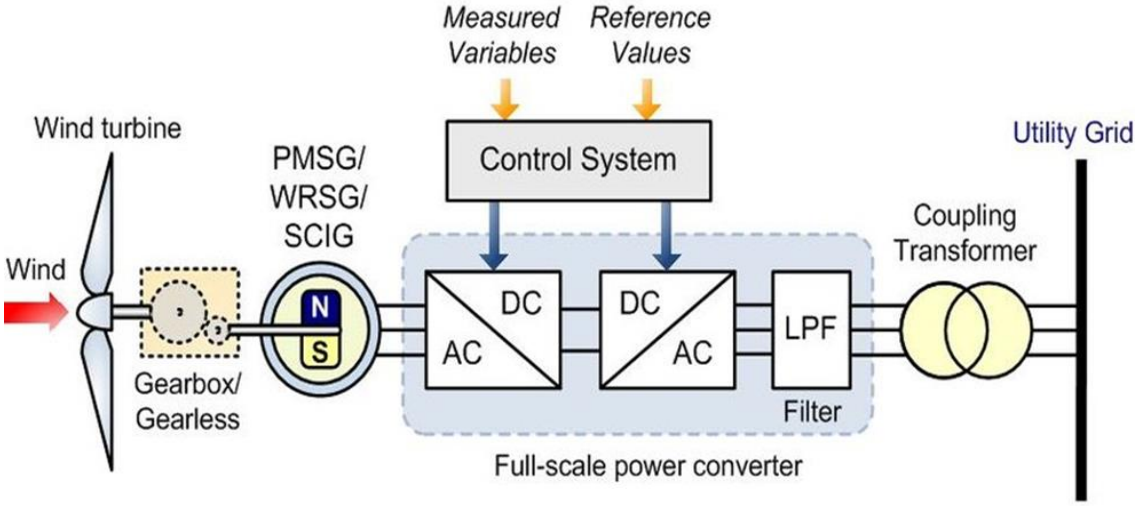

Note: Molina, M., & Alvarez, J. (2011). Technical and regulatory exigencies for grid connection of wind generation. Wind Farm-Technical Regulations, Potential Estimation and Siting Assessment

Figure 2.7
Buck converter circuit

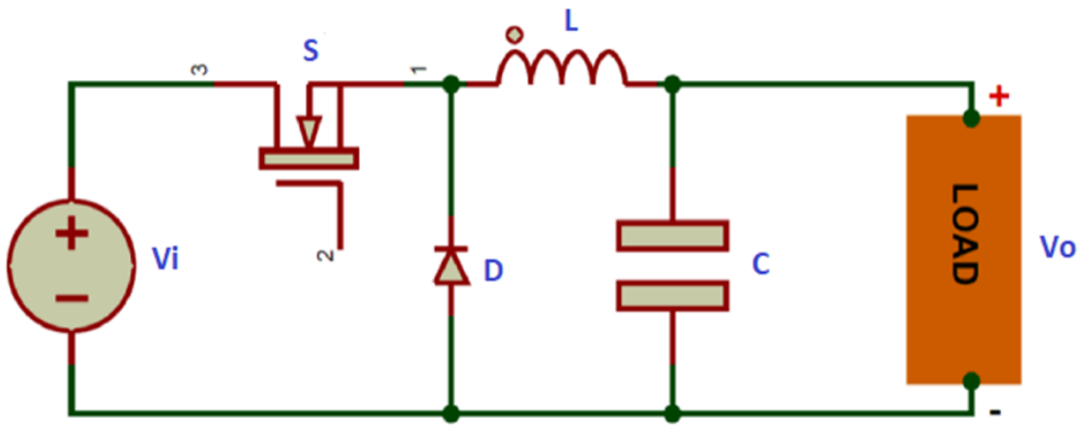

Note: Majumder, D., Mehta, M., Mukherjee, S., & Mondal, S. (n.d.). ELECTRICAL ENGINEERING.

Figure 2.8
Principle of DC buck converter operation during Ton period

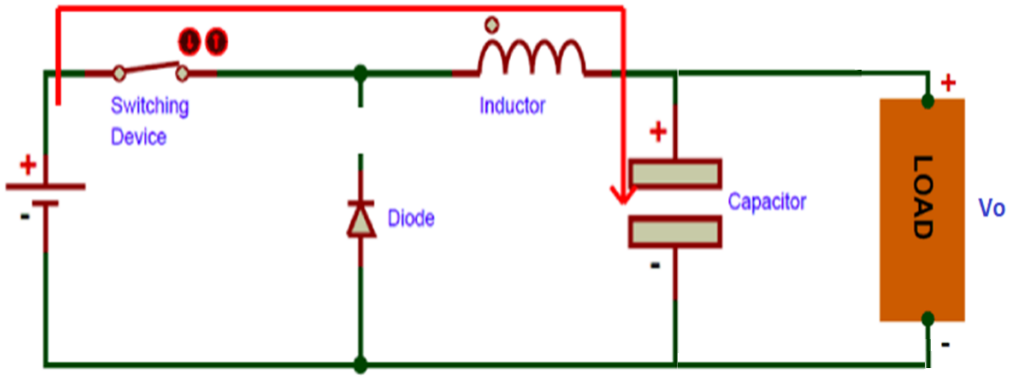

Note: Majumder, D., Mehta, M., Mukherjee, S., & Mondal, S. (n.d.). ELECTRICAL ENGINEERING

Figure 2.9
Principle of DC buck converter operation during Toff period

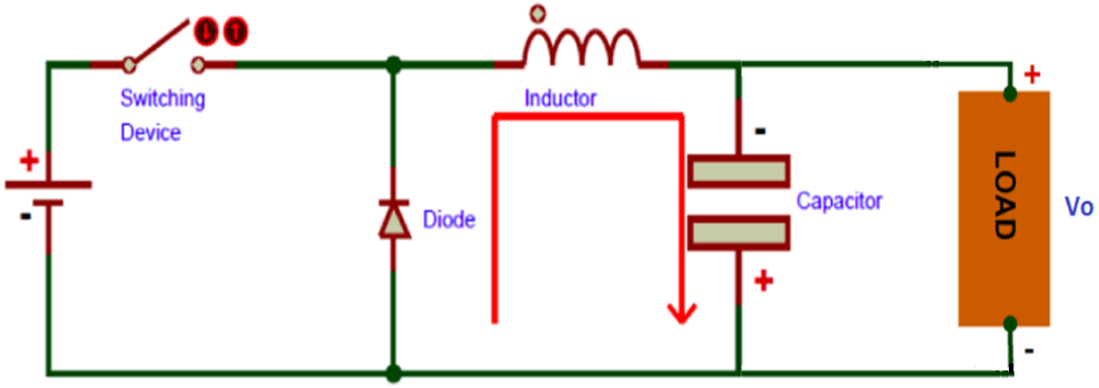

Note: Majumder, D., Mehta, M., Mukherjee, S., & Mondal, S. (n.d.). ELECTRICAL ENGINEERING

Figure 2.10
(a)CCM (b) DCM

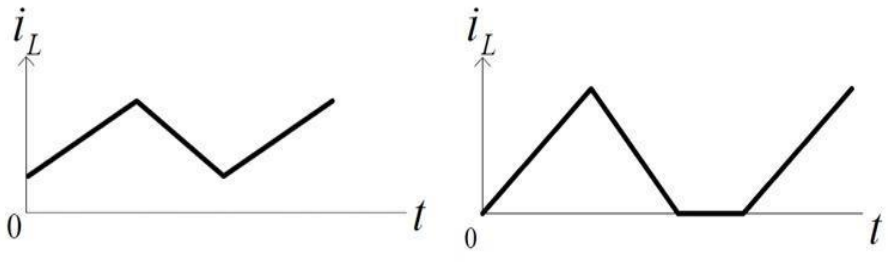

Note: Majumder, D., Mehta, M., Mukherjee, S., & Mondal, S. (n.d.). ELECTRICAL ENGINEERING

Figure 2.11
Waveforms of buck converter modes

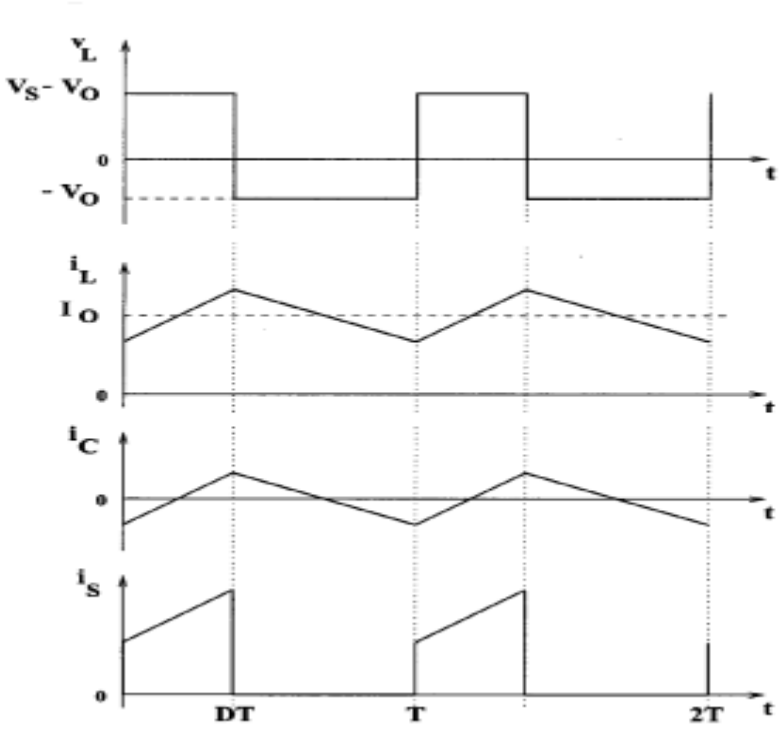

Note: KWIZERA, J. (2020). DC converter design for a DC direct use. Case study solar powered irrigation system at Kabuga. Rwanda. Diss: College of science and Technology

Figure 3.1

principle operation of a mulit-level inverter (A) two-level, (B) three-level, and (C) n-level

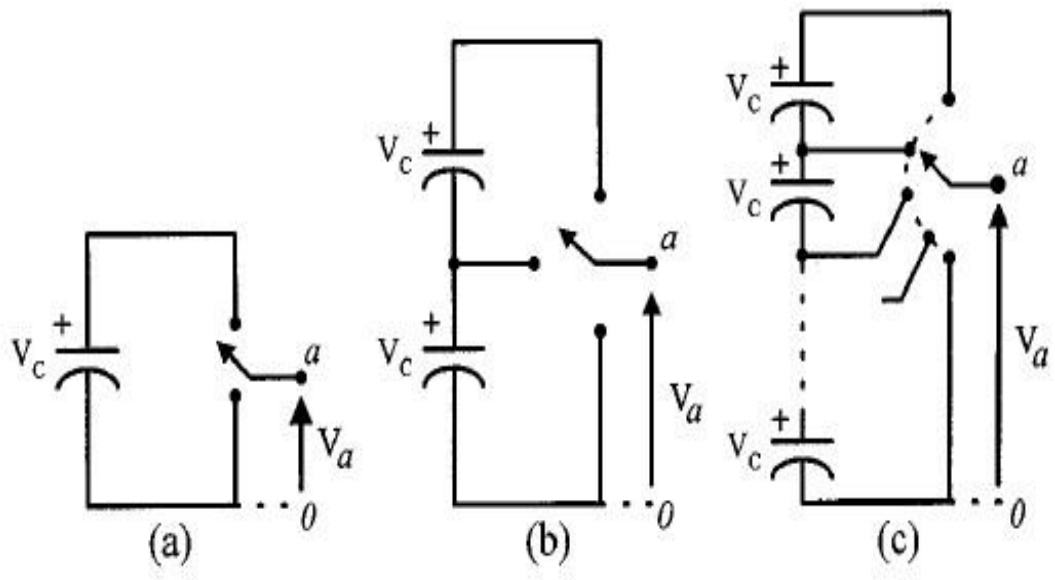

Note: Mittal, N., Singh, B., Singh, S. P., Dixit, R., & Kumar, D. (2012). Multilevel inverters: A literature survey on topologies and control strategies. 2012 2nd International Conference on Power, Control and Embedded Systems. Allahabad, India

Figure 3.2

Multilevel inverter topologies

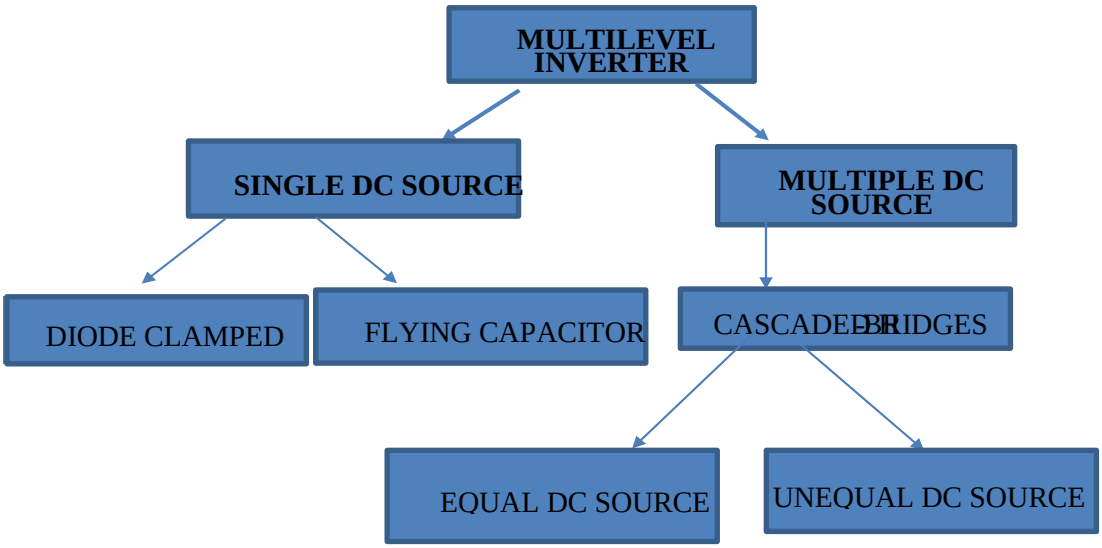

Note: Divya, K., & Srinivasan, S. (2015). International Research Journal of Engineering and Technology (IRJET)

Figure 3.3

Three level inverter using diode-clamped inverter topology

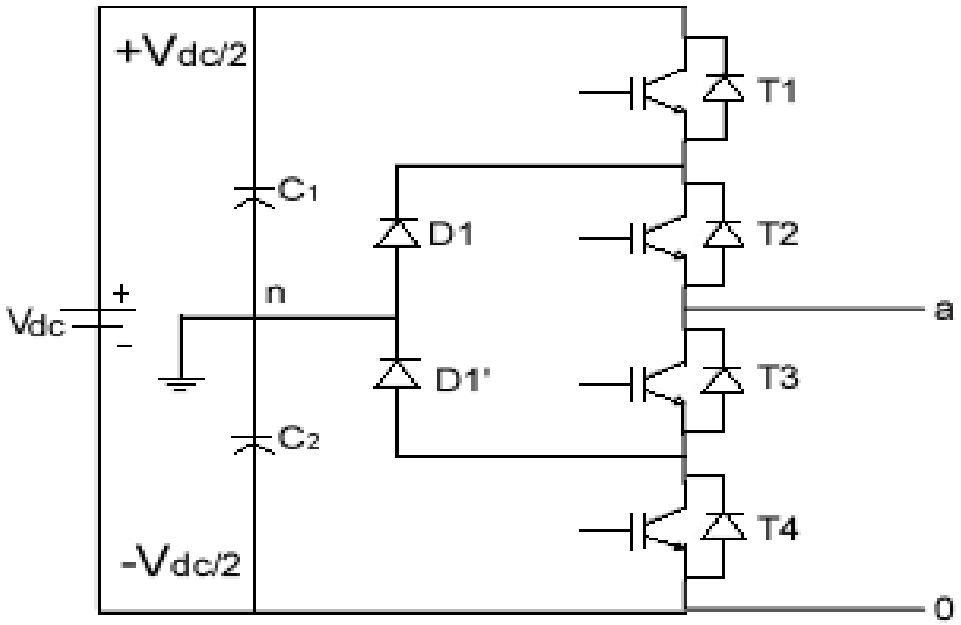

Note: Divya, K., & Srinivasan, S. (2015). International Research Journal of Engineering and Technology (IRJET)

Figure 3.4

Flying capacitor multilevel inverter circuit topology for 3- level inverter

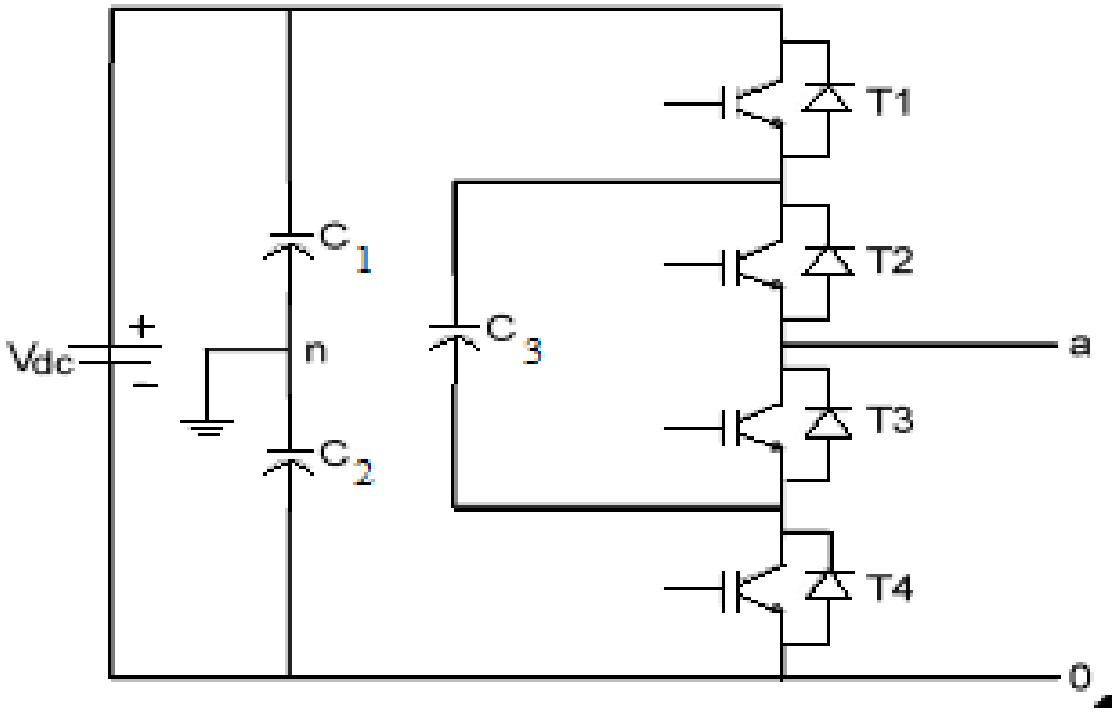

Note: Divya, K., & Srinivasan, S. (2015). International Research Journal of Engineering and Technology (IRJET)

Figure 3.5

Three-level Cascaded multilevel inverter topology (Y-configuration) (A) three-level, (B) five-level

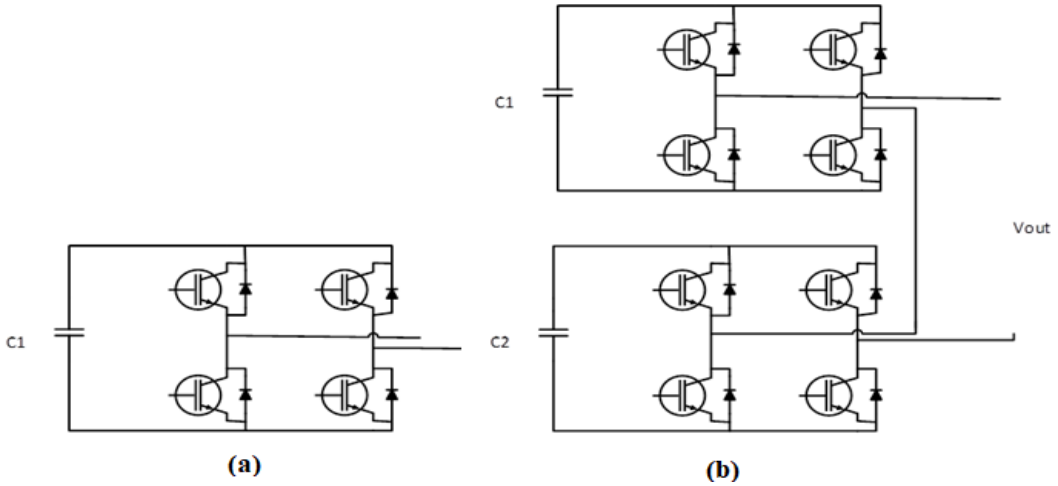

Note: Mittal, N., Singh, B., Singh, S. P., Dixit, R., & Kumar, D. (2012). Multilevel inverters: A literature survey on topologies and control strategies. 2012 2nd International Conference on Power, Control and Embedded Systems. Allahabad, India

Figure 3.6
27 level asymmetric cascaded h-bridge inverter

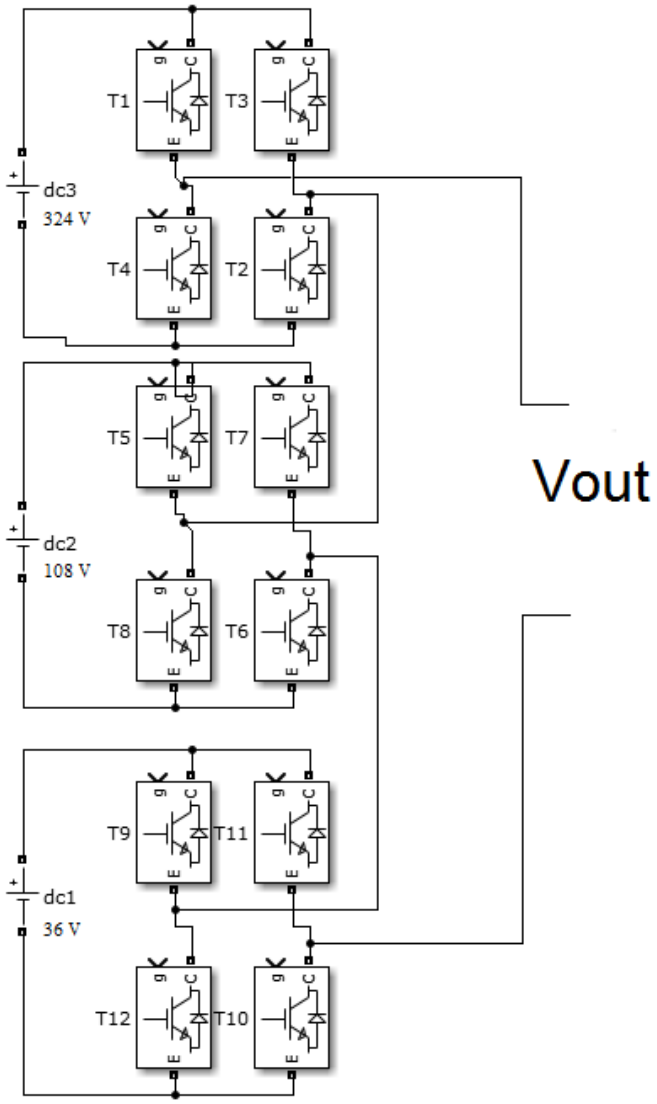

Figure 3.7
Flow chart of multi-level inverter controller

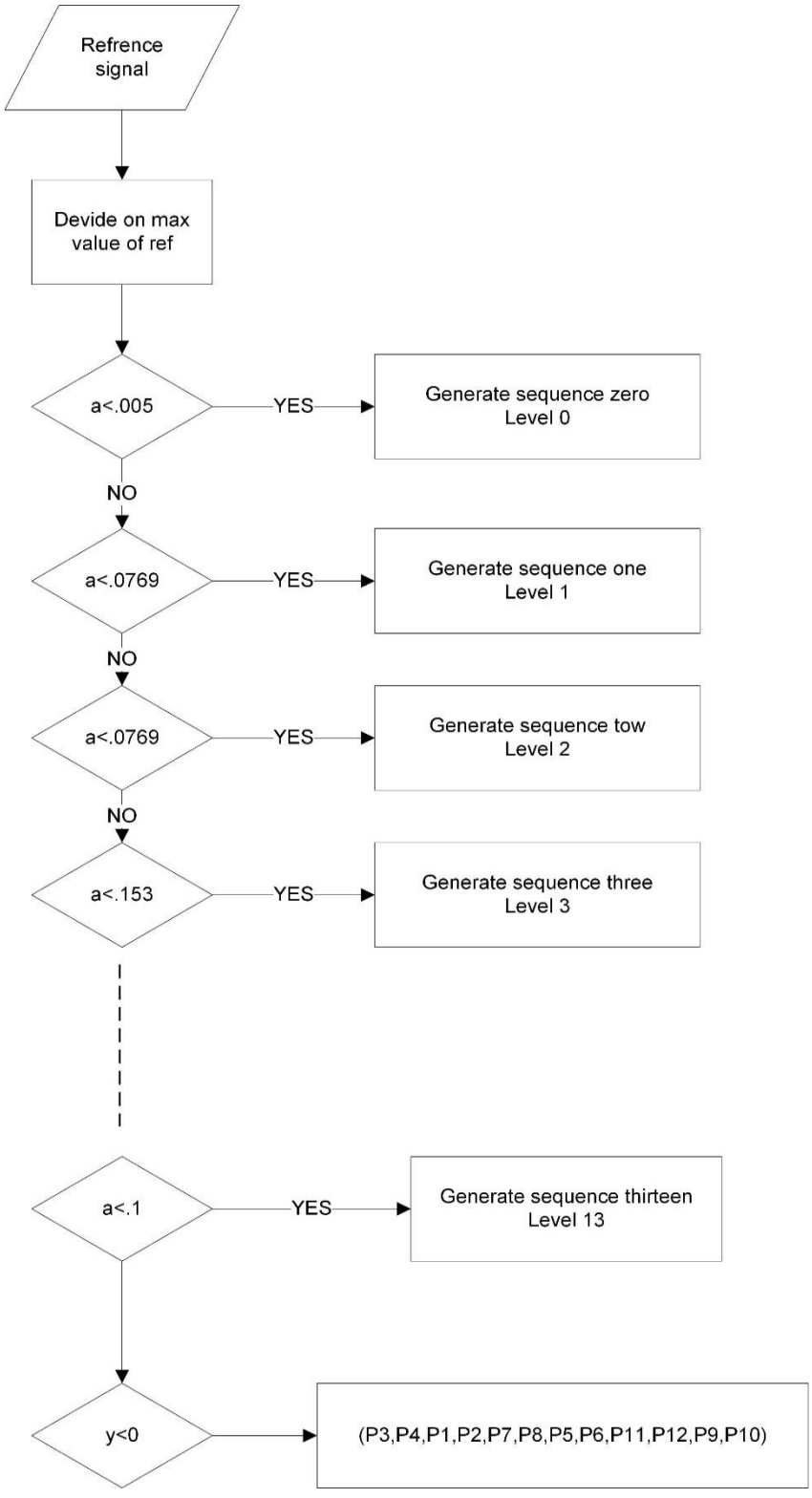

Figure 4.1
Passive filter

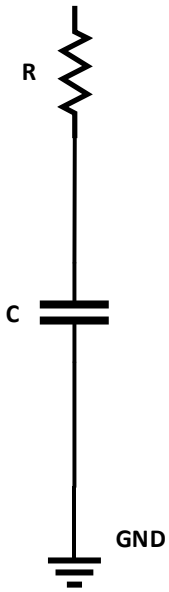

Note: Patil, A., Katkar, R., & Vijay, C. (2017). Harmonic metigation using Passive Filter. International Journal of Engineering Trends and Technology (IJETT)

Figure 4.2
Classifications of active power filter

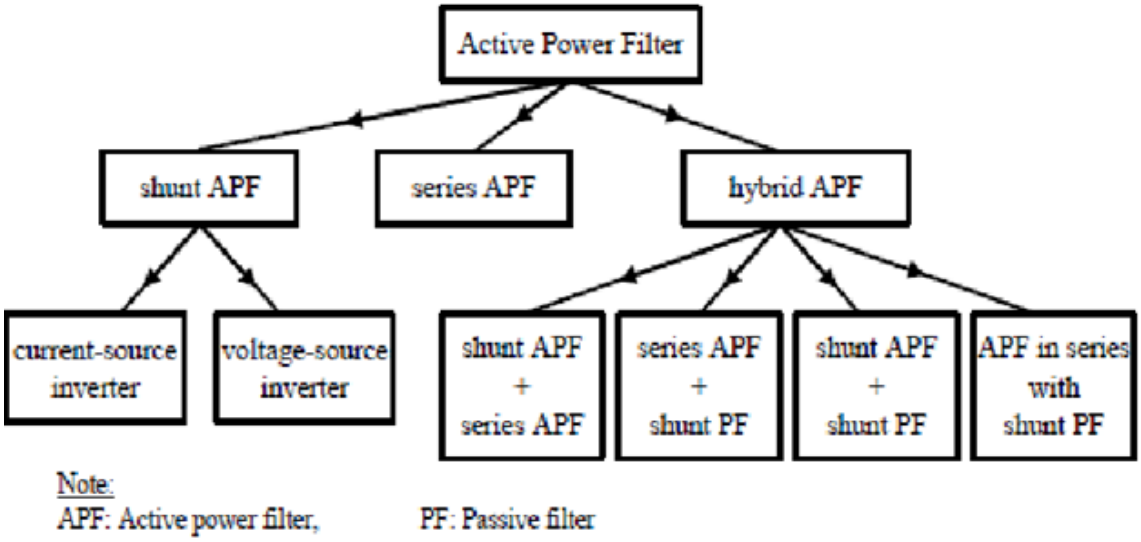

Note: Anju, J., & et al. (2014). A review of active power filters in power system applications. International Journal of Advanced Research in Electrical, Electronics and Instrumentation Engineering 3.6

Figure 4.3
Block diagram of the shunt active power filters

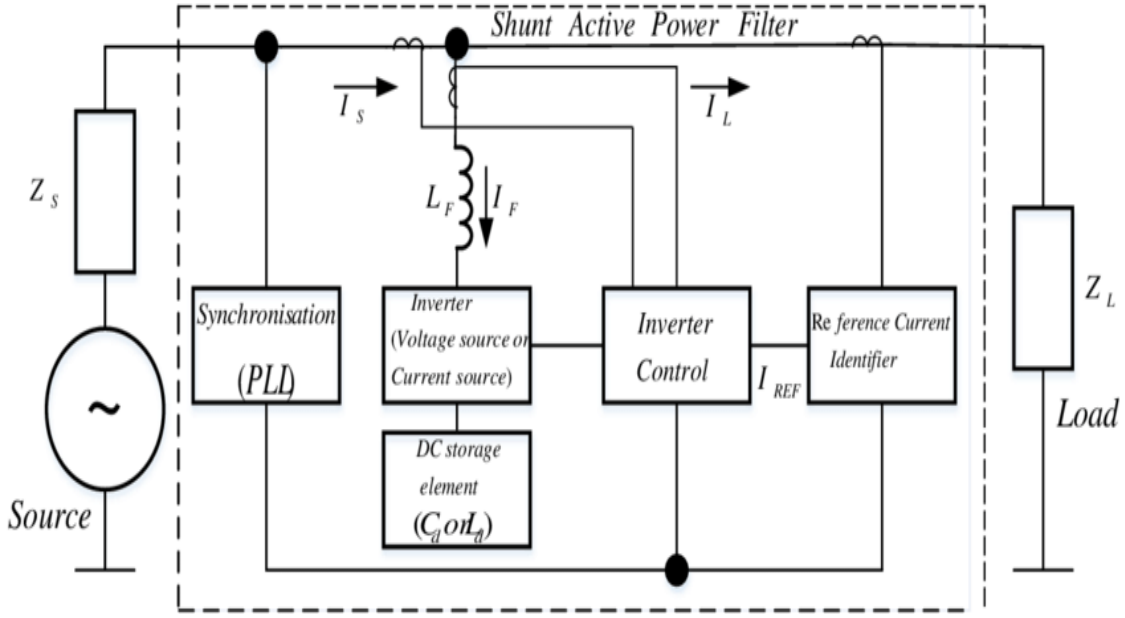

Note: Antchev, M. (2018). Classical and recent aspects of active power filters for power quality improvement. Classical and Recent Aspects of Power System Optimization. Academic Press

Figure 4.4
Block diagram of the series active power filters

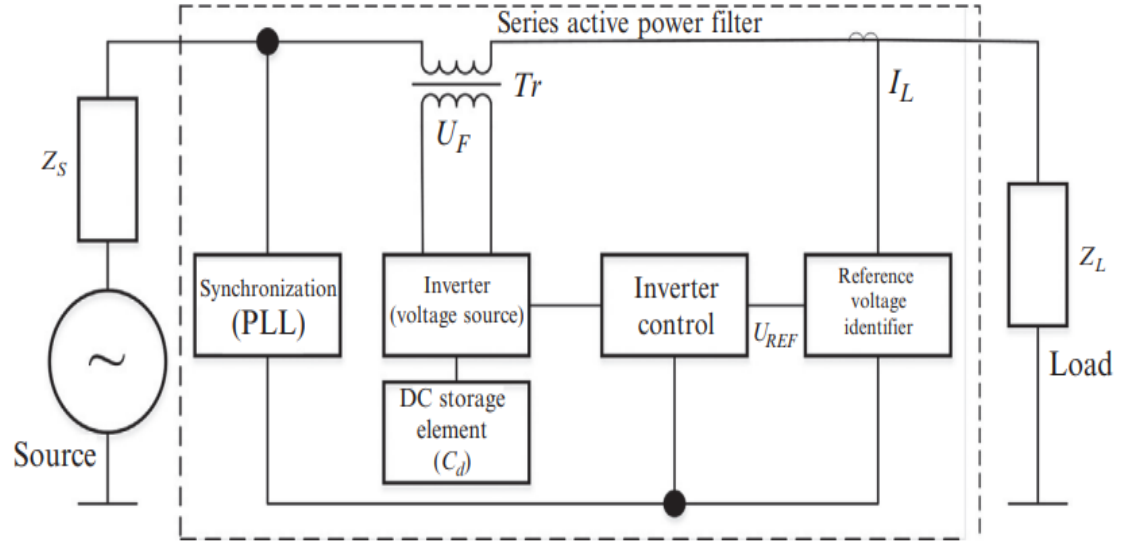

Note: Antchev, M. (2018). Classical and recent aspects of active power filters for power quality improvement. Classical and Recent Aspects of Power System Optimization. Academic Press

Figure 4.5

Block diagram of a hybrid active power filters (series connection of a shunt APF and passive filter)

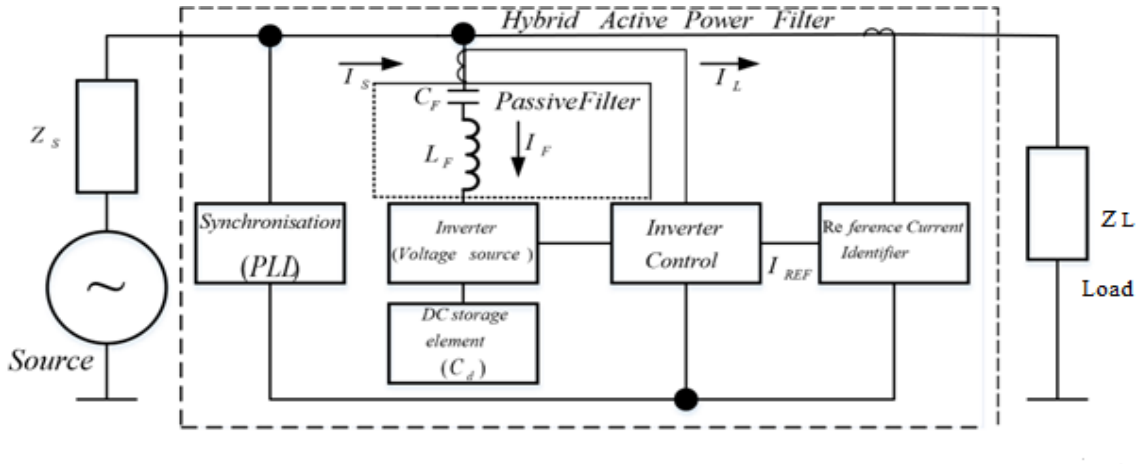

Note: Antchev, M. (2018). Classical and recent aspects of active power filters for power quality improvement. Classical and Recent Aspects of Power System Optimization. Academic Press

Figure 4.6

Hybrid APFs

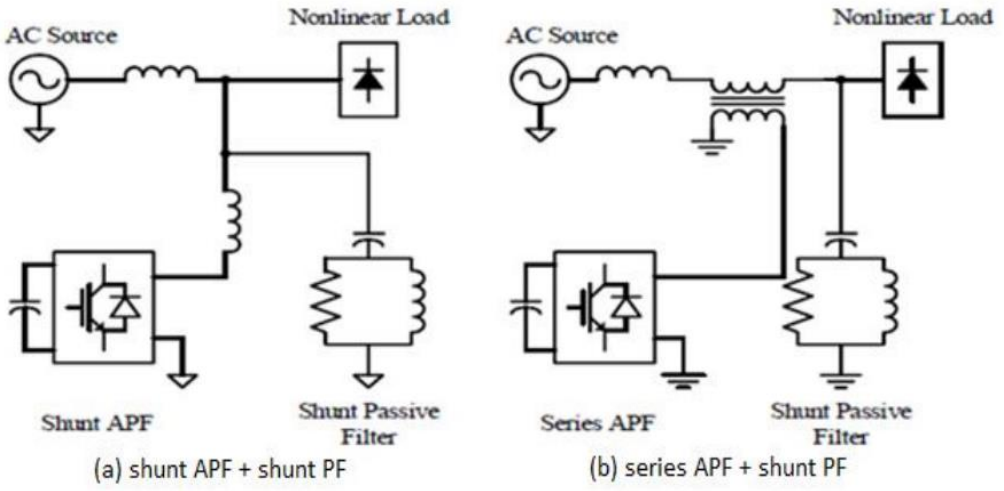

Note: Anju, J., & et al. (2014). A review of active power filters in power system applications. International Journal of Advanced Research in Electrical, Electronics and Instrumentation Engineering 3.6

Figure 4.7

Diagram of p-q theory principle (a-b-c to the 0-α-β system)

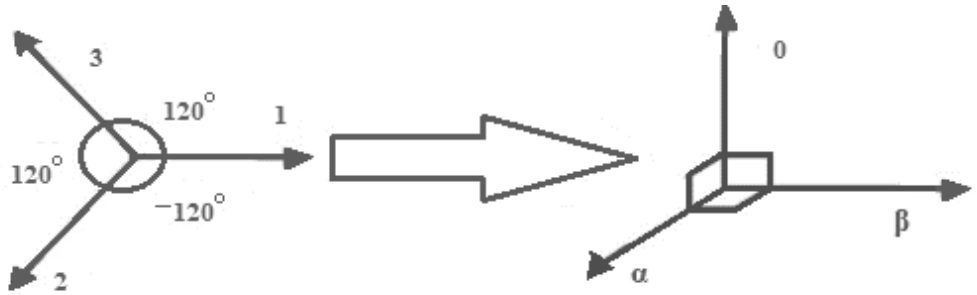

Figure 4.8

Power components of the p-q theory in a-b-c coordinate

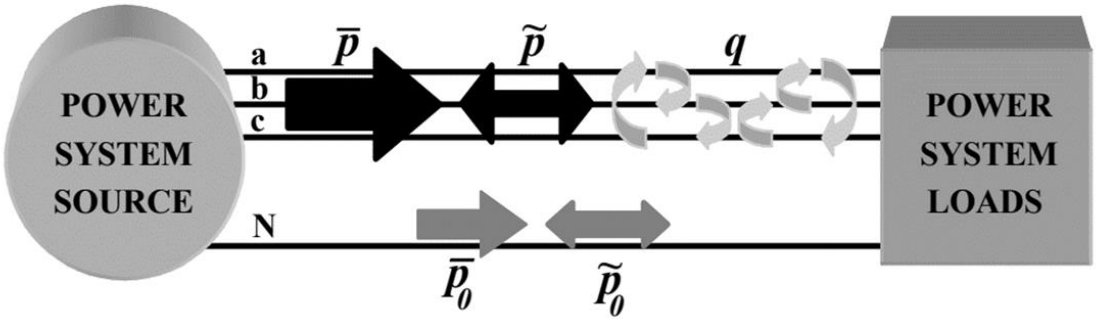

Note: Afonso, L., Feritas, M., & Martins, S. (2003). p-q Theory Power Components Calculations. IEEE

Figure 4.9

Schematic of the p-q theory to remove harmonics

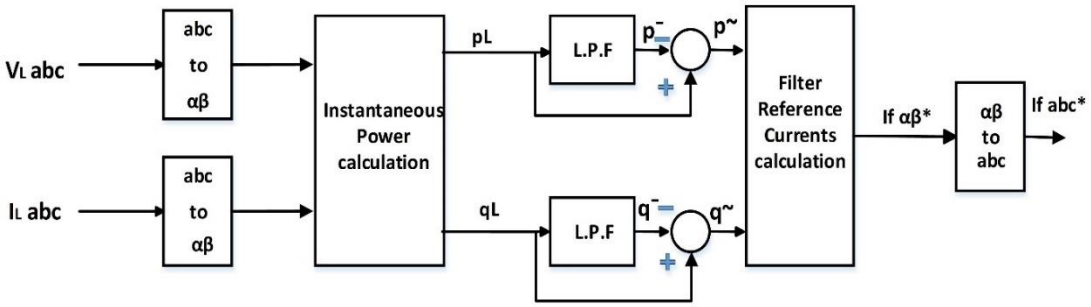

Note: Anju, J., & et al. (2014). A review of active power filters in power system applications. International Journal of Advanced Research in Electrical, Electronics and Instrumentation Engineering 3.6

Figure 4.10

Diagram of the p-q theory for removing harmonics and improving PF

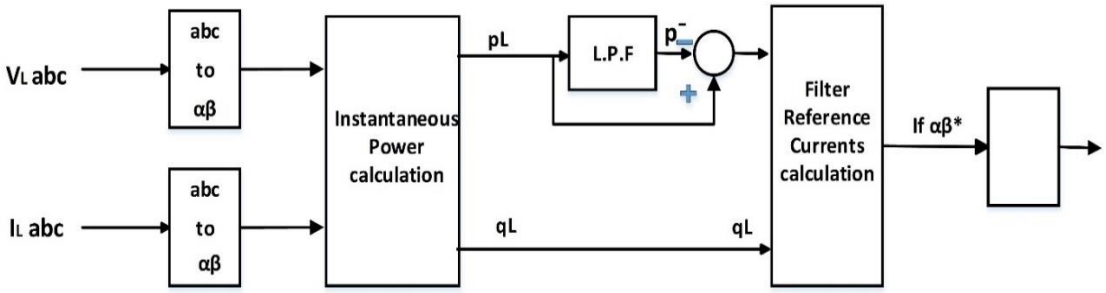

Note: Anju, J., & et al. (2014). A review of active power filters in power system applications. International Journal of Advanced Research in Electrical, Electronics and Instrumentation Engineering 3.6

Figure 4.11

Illustration of id-iq theory for reference current extraction

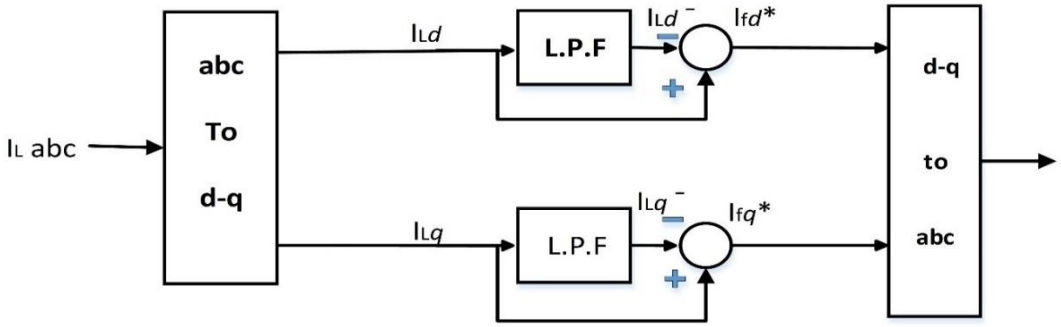

Note: Anju, J., & et al. (2014). A review of active power filters in power system applications. International Journal of Advanced Research in Electrical, Electronics and Instrumentation Engineering 3.6

Figure 4.12

Direct control using PI controllers in Synchronous Reference

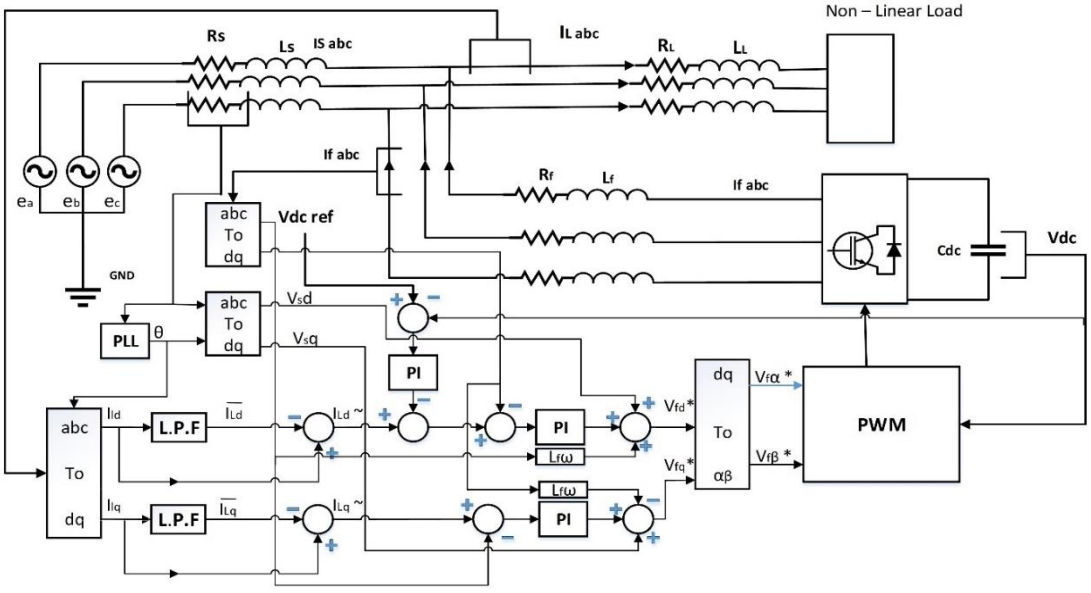

Note: Noguchi, T., Tomiki, H., Kondo, S., & Takahashi, I. (2001). Direct Power Control of PWM converter without power-source voltage sensors. IEEE

Figure 4.13

Schematic of SAF with switches and Dc source

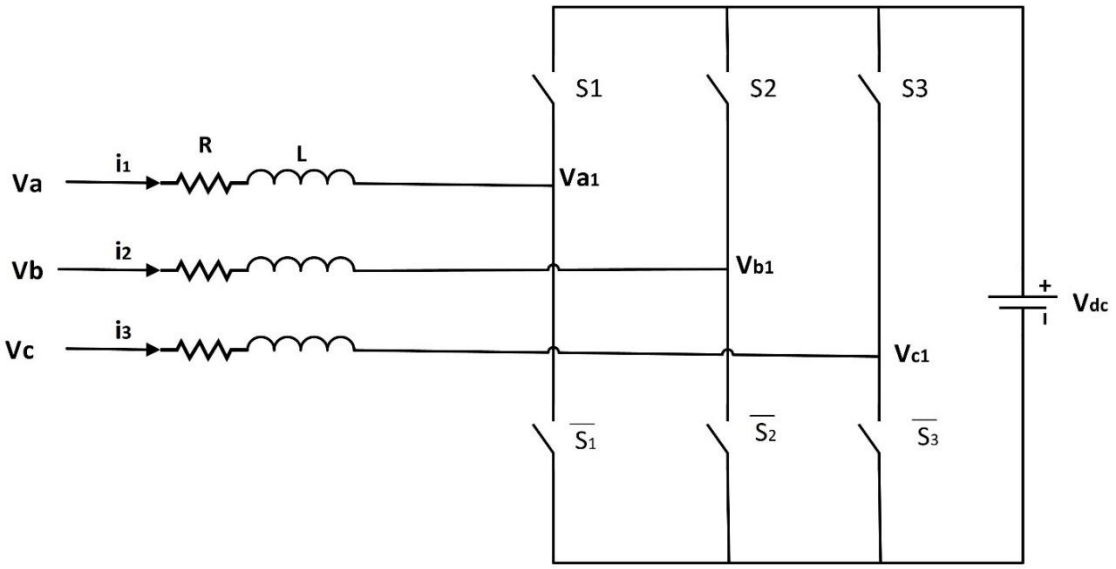

Note: Chelladurai, J., Saravana Ilango, G., Nagamani, C., & Senthil Kumar, S. (2008). Investigation of Various PWM Techniques for Shunt Active Filter. International Journal of Electrical, Computer, Energetic, Electronic and Communication Engineering

Figure 4.14

Diagram of Instantaneous current controller with PI control

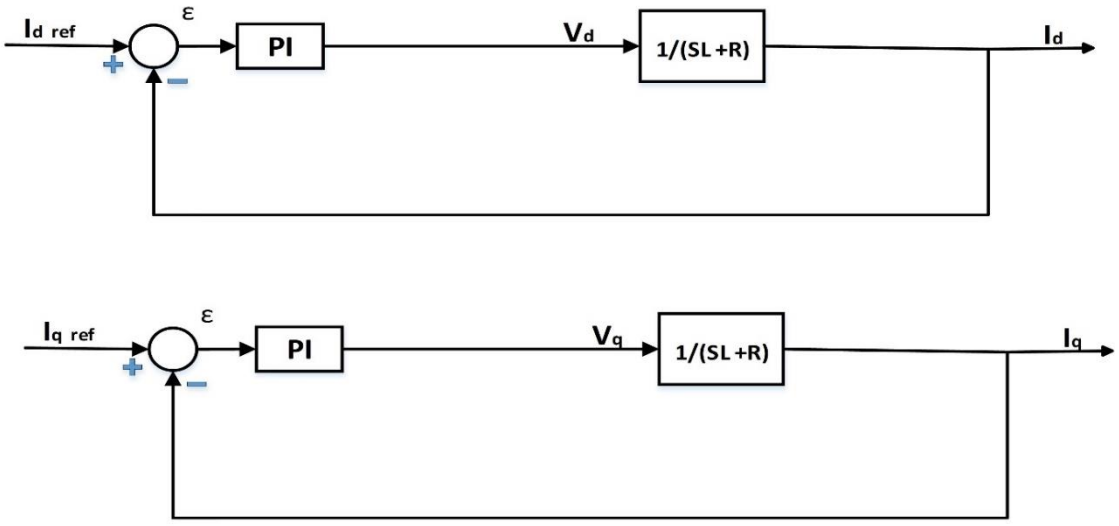

Note: Chelladurai, J., Saravana Ilango, G., Nagamani, C., & Senthil Kumar, S. (2008). Investigation of Various PWM Techniques for Shunt Active Filter. International Journal of Electrical, Computer, Energetic, Electronic and Communication Engineering

Figure 5.2
Results of source active and reactive power behavior under different operation scenarios

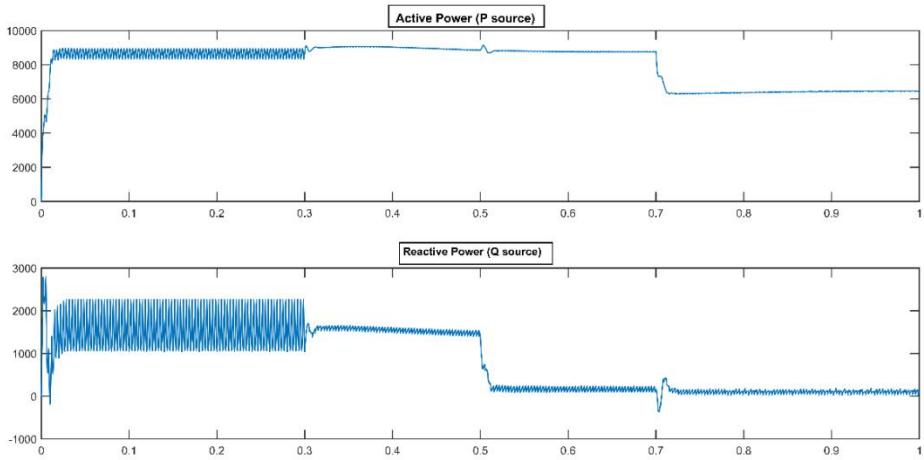

Figure 5.3
Results of inverter active and reactive power behavior under different operation scenarios

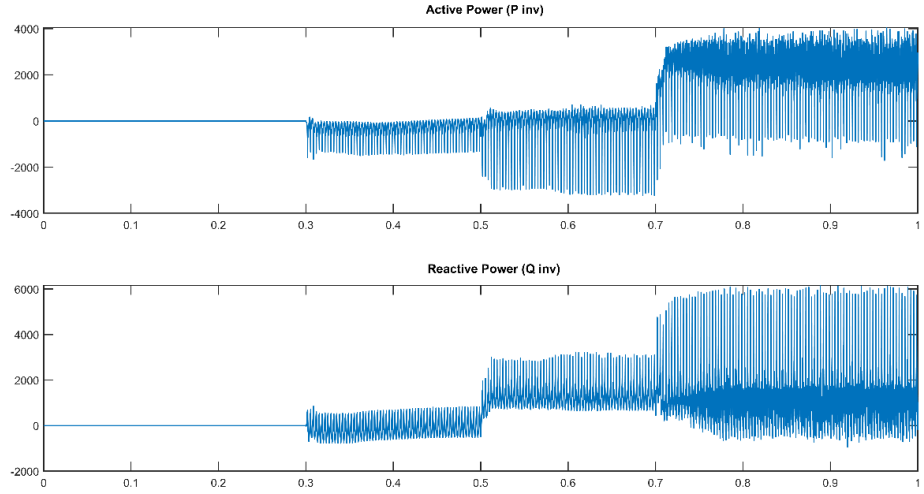

Figure 5.4
Results of load active and reactive power behavior under different operation scenarios

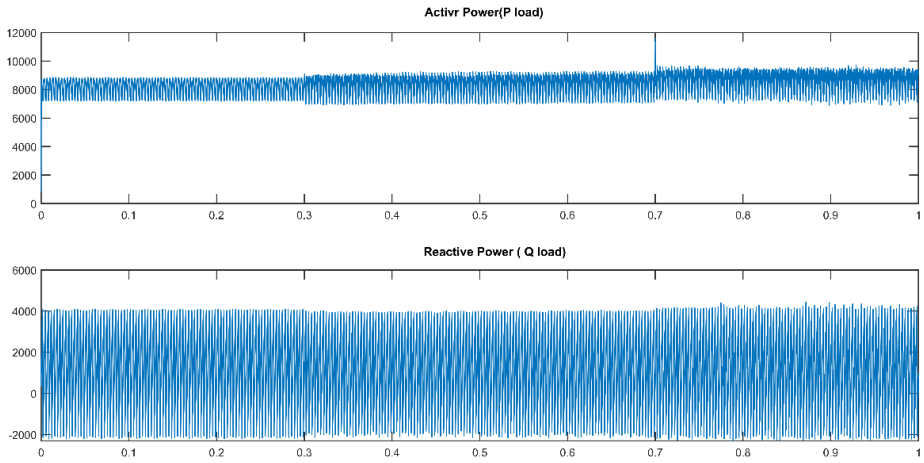

Figure 5.5
Result of source current behavior during first and second scenarios

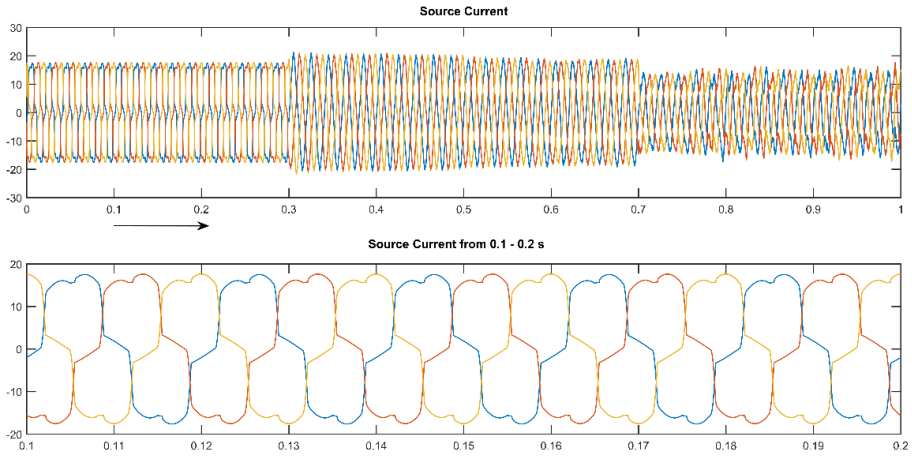

Figure 5.6
Result of source current behavior during third scenario

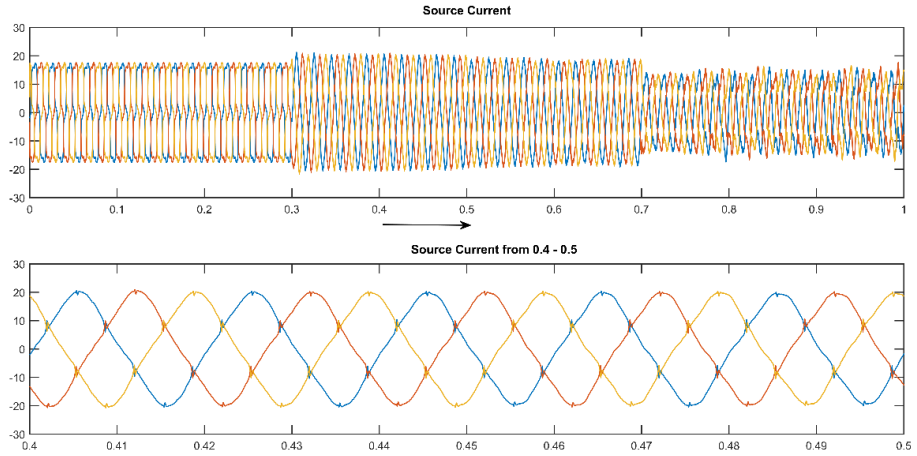

Figure 5.7
Result of source current behavior during fourth scenario

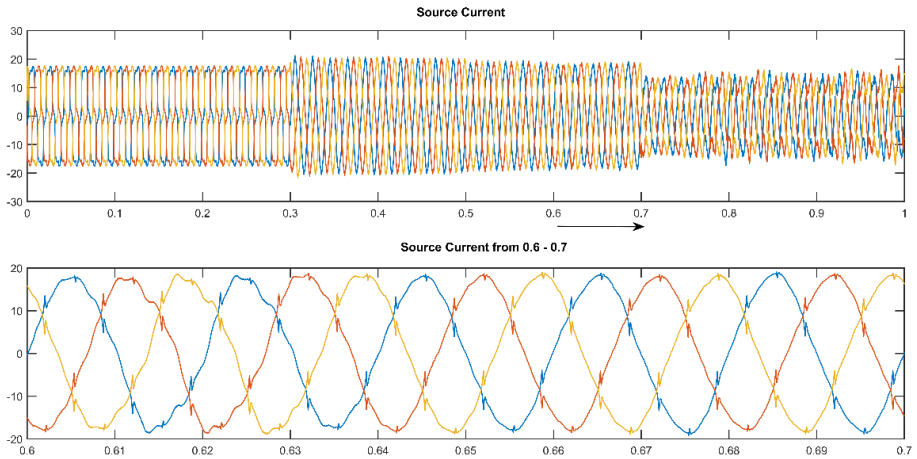

Figure 5.8
Result of source current behavior during fifth scenario

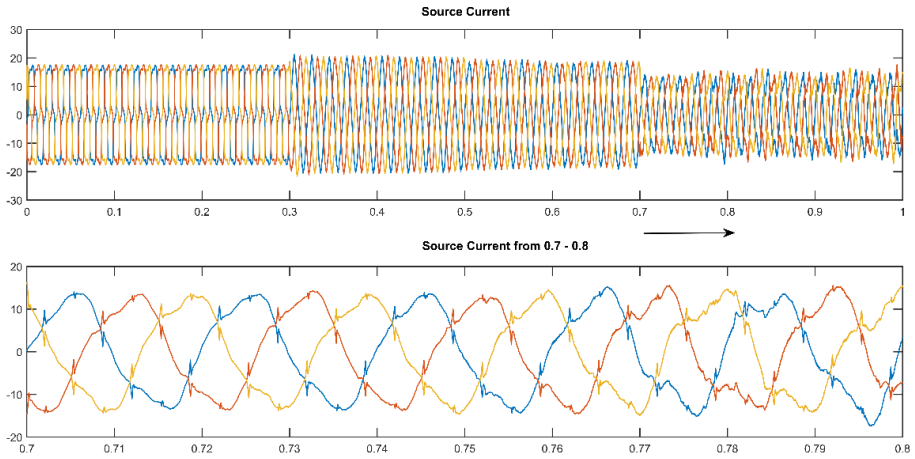

Figure 5.9
Result of inverter current behavior during first and second scenarios

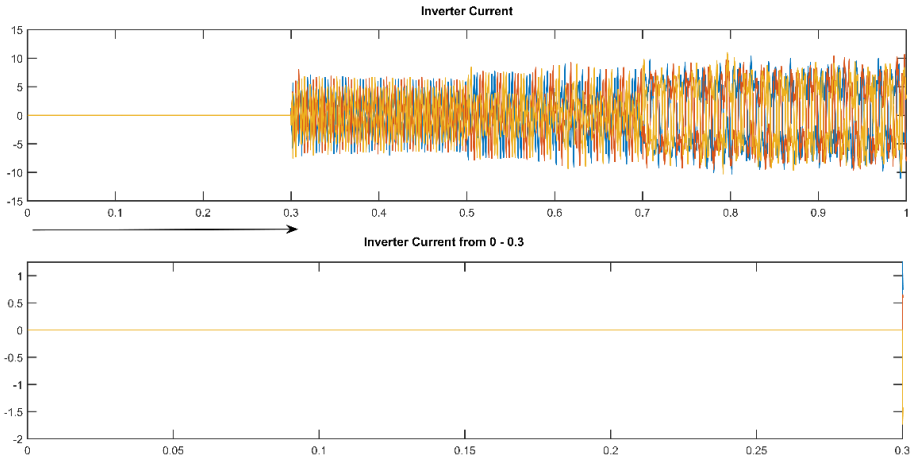

Figure 5.10
Result of inverter current behavior during third scenario

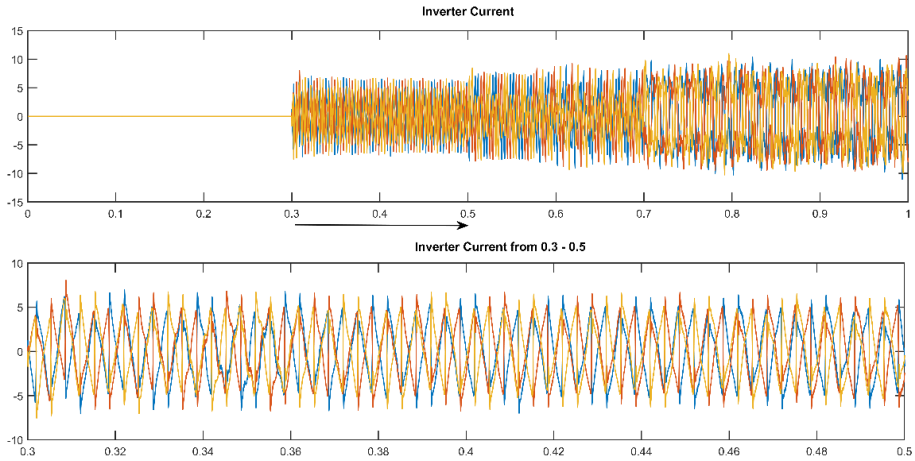

Figure 5.11
Result of inverter current behavior during fourth scenario

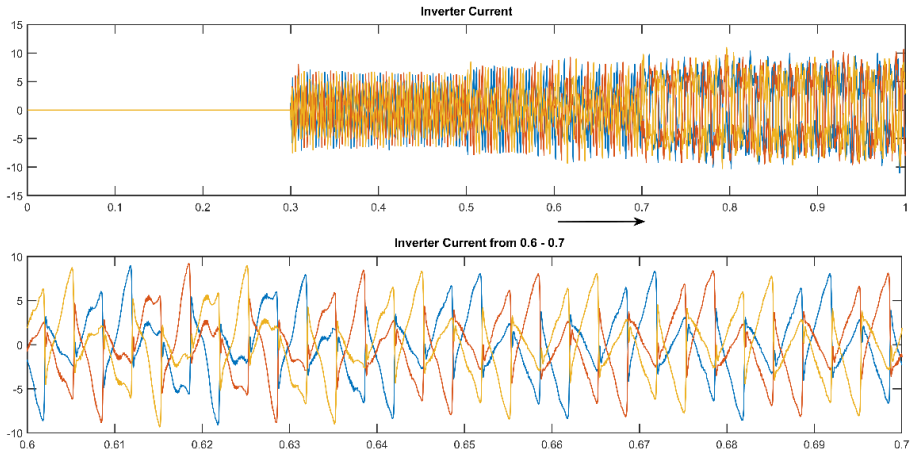

Figure 5.12
Result of inverter current behavior during fifth scenario

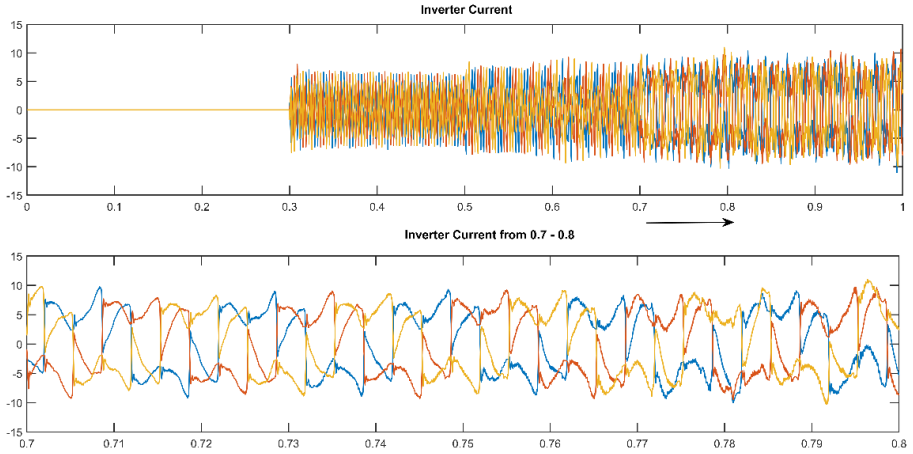

Figure 5.13
Total harmonics distortion of source output current during first and second scenarios

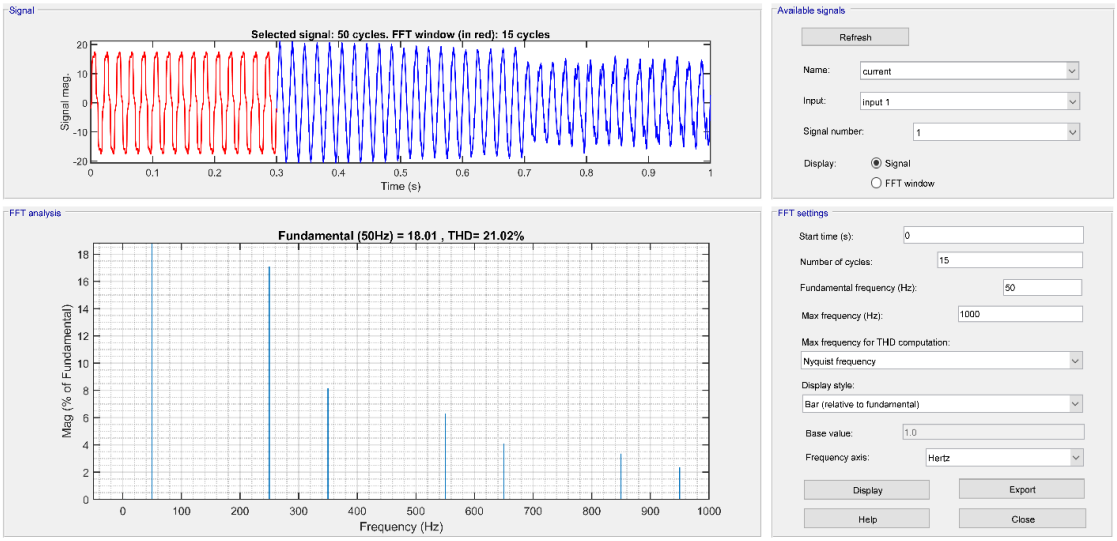

Figure 5.14

Total harmonics distortion of source output current during third scenario

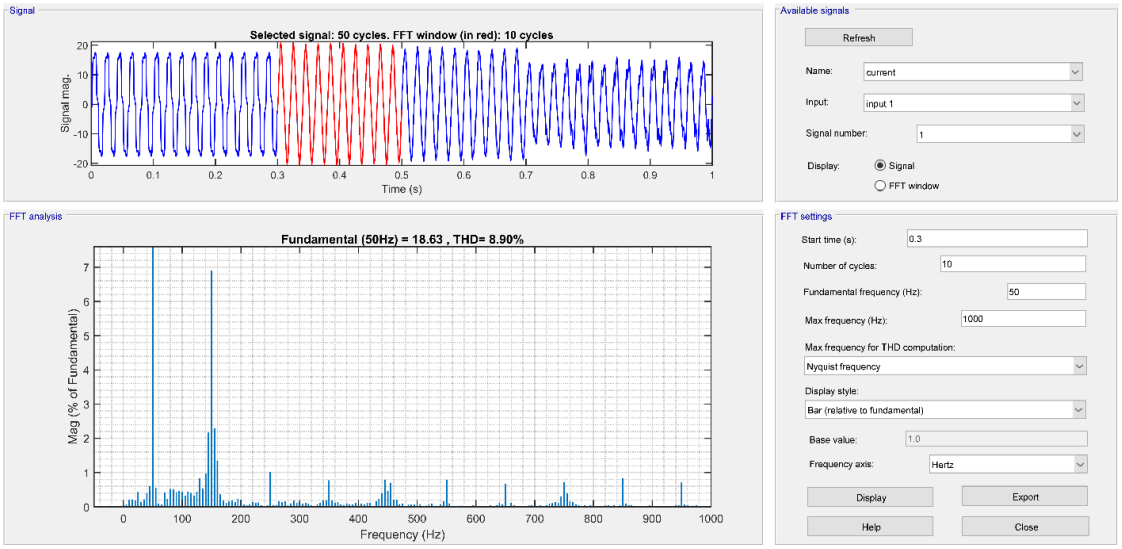

Figure 5.15

Total harmonics distortion of source output current during fourth scenario

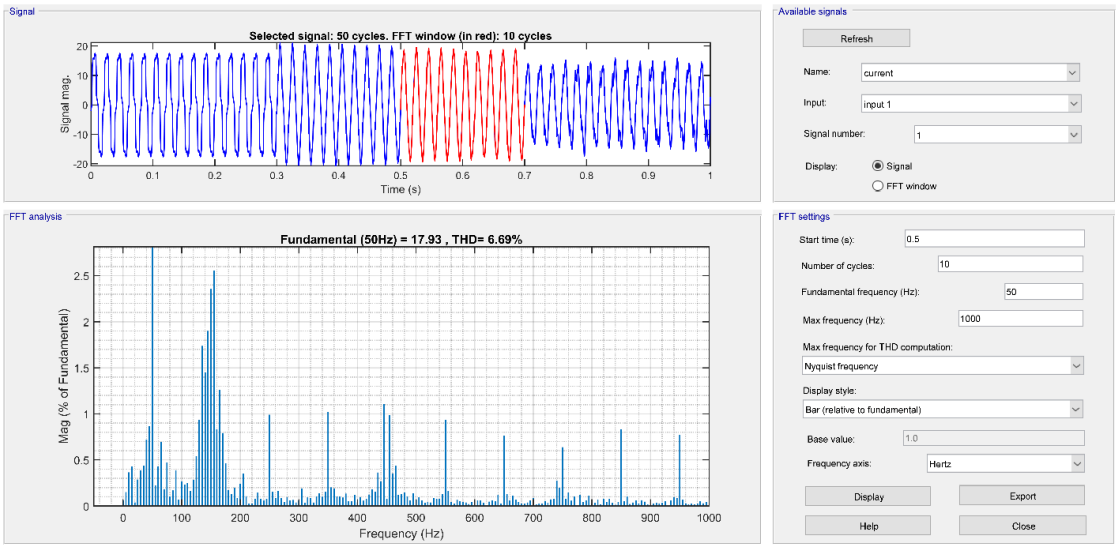

Figure 5.16

Total harmonics distortion of source output current during fifth scenario

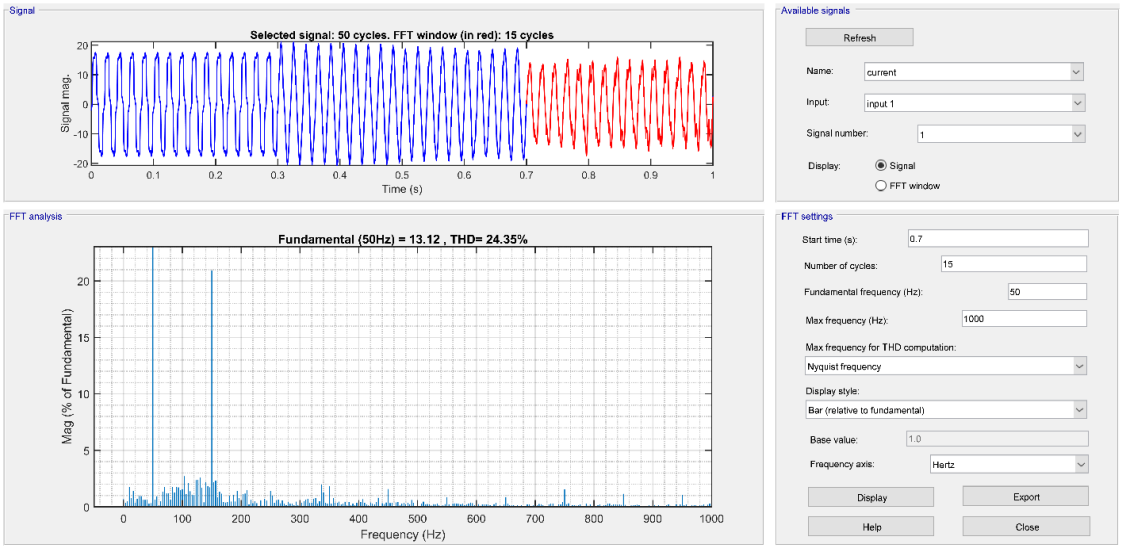

Figure 5.17

Total harmonics distortion of Inverter output current during first and second scenarios

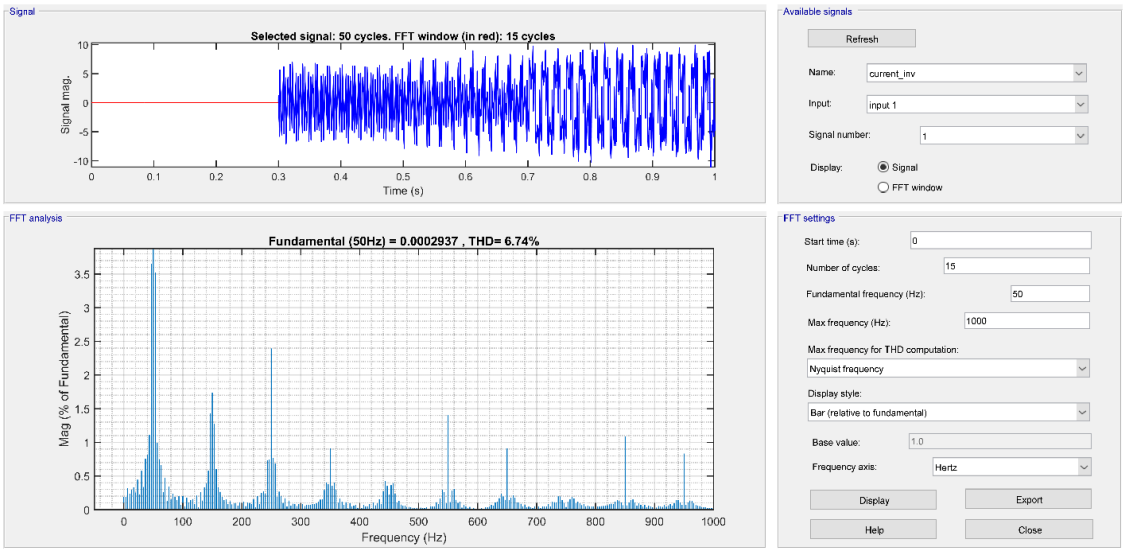

Figure 5.18

Total harmonics distortion of Inverter output current during third scenario

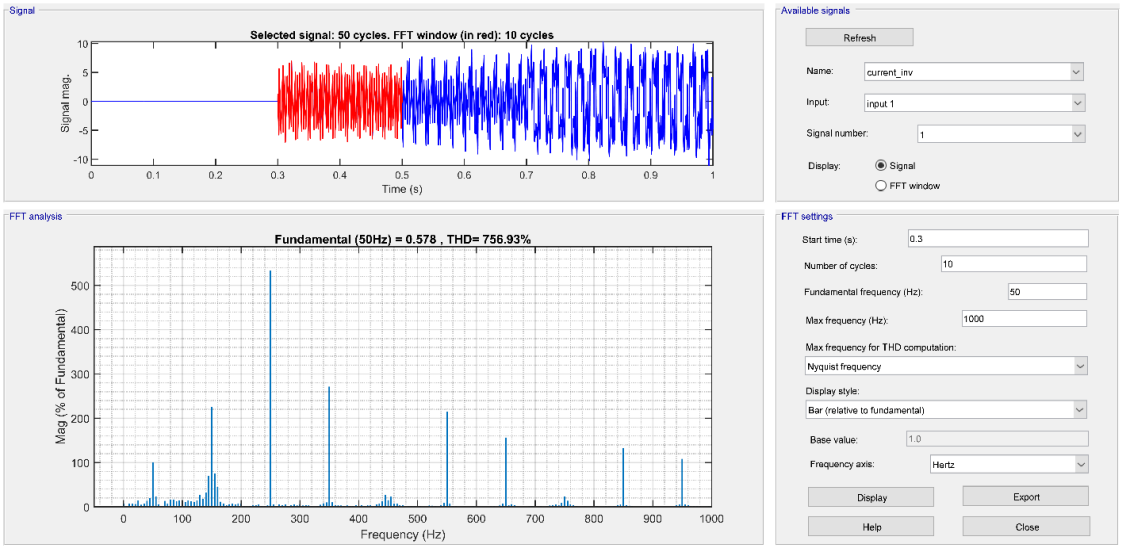

Figure 5.19

Total harmonics distortion of Inverter output current during fourth scenario

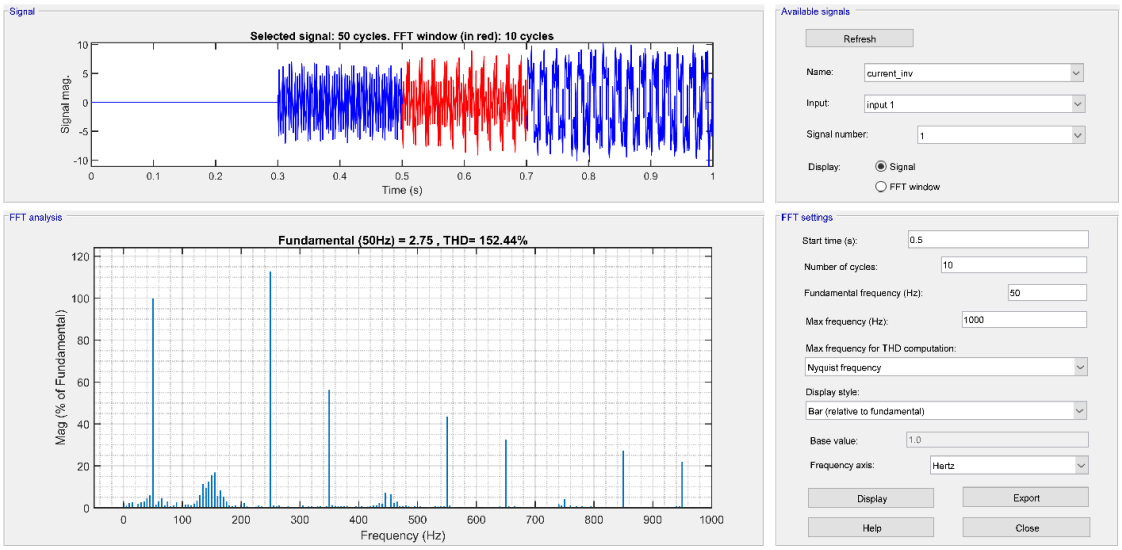

Figure 5.20
Total harmonics distortion of Inverter output current during fifth scenario

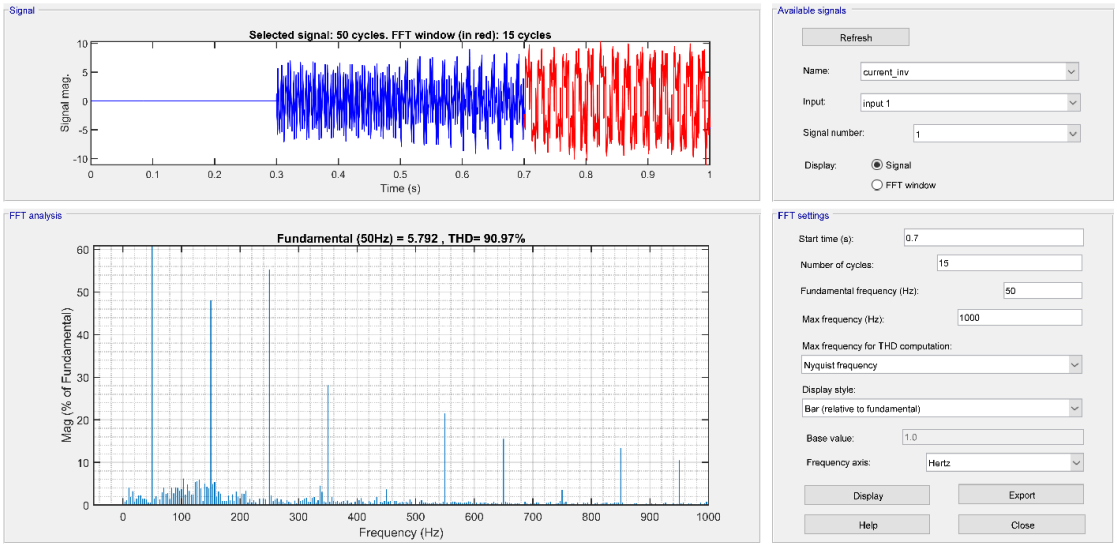

Figure 5.21
Results of source voltage behavior

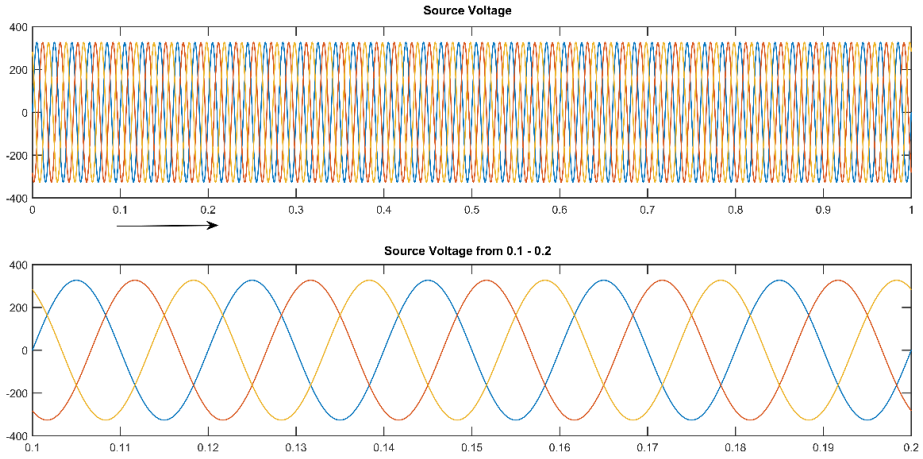

Figure 5.22
Results of Inverter voltage behavior during first and second scenarios

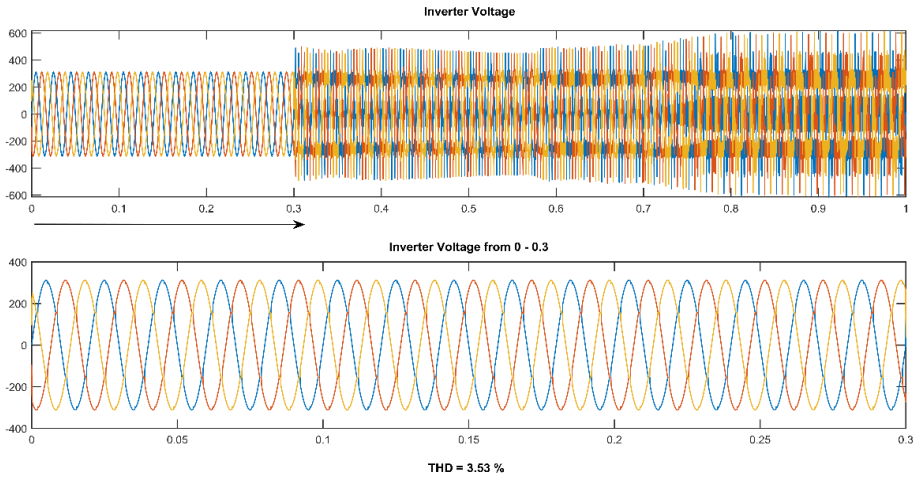

Figure 5.23
Results of Inverter voltage behavior during third scenario

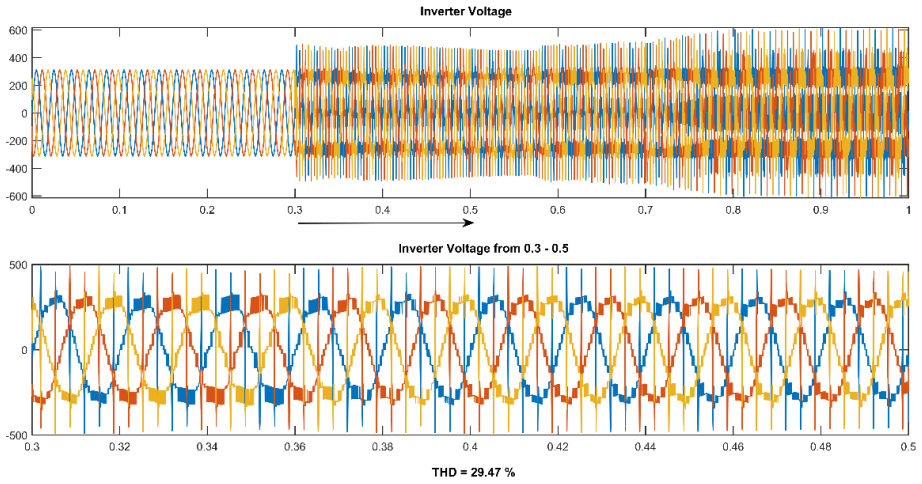

Figure 5.24
Results of Inverter voltage behavior during fourth scenario

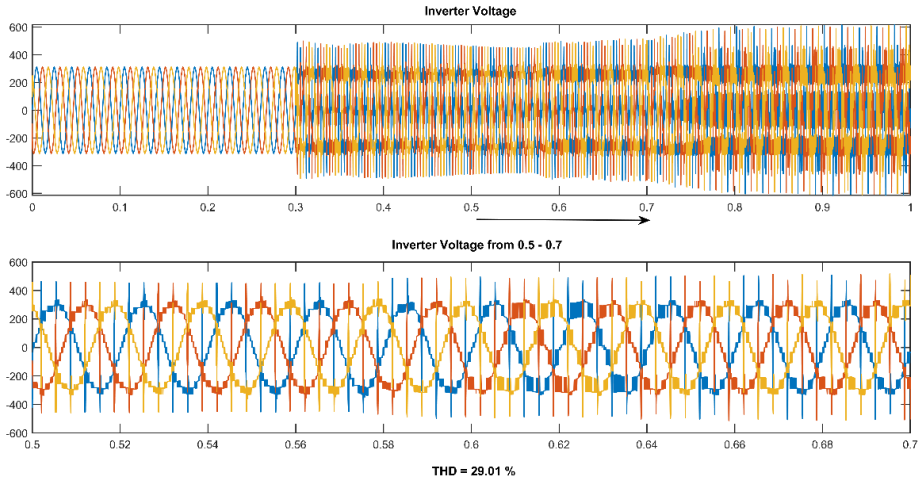

Figure 5.25
Results of Inverter voltage behavior during fifth scenario

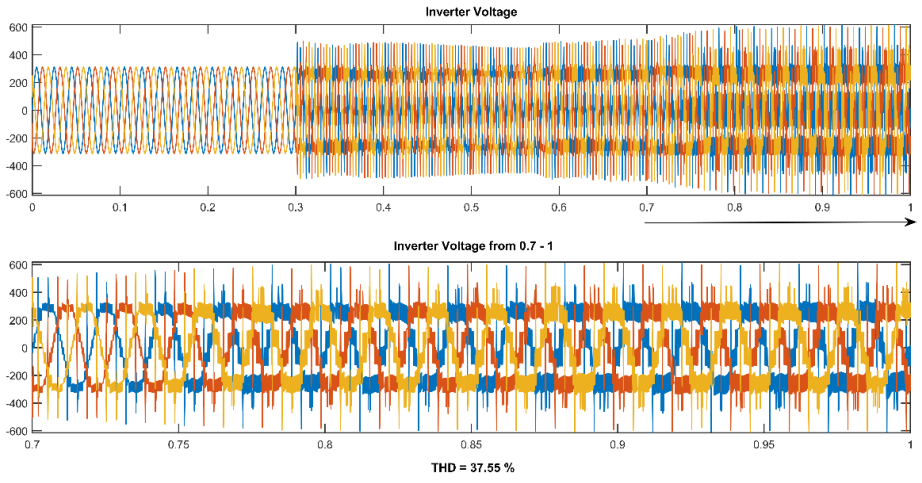

Figure 5.26
Id measured and Id reference.

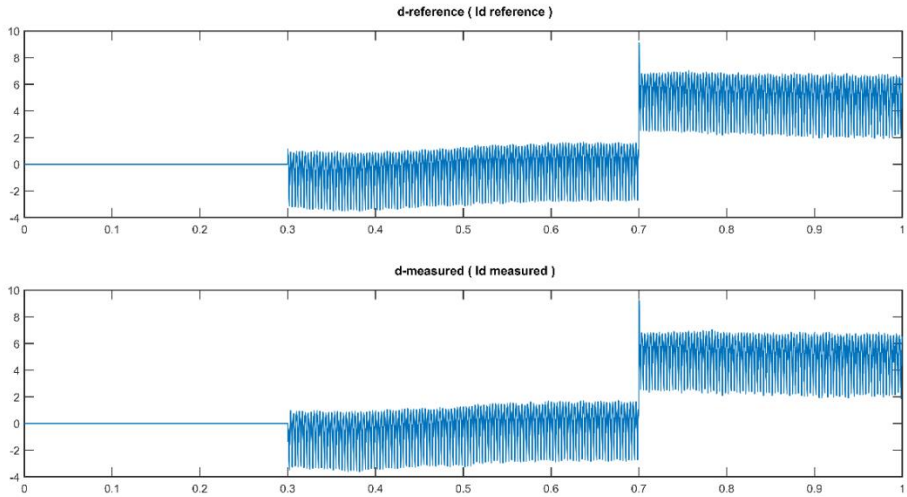

Figure 5.27
Iq measured and Iq reference

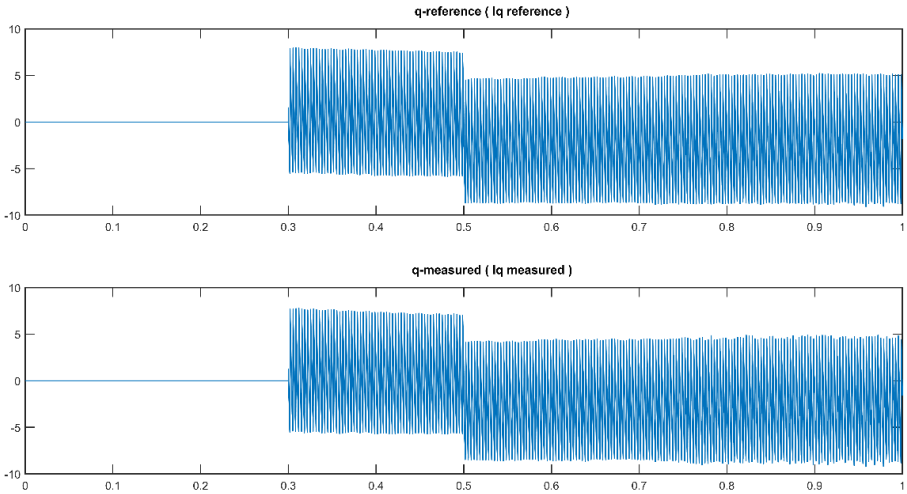

Figure 5.29
Result of source voltage behavior when SAPF connected to bus no 1 of the IEEE 15 bus network

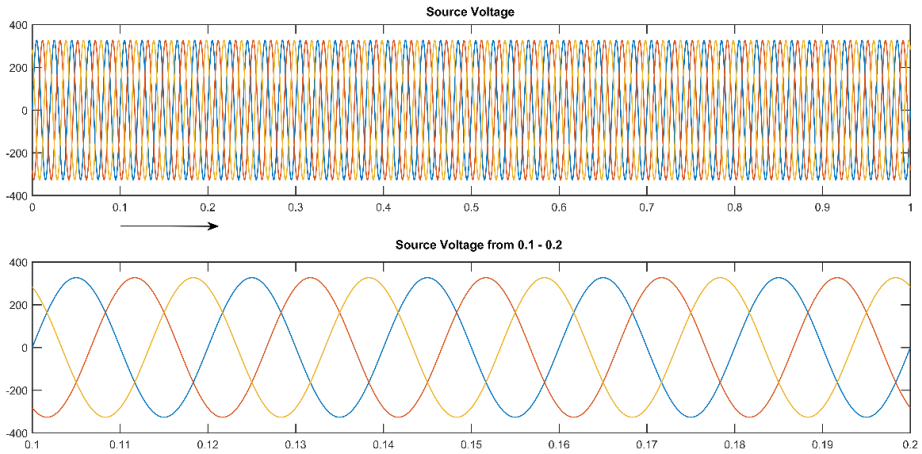

Figure 5.30
Result of source current behavior during first and second scenarios when SAPF connected to bus no 1 of the IEEE 15 bus network

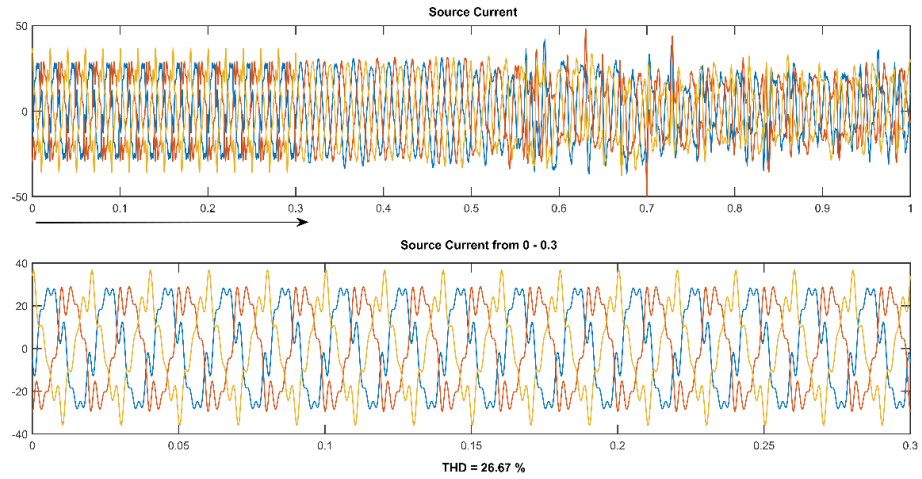

Figure 5.31

Result of source current behavior during third scenario when SAPF connected to bus no 1 of the IEEE 15 bus network

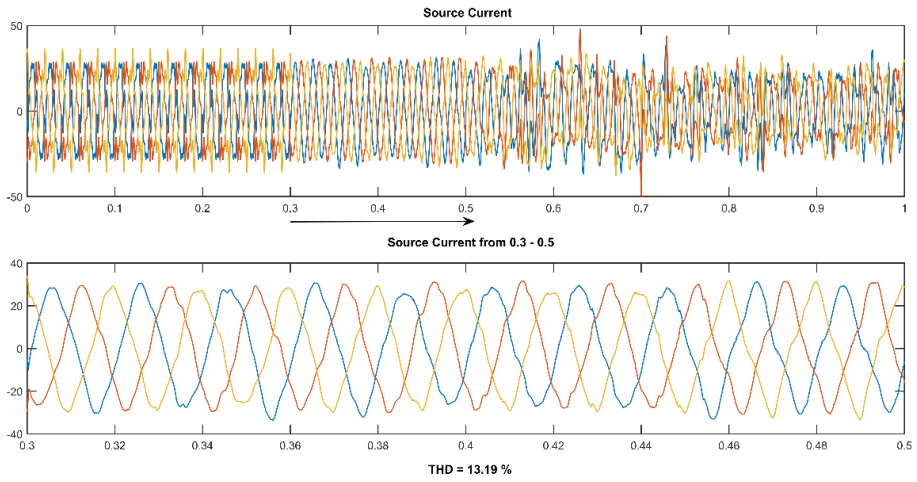

Figure 5.32

Result of source current behavior during fourth scenario when SAPF connected to bus no 1 of the IEEE 15 bus networ

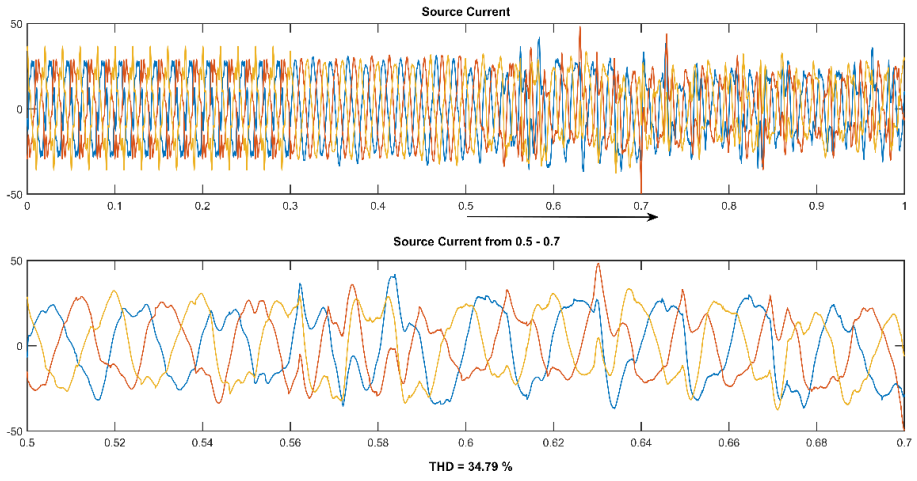

Figure 5.33

Result of source current behavior during fifth scenario when SAPF connected to bus no 1 of the IEEE 15 bus network

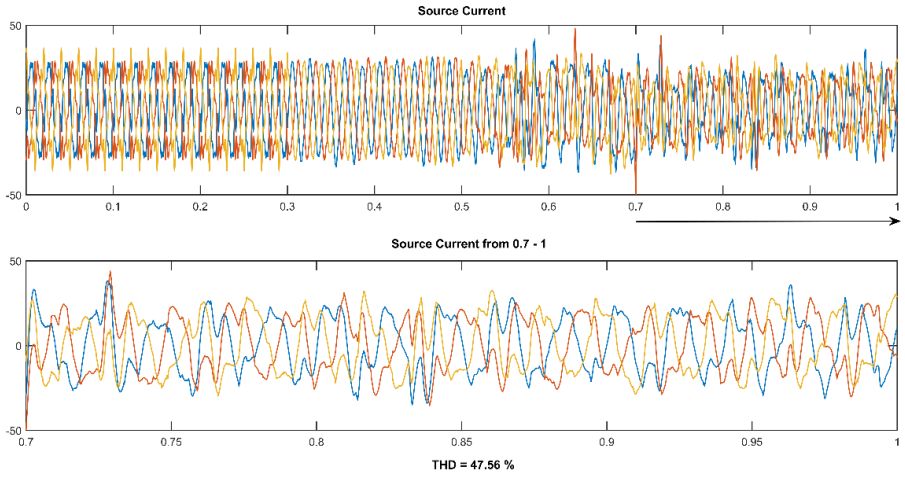

Figure 5.34

Total harmonics distortion of source output current during first and second scenarios in the first test

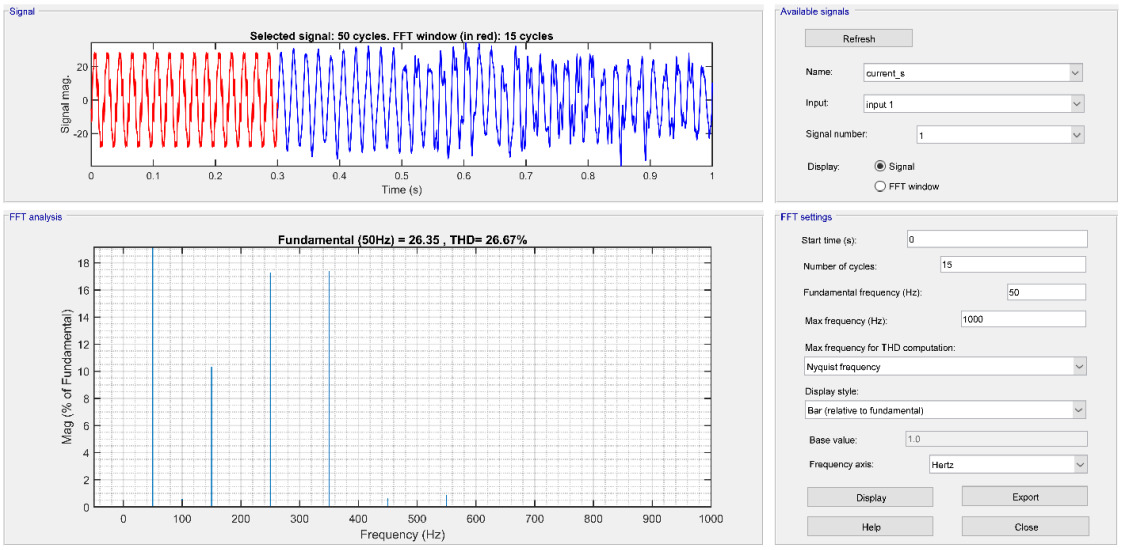

Figure 5.35

Total harmonics distortion of source output current during third scenario in the first test

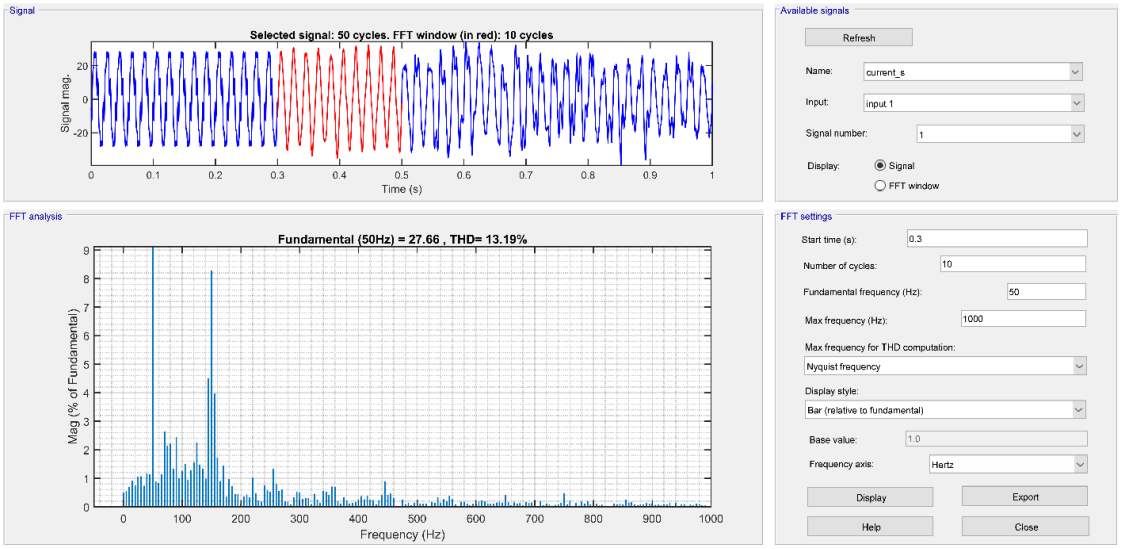

Figure 5.36

Total harmonics distortion of source output current during fourth scenario in the first test

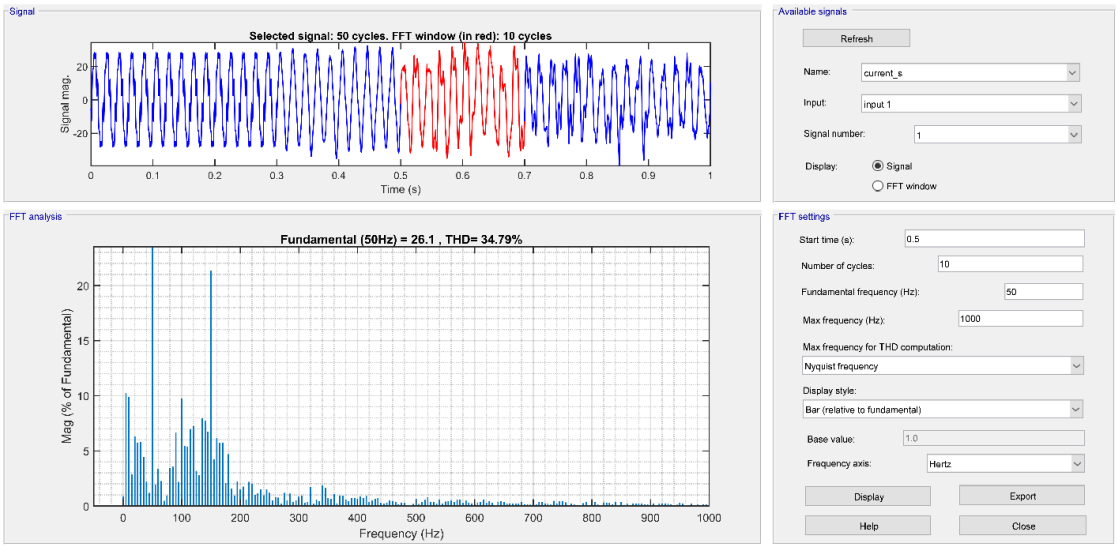

Figure 5.37

Total harmonics distortion of source output current during fifth scenario in the first test

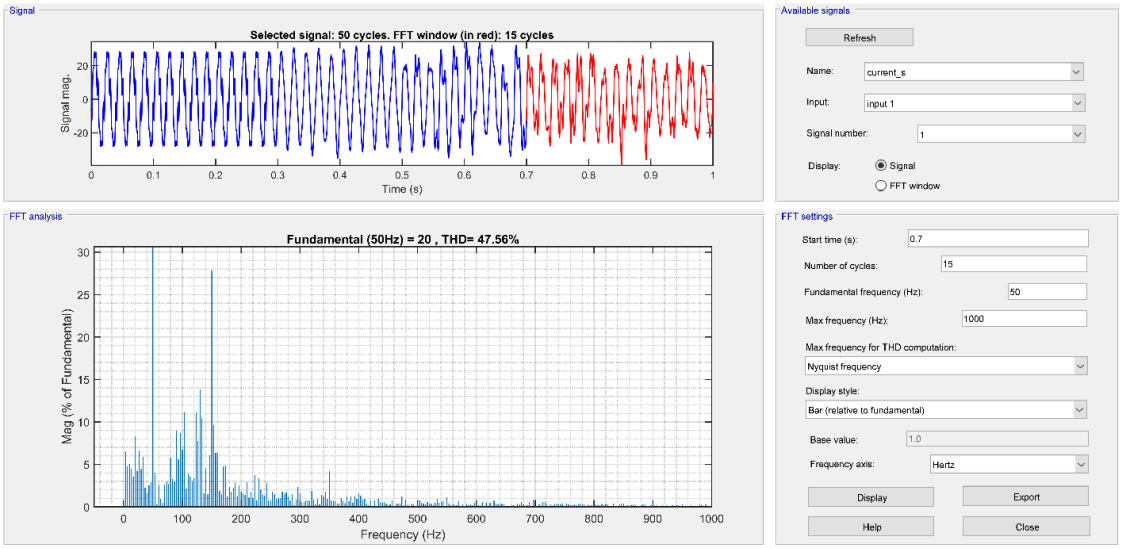

Figure 5.38

Results of current waveforms at buses 7, 9, 11, 15 when SAPF connected to bus no 1 of the IEEE 15 bus network

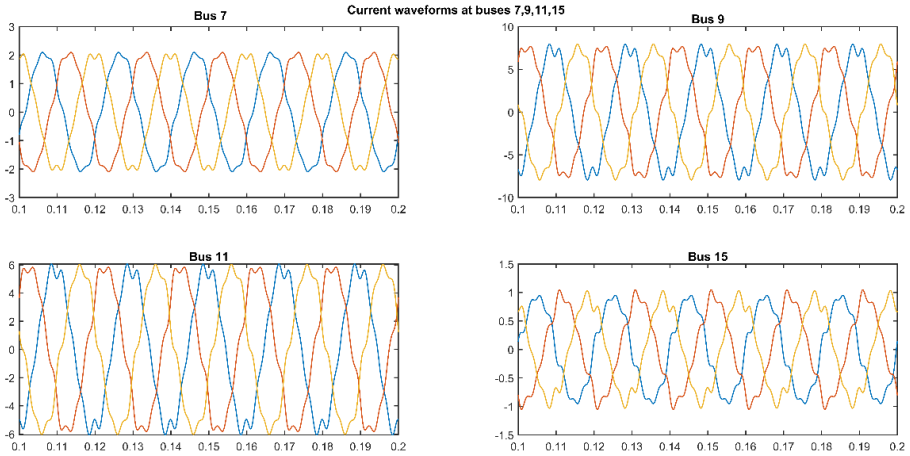

Figure 5.39

Results of voltage waveforms at buses 7, 9, 11, 15 when SAPF connected to bus no 1

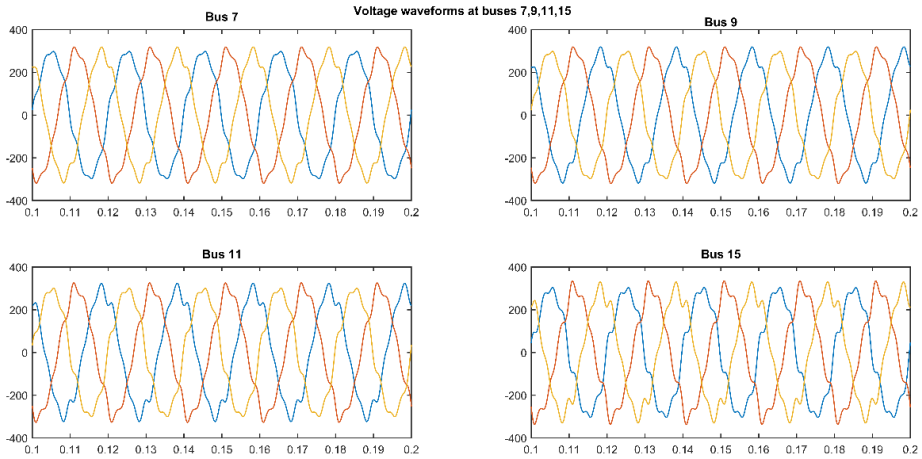

Figure 5.41

Result of source voltage behavior when SAPF connected to bus no 5 of the IEEE 15 bus network

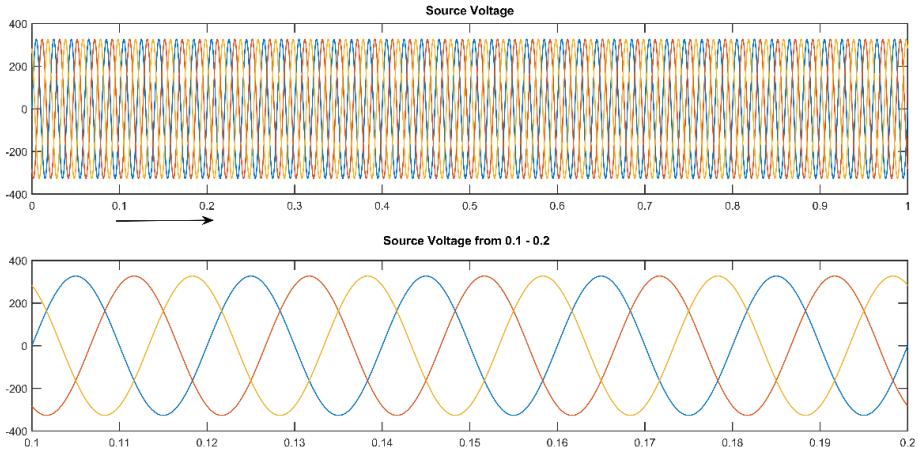

Figure 5.42

Result of source current behavior during first and second scenarios when SAPF connected to bus no 5 of the IEEE 15 bus network

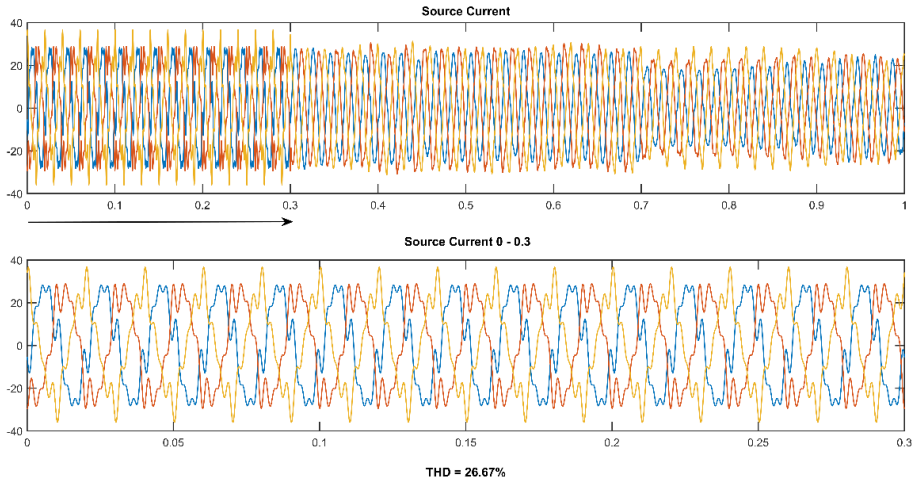

Figure 5.43

Result of source current behavior during third scenario when SAPF connected to bus no 5 of the IEEE 15 bus network

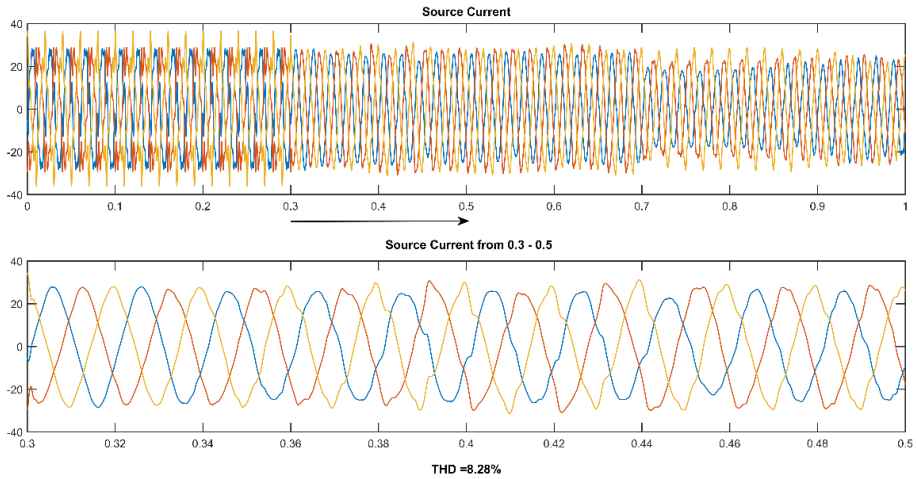

Figure 5.44
Result of source current behavior during fourth scenario when SAPF connected to bus no 5 of the IEEE 15 bus network

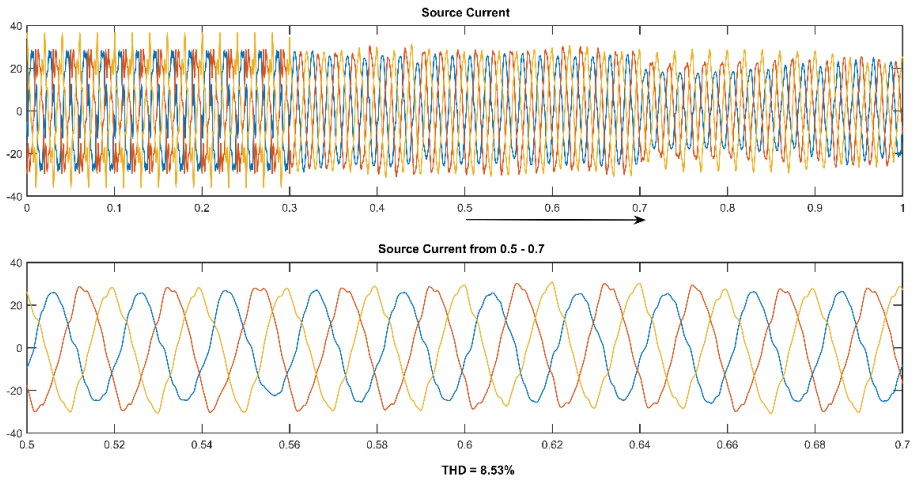

Figure 5.45
Result of source current behavior during fifth scenario when SAPF connected to bus no 5 of the IEEE 15 bus network

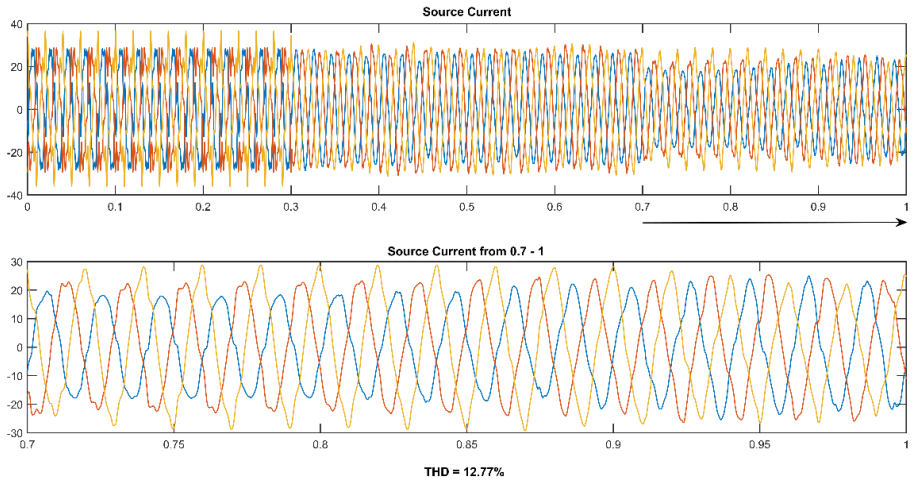

Figure 05.46

Total harmonics distortion of Source output current during first and second scenarios in the second test

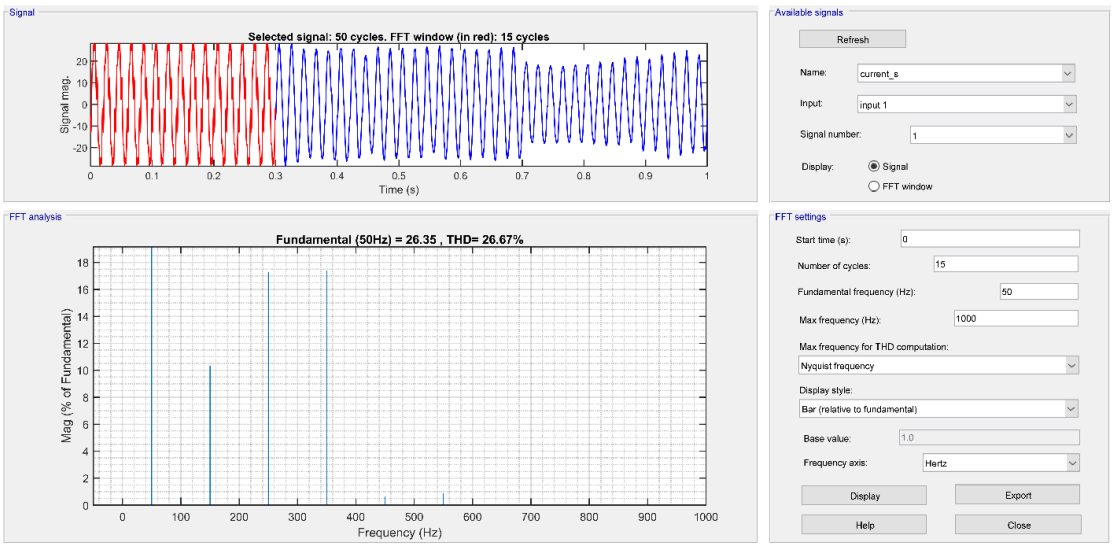

Figure 5.47

Total harmonics distortion of Source output current during third scenario in the second test

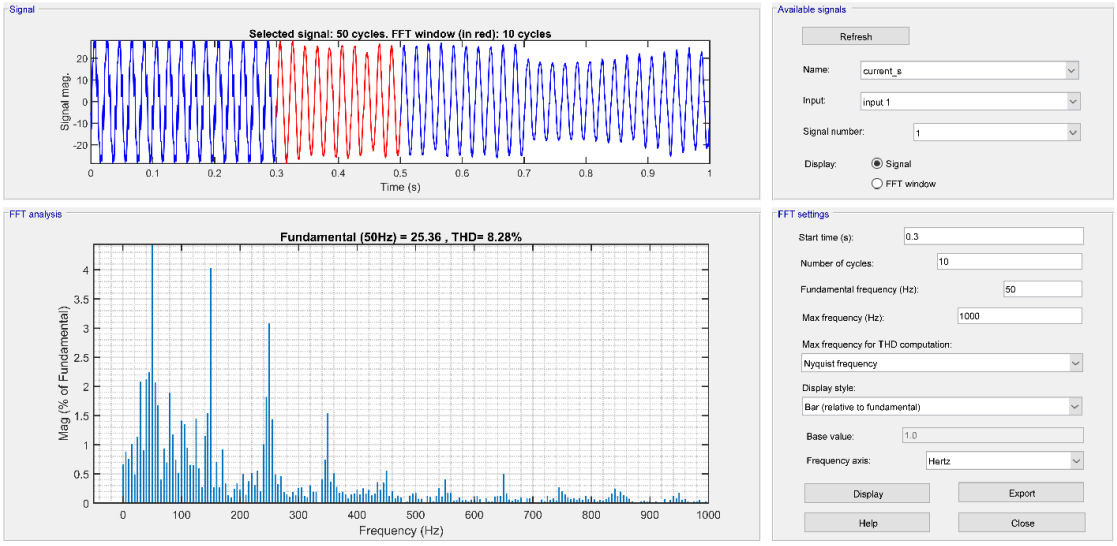

Figure 5.48

Total harmonics distortion of Source output current during fourth scenario in the second test

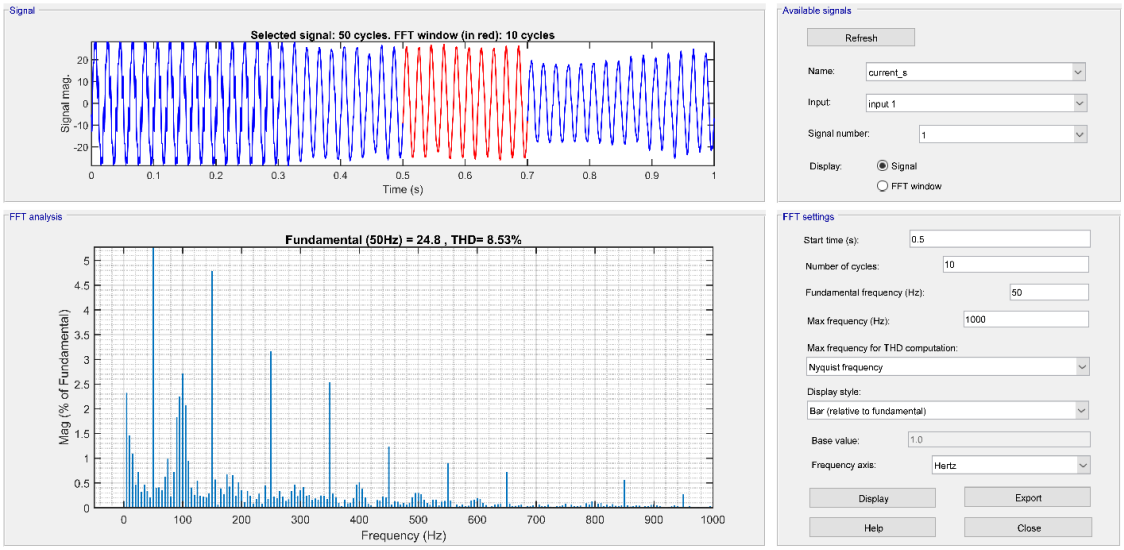

Figure 5.49

Total harmonics distortion of Source output current during fifth scenario in the second test

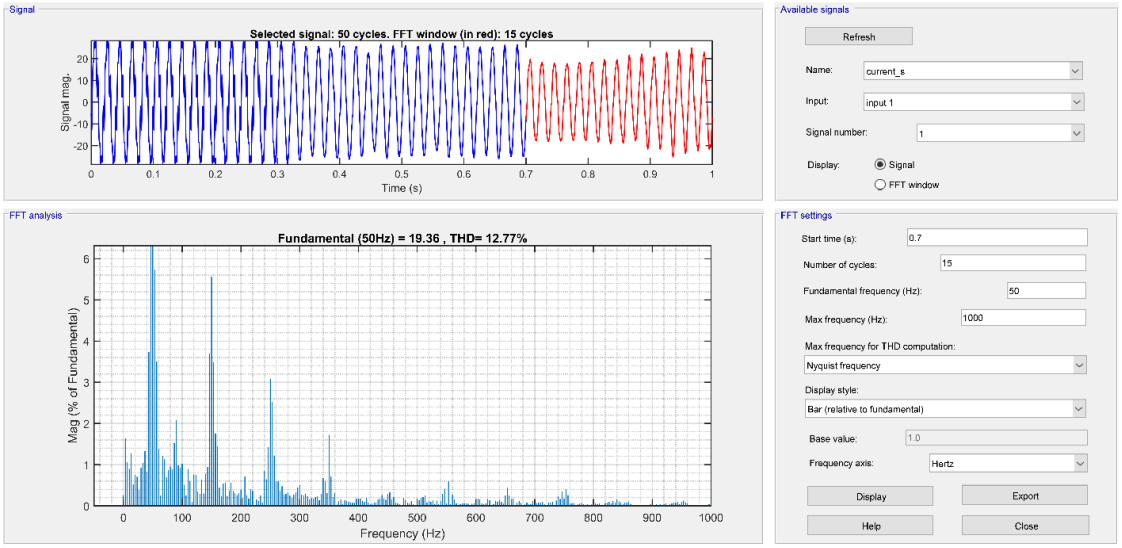

Figure 5.50

Results of current waveforms at buses 7,9,11,15 when SAPF connected to bus no 5 of the IEEE 15 bus network

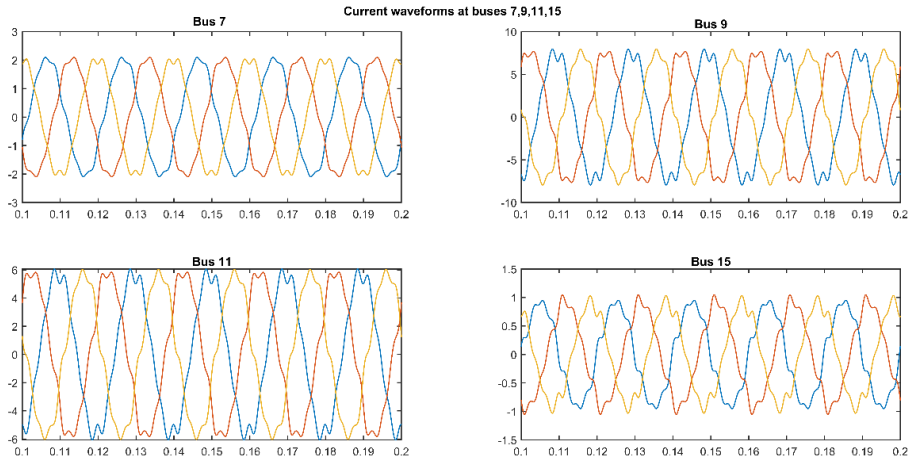

Figure 5.51

Results of voltage waveforms at buses 7,9,11,15 when SAPF connected to bus no 5 of the IEEE 15 bus network

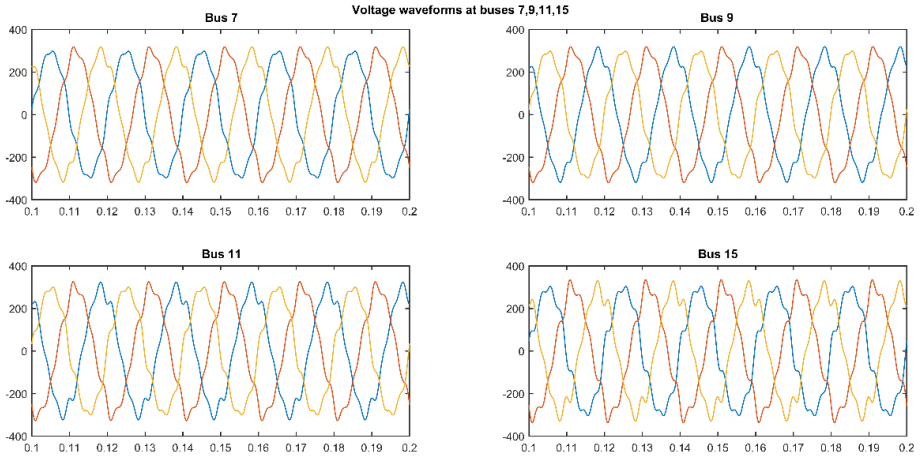

Figure 5.52
THD of current waveforms at buses 7,9,1,15 when SAPF connected to bus no 1, and bus no 5 of the IEEE 15 bus network

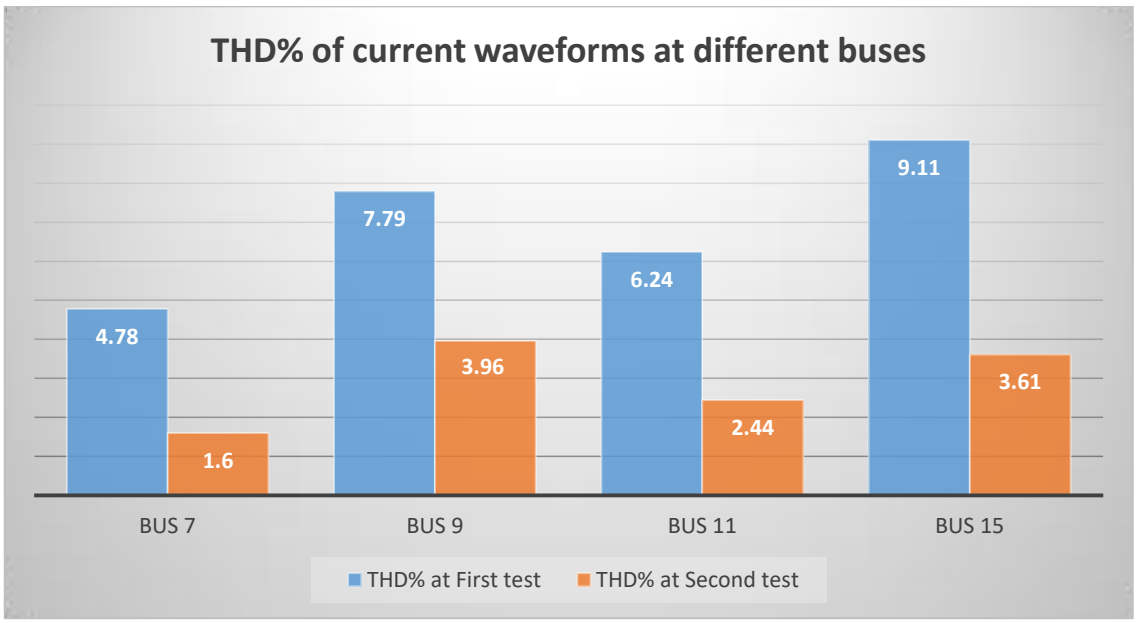

Figure 5.53
THD of voltage waveforms at buses 7,9,1,15 when SAPF connected to bus no 1, and bus no 5 of the IEEE 15 bus network

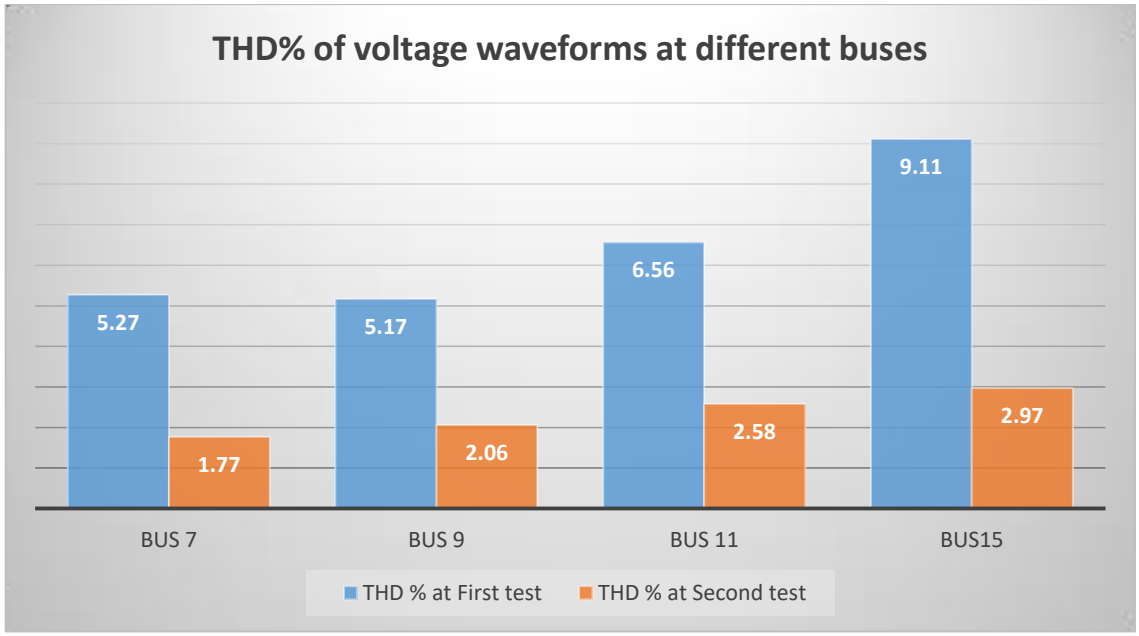

جـامعـــة النجاح الوطنية

كليـــة الدراســـات العليـــا

تصميم مرشح باستخدام انفيرتر متعدد المستويات وتربينة رياح

إعداد

منار وائل شتية

إشراف

د. كامل صالح

قدمت هذه الرسالة استكمالا لمتطلبات الحصول على درجة الماجستير في هندسة القوى الكهربائية، من كلية الدراسات العليا، في جامعة النجاح الوطنية، نابلس –فلسطين.

2023

تصميم مرشح باستخدام انفيرتر متعدد المستويات وتربينة رياح

إعداد

منار وائل شتية

إشراف

د. كامل صالح

الملخص

تتزايد الحاجة إلى الطاقة بسرعة مع عدد سكان العالم. يفترض توليد القوة دورا حاسما في تسهيل التنمية الوطنية من خلال تلبية مطالب السكان. لقد تم استخدام مصادر الطاقة المتجددة، بما في ذلك الطاقة الشمسية وطاقة الرياح وغيرها، لعدة قرون سبقت العصر الحالي. من المعترف به عمومًا أن الطاقة الشمسية وطاقة الرياح من أكثر الطرق الواعدة للطاقة المتجددة، وقد أصبح استخدامها منتشرًا بشكل متزايد.

يؤدي الاستخدام الواسع النطاق للأحمال غير الخطية في الأنظمة الكهربائية الحديثة إلى التلوث التوافقي للشبكة الرئيسية. بصرف النظر عن المشكلات التي تثيرها التيارات التوافقية، تمثل الطاقة التفاعلية تحديًا إضافيًا في أنظمة الطاقة.

لتعزيز جودة التوصيل للنظام وتحقيق عامل قدرة يساوي واحد، لا بد من استخدام المرشحات الكهربائية للقضاء على التوافقيات والطاقة التفاعلية. لتحسين جودة الكهرباء، يتم استخدام مرشح نشط موازي.

في هذا البحث تم دمج عاكس متعدد المستويات ذي 27 مستوى بالإضافة إلى مرشح الطاقة النشط مع توربينات الرياح كمصدر للطاقة المتجددة باستخدام . MATLAB/SIMULINKبرنامج

في هذا المشروع تمت محاكاة مرشح الطاقة النشط باستخدام برنامج الماتلاب ، وكانت النتائج التي تم الحصول عليها على النحو التالي: في حالة التشغيل الأولى، عند توصيل النظام بحمل غير خطي

منفصل، تم تقليل التشوه التوافقي الكلي لتيار المصدر من 21.02% إلى 8.90% بعد بدء عمل العاكس. علاوة على ذلك، تم زيادة التشوه التوافقي الكلي لتيار العاكس من 6.74% إلى 756.93%.

في حالة التشغيل الثانية، يتم شبك النظام بشبكة شعاعية مكونة من خمسة عشر نقطة توزيع، فعندما يتم توصيل الفلتر النشط بالقرب من مصدر الطاقة، ينخفض التشوه التوافقي الكلي لتيار خرج المصدر من 26.67% إلى 13.19%، ولكن على العكس من ذلك، عندما يتم توصيل الفلتر النشط بالقرب من الحمل، تم تخفيض التشوه التوافقي الكلي لتيار خرج المصدر من 26.67% إلى 8.28%. تؤكد النتائج أن المرشح النشط في هذا الموقع فعال في تقليل قيم التشوه التوافقي الكلي.

الكلمات المفتاحية: مصادر الطاقة المتجددة، مرشح الطاقة النشط، العاكس متعدد المستويات، توربينات الرياح، الأحمال غير الخطية، الشبكة الشعاعية، التشوه التوافقي الكلي.